Titre: Title:	New Strategies for Desensitizing Aero-Engine Axial Compressor Performance and Stability to Tip Clearance Increase
Auteur: Author:	Yassine Souleimani
Date:	2017
Type:	Mémoire ou thèse / Dissertation or Thesis
Référence: Citation:	Souleimani, Y. (2017). New Strategies for Desensitizing Aero-Engine Axial Compressor Performance and Stability to Tip Clearance Increase [Master's thesis, École Polytechnique de Montréal]. PolyPublie. https://publications.polymtl.ca/2754/

UNIVERSITÉ DE MONTRÉAL

NEW STRATEGIES FOR DESENSITIZING AERO-ENGINE AXIAL COMPRESSOR PERFORMANCE AND STABILITY TO TIP CLEARANCE INCREASE

YASSINE SOULEIMANI

DÉPARTEMENT DE GÉNIE MÉCANIQUE

ÉCOLE POLYTECHNIQUE DE MONTRÉAL

MÉMOIRE PRÉSENTÉ EN VUE DE L'OBTENTION

DU DIPLÔME DE MAÎTRISE ÈS SCIENCES APPLIQUÉES

(GÉNIE MÉCANIQUE)

AOÛT 2017

UNIVERSITÉ DE MONTRÉAL

ÉCOLE POLYTECHNIQUE DE MONTRÉAL

Ce mémoire intitulé :

NEW STRATEGIES FOR DESENSITIZING AERO-ENGINE AXIAL COMPRESSOR PERFORMANCE AND STABILITY TO TIP CLEARANCE INCREASE

présenté par : SOULEIMANI Yassine

en vue de l'obtention du diplôme de : Maîtrise ès sciences appliquées

a été dûment accepté par le jury d'examen constitué de :

M. REGGIO Marcelo, Ph. D., président

M. VO Huu Duc, Ph. D., membre et directeur de recherche

M. VÉTEL Jérôme, Ph. D., membre

ACKNOWLEDGEMENTS

I would first like to thank Pratt & Whitney Canada (P&WC) for sponsoring this research and for providing all the necessary resources to successfully carry out this project. I am particularly grateful to Hong Yu, Hien Duong and Jonathan Driver from P&WC Compressor Aerodynamics department for their technical training and administrative support. I would like also to thank Barry Barnett from P&WC Research and technology department for his technical advices and the successful coordination of the entire project. A special thank is also addressed to Sean Nolan and Matthew Bennington from Pratt & Whitney East Hartford (P&WEH) for their insightful technical feedback. Due to the large scope and complexity of this project as well as the diversity of the disciplines involved, I also had to draw on the expertise of many P&WC other departments to complete this work and I am grateful for their help.

I would like to thank the other funding partners for this research, namely Green Aviation Research and Development Network (GARDN), the National Sciences and Engineering Research Council of Canada (NSERC), the Fond Québécois de Recherche sur la Nature et les Technologies (FRQNT), Pratt & Whitney East Hartford (P&WEH).

I also owe many thanks to Thierry Lafrance from MEKANIC Research and Technology for his countless advices during the long evenings spent on assembling and putting into operation the state-of-the-art new compressor rig at École Polytechnique de Montréal.

Finally, I would like to express my profound gratitude to my research director Huu Duc Vo for his constant guidance and patience throughout the project. Although his supervision was mostly technical, he also contributed significantly to the enhancement of my soft skills which is greatly appreciated.

RÉSUMÉ

Le jeu d'aube correspond à l'espace minuscule qui se trouve entre le bout des aubes d'un rotor de turbomachine et son carter fixe. Dans un compresseur de moteur d'avion, le jeu d'aube cause des pertes en performance et des problèmes de stabilité aérodynamique qui nuisent à la consommation en carburant et à l'enveloppe d'opération des moteurs d'avion. Les variations de la vitesse de rotation ainsi que des températures internes du compresseur durant un cycle de vol entraînent la dilation ou le rétrécissement de ses composants (rotor, disque ou carter), ce qui augmente temporairement ou de façon permanente (par frottement) le jeu d'aube. Cet agrandissement inévitable du jeu d'aube durant le cycle de vie du moteur résulte en une dégradation à long terme du moteur au niveau de sa consommation en carburant et de son enveloppe d'opération.

La majorité des études effectuées se sont concentrées sur l'amélioration de la performance (rapport de pression totale et rendement) et la stabilité aérodynamique (marge de décrochage) à un jeu d'aube nominal. Toutefois, très peu d'études se sont attaquées directement à l'atténuation de la réduction (sensibilité) de la performance et de la stabilité aérodynamique face à l'agrandissement du jeu d'aube. Ces travaux incluent deux récentes études numériques très prometteuses à l'École Polytechnique de Montréal qui ont proposé deux stratégies de conception d'aubes et un nouveau traitement de carter pour réduire la sensibilité de la performance et de la marge de décrochage à l'agrandissement du jeu d'aube pour un compresseur axial.

La phase actuelle de cette recherche vise à appliquer les conclusions de ces deux études à un vrai rotor de compresseur axial de moteur d'avion. Les objectifs de ce projet sont de concevoir un traitement de carter pour ce rotor afin de réduire la sensibilité de sa performance et de sa marge de décrochage face à l'agrandissement du jeu d'aube, et de changer le design de l'aube du rotor pour obtenir le même effet (sans traitement de carter). Ces deux designs seront testés dans un nouveau banc d'essai de compresseur transsonique à l'École Polytechnique de Montréal pour valider expérimentalement cette technologie. En cas de succès, cette technologie donnera des moteurs d'avion aérodynamiquement plus robustes qui seront capables de maintenir leur performance et enveloppe d'opération avec l'âge.

La méthodologie choisie pour atteindre ces objectifs passe par une approche numérique basée sur des simulations numériques de l'écoulement (CFD) et est composée de trois étapes. La première étape est la simulation du rotor de référence pour évaluer sa performance et stabilité

aérodynamique, leurs sensibilités à l'agrandissement du jeu d'aube ainsi que la source de ces sensibilités. Ensuite, le nouveau traitement de carter est adapté au rotor de référence par une étude paramétrique pour minimiser la pénalité en performance nominale et maximiser la réduction de la sensibilité de la performance à l'agrandissement du jeu d'aube. Une analyse comparative s'en suit afin de comprendre l'influence du traitement de carter appliqué sur la valeur nominale et la sensibilité face à l'agrandissement du jeu d'aube de la performance et de la marge de décrochage. Finalement, les deux stratégies de conception d'aubes sont appliquées sur le rotor de référence pour essayer de produire un nouveau rotor dont la performance et stabilité aérodynamique sont moins sensibles à l'agrandissement du jeu d'aube tout en minimisant les pertes de performance nominale. Une étude comparative du champ d'écoulement est faite pour expliquer les améliorations observées.

Les simulations du rotor de référence montrent que la région inférieure du passage d'aube contribue autant à la sensibilité du rapport de pression totale à l'agrandissement du jeu d'aube que la région supérieure du passage d'aube qui est dominée par l'écoulement de jeu (i.e. l'écoulement qui passe à travers le jeu d'aube). Par contre, la sensibilité du rendement à l'agrandissement du jeu d'aube est due principalement aux pertes de mélange dans la région supérieure du passage d'aube.

Le nouveau traitement de carter a été appliqué au rotor de référence à travers une optimisation du design. Bien qu'il cause une perte de performance nominale, le traitement de carter a complètement inversé la sensibilité du rapport de pression totale à l'agrandissement du jeu d'aube et réduit la sensibilité du rendement. Le premier phénomène peut être expliqué par la rotation du noyau de l'écoulement du passage d'aube dans la partie inférieure du passage, cette rotation étant induite indirectement par l'injection radiale de fluide par les fentes du traitement de carter. Le deuxième phénomène vient de la réduction de la quantité d'écoulement qui traverse les jeux de deux aubes adjacentes, appelé double écoulement de jeu.

Finalement, les deux stratégies de conception d'aubes proposées antérieurement n'ont pas fonctionné pour ce rotor. Une nouvelle stratégie de conception d'aube a été appliquée pour induire de la rotation au noyau de l'écoulement du passage d'aube dans la partie inférieure du passage. Le nouveau rotor qui en résulte a réduit avec succès la sensibilité du rapport de pression totale et du rendement à l'agrandissement du jeu d'aube tout en améliorant la performance et stabilité aérodynamique nominales.

ABSTRACT

The tip clearance is the small gap found in turbomachine rotors that is left between the tip of the rotating blades and the stationary shroud. In an aero-engine compressor, this tip clearance is responsible for performance losses and stability issues which respectively increase the engine fuel consumption and reduce its operating envelope. During a given flight mission, the variations experienced by the compressor rotational speed and temperatures lead to the expansion/shrinkage of the compressor components (rotor, disc or shroud) which increase temporarily or permanently (from rubbing) the size of the tip clearance. This inevitable increase in tip clearance throughout the engine life translates into a long-term degradation of the engine in terms of fuel consumption and operating envelope.

Many studies in the literature have focused on improving the performance (i.e. total pressure ratio and efficiency) and aerodynamic stability (stall margin) of the compressor at a nominal tip clearance. However, very few of them explicitly dealt with alleviating the drop (sensitivity) of these parameters with tip clearance increase. These include two highly promising recent numerical studies at Polytechnique of Montréal that proposed two new blade design strategies and a novel casing treatment to decrease the performance and stall margin sensitivity of an axial compressor rotor to tip clearance increase.

The current phase of this research aims to apply the findings from these two studies to a real aero-engine axial compressor rotor. The objectives of this project are to design a casing treatment for this rotor to reduce its performance and stall margin sensitivity to tip clearance, and to redesign the rotor itself to achieve the same goal (without casing treatment). These two designs will be tested in the new transonic compressor test rig at Polytechnique of Montréal to experimentally validate this technology. If successful, this technology will lead to more aerodynamically robust aero-engines capable of maintaining their performance and operating envelope with age.

The methodology to attain these objectives uses a computational approach using CFD simulations and consists of three steps. First, the baseline rotor is simulated to assess its nominal performance/stall margin and their sensitivities to tip clearance as well as the source of these sensitivities. Second, the novel casing treatment configuration is adapted to the baseline rotor through a parametric study in order to minimize nominal performance penalty and maximize improvements in sensitivity. A comparative analysis of the flow field is carried out to explain the

effect of the casing treatment on the performance and stall margin and their sensitivities to tip clearance. Finally, desensitizing blade design strategies are applied to obtain a new rotor with reduced sensitivity to tip clearance increase of performance and stall margin while minimizing the penalty to the nominal values of these parameters. A comparative study of the flow field is also carried out to explain the observed improvements.

Simulations of the baseline rotor showed that the lower span region contribute as much to the pressure ratio sensitivity as the tip region which is dominated by tip leakage flow (flow through the tip clearance gap). In contrast, the efficiency sensitivity is mainly driven by losses occurring in the tip region.

The novel casing treatment was successfully applied to the baseline rotor through a design refinement. Although the casing treatment causes some penalty in nominal performance, it completely reversed the pressure ratio sensitivity and reduced the efficiency sensitivity. The first phenomenon is explained by rotation in the core flow at the lower span region indirectly induced by the flow injection from the casing treatment. The latter comes from a reduction in the amount of fluid that crosses the tip clearance of two adjacent blades, known as double leakage.

Finally, the previously proposed desensitizing blade design strategies did not work for this rotor. A new blade design strategy was applied to generate rotation in the lower span flow. The resulting new rotor successfully reduces performance sensitivity while improving nominal performance and stall margin.

TABLE OF CONTENTS

LIST OF TABLES

LIST OF FIGURES

LIST OF SYMBOLS AND ABBREVIATIONS

V_{abs}	Absolute velocity
$V_{abs, circ}$	Circumferential component of the velocity in the absolute frame of reference
V_{rel}	Relative velocity
$V_{rel, circ}$	Circumferential component of the velocity in the relative frame of reference
V_x	Axial velocity
V_{span}	Spanwise velocity
M_{rel}	Mach number in the relative frame of reference
U	Rotational velocity
s	Static entropy
i	Incidence
β_{rel}	Relative flow angle
P_T	Total pressure
P_S	Static pressure
T_T	Total temperature
h_T	Total enthalpy
$\dot{m}$	Mechanical mass flow rate
$\dot{m}_{COR}$	Corrected mass flow rate
PR_{TT}	Total-to-total pressure ratio
PR_{TS}	Total-to-static pressure ratio
η_{TT}	Total-to-total efficiency
γ	Specific heat ratio
P&WC	Pratt & Whitney Canada
P&WEH	Pratt & Whitney East Hartford (USA)

LIST OF APPENDICES

CHAPTER 1 INTRODUCTION

1.1 Background

Three fundamental components are shared by all aircraft engines: a compressor, a combustion chamber and a turbine. The compressor pressurises the incoming air, the combustion chamber burns it with jet fuel and the turbine extracts energy from the resulting hot mixture of gas. A portion of that extracted energy drives the compressor while the remainder is used to produce thrust through other components depending on the application of the engine.

An aero-engine's mission is made up of different flight phases. A typical mission of a commercial aircraft is illustrated in Figure 1.1[1] along with the variation of the rotational speed and average temperature of the core engine at each phase.

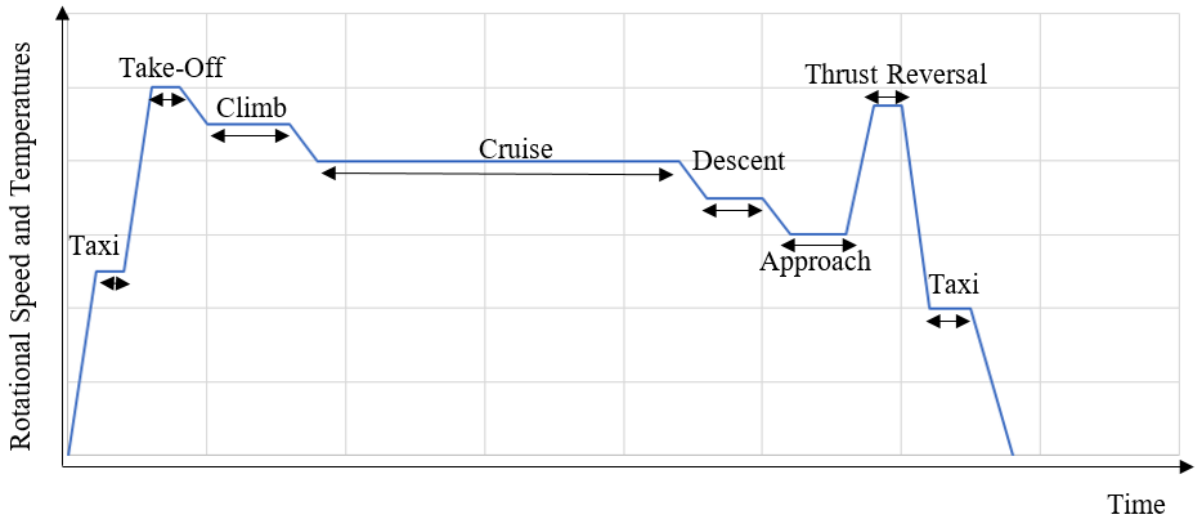

Figure 1.1: Typical mission of an aircraft engine

The rotational speed as well as the temperatures reach a maximum during the take-off phase. Therefore, the take-off conditions serve as the basis for the structural design of the engine components. On the other hand, the longest period corresponds to the cruise phase. As a result, the

[1] Courtesy of Ghislain Plante, Pratt & Whitney Canada

aerodynamic design is typically made based on the conditions of the cruise phase to ensure that the engine operates at its optimum performance for the longest period in a given mission.

This study focuses on compressors, in particular axial compressors which is the most common type of compressors used in aero-engines. This type of compressors is characterized by the mean radius of the gas path remaining more or less constant. Figure 1.2 depicts a five stage axial compressor, each stage being composed of a rotor and a stator.

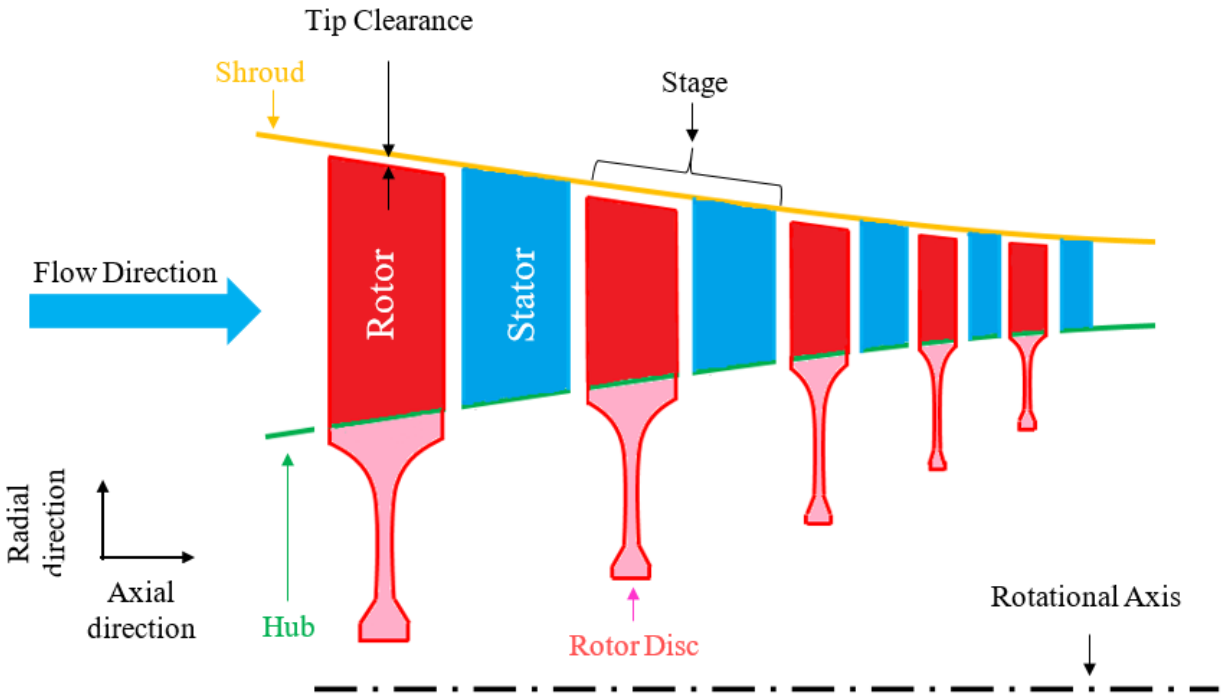

Figure 1.2: Cross-section of a five-stage axial compressor

Figure 1.3 illustrates the workings of an axial compressor through a radial cut of an axial compressor stage. The velocity triangles show that by deviating the flow in the relative (rotating) frame of reference, the rotor increases the circumferential component of the velocity in the absolute (stationary) frame. From the Euler turbomachinery equation, an increase in the absolute circumferential velocity corresponds to the work imparted to the flow to increase its kinetic energy and leads to total pressure rise. At the same time, the illustration below in Figure 1.3 shows that the flow in the relative frame slows down across the rotor passage due to a cross-sectional area increase, similar to the flow across a diffuser, leading to static pressure increase. When the flow exiting the rotor travels (in the stationary frame) across the stator, it is slowed down in the same

matter allowing the kinetic energy added by the rotor to the flow to be converted to static pressure rise.

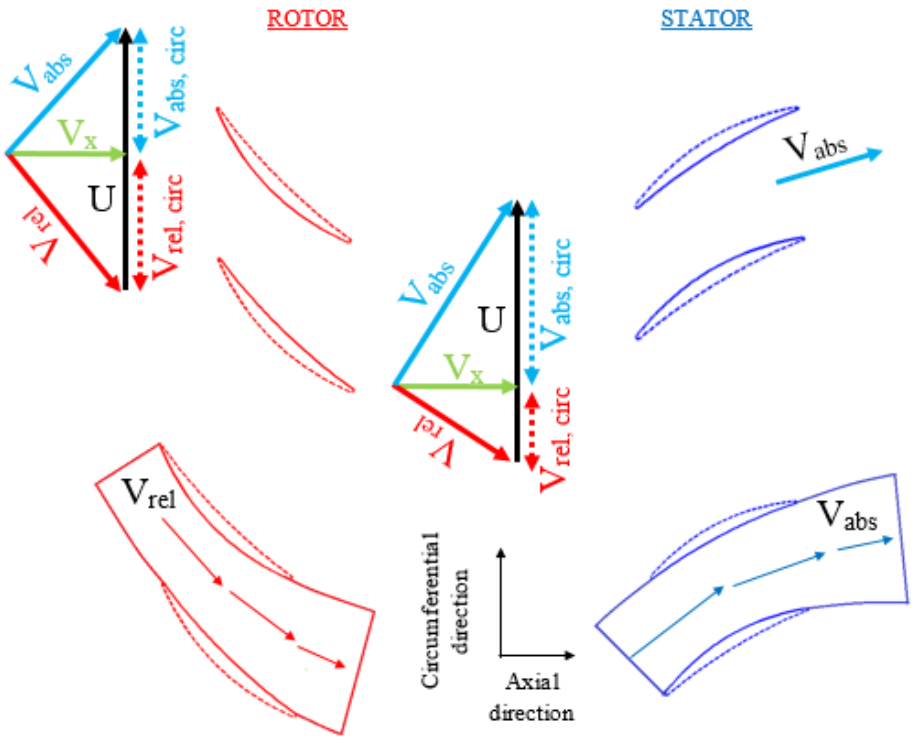

Figure 1.3: Working of an axial compressor

The performance of a compressor is generally described by two parameters: the total-to-total pressure ratio and the total-to-total adiabatic efficiency, often referred to simply as *total pressure ratio* and *efficiency*, respectively. The total pressure ratio is the ratio of the outlet total (stagnation) pressure over the inlet total pressure. The efficiency is the ratio of ideal adiabatic work over actual work consumed by the compressor to produce a given pressure ratio. It is calculated from total pressure and total temperature at the inlet and exit of the compressor. These two parameters will be presented in further detail in chapter 3.

The plots of the left of Figure 1.4 shows the variation of the total pressure ratio and efficiency of the compressor with mass flow at a particular speed. Each of these two curves is called a *speedline* and features three important points: the peak-efficiency point, the stall point and the choke point. The choke point on the far right of the speedline is when the flow in the throat of the blade passage reaches Mach 1 and the mass flow can no longer increase regardless of the pressure difference across the compressor. As the mass flow is reduced from the choke point, the pressure ratio and

efficiency increases until a peak-efficiency point is reached. At design speed, this point is called the design point. If the mass flow is reduced further, the pressure ratio continues to increase until the stall point where aerodynamic instabilities appear in the form of rotating stall, when a cell of velocity deficiency rotates at part of the speed of the compressor accompanied by a drop in compressor pressure ratio. In an engine, this usually triggers surge, a catastrophic aerodynamic instability where the entire flow oscillates axisymmetrically across the engine causing a sudden drop in engine power.

A compressor map, as illustrated on the right of Figure 1.4, is composed of multiple speedlines and helps define the operating envelope of the compressor. Three important lines on the compressor map are the working line, the surge line and the choke line. The working line is the line along which the compressor operates as it changes speed in a quasi-steady manner. It crosses the design point of the compressor and often links peak efficiency points at different speeds. The surge line links the stall points of each speed line. Finally, the choke line links the choke points of each speedline. The distance between the operating line and the surge line is the *stall margin*, a safety margin against rotating stall/surge. Such margin is necessary because the stall line can drop with distortion of the inlet flow due to non-standard operating environment such as engine intake asymmetry and cross-winds, or the operating line can deviate upward during rapid engine acceleration causing the operating and stall lines to intersect resulting in engine surge.

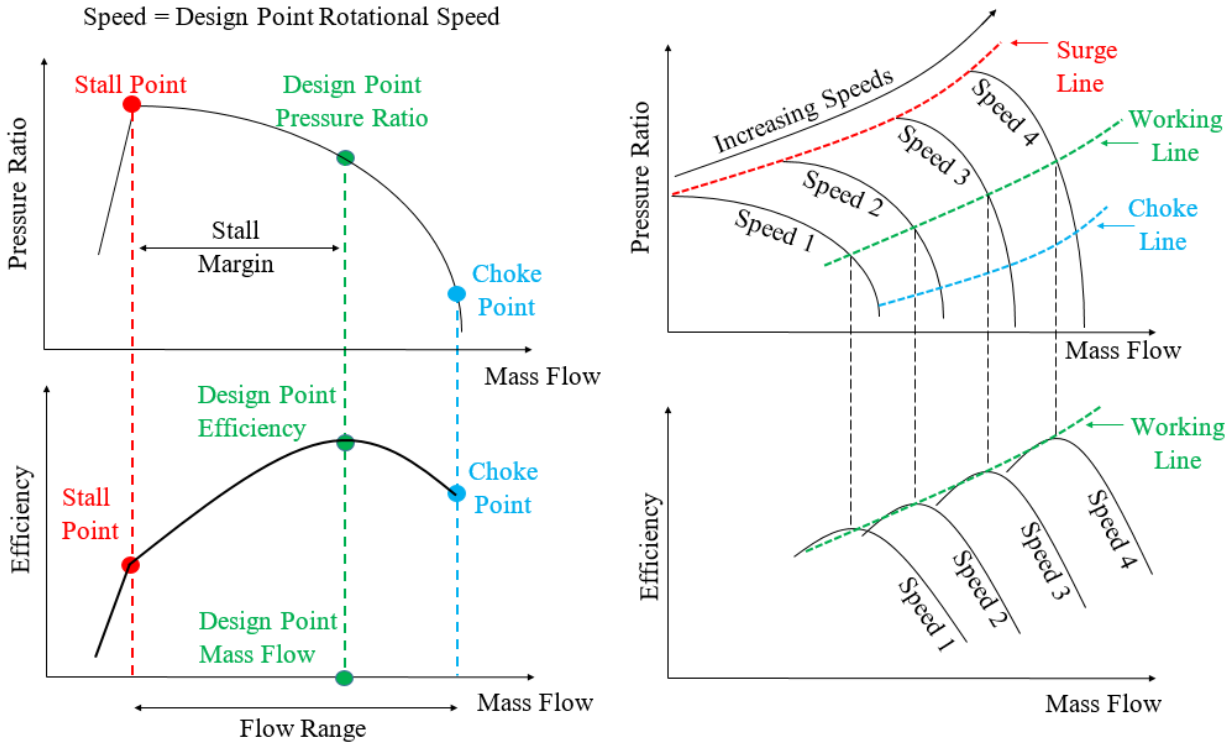

Figure 1.4: Compressor speedline and map

As indicated previously, the cruise flight phase is the most important phase in the aerodynamic design of the engine. As a result, this study focuses on the design operating speed and the design operating point which corresponds to the cruise condition. Moreover, the word *performance* will refer to the total pressure ratio *and* the efficiency at the *design point* while the word *stability* will relate to the stall margin at the *design speed*.

1.2 The tip clearance problem

As depicted in Figure 1.2, a small gap referred to as *tip clearance* exists between the tip of the rotor blade, which is rotating, and the stationary shroud of the compressor. Although also present in turbines [1], this gap has a more serious detrimental impact on the performance and stability of a compressor. Studies [2] have shown that the flow through the tip clearance, called *tip clearance flow* or *tip leakage flow*, is associated with a penalty in pressure ratio and efficiency. Moreover, other studies [3] suggested that this flow is directly responsible for the early onset of rotating stall which leads to lower stall margins. These effects are taken into account in the design of the compressor for a nominal (design) tip clearance value.

However, the tip clearance size changes during a flight cycle. Two main factors impact the size of the tip clearance [4]. On one hand, changes in rotational speed causes the rotor disc and the rotor blade to deform as a result of the changing centrifugal force. On the other hand, the change in temperatures translates into a change in the thermal expansion of the rotor disc, the rotor blade and the shroud. The *differential* expansion between these components reflects directly on the tip clearance size. While this change in tip clearance may be temporary, rubbing can occur between the blade tip and shroud because of temporary decreases in tip clearance, leading to general increase in compressor operating tip clearance over the life of the engine.

Berdanier and Key [5] carried out an experimental study on the effect of the tip clearance size on a three-stage axial compressor. Three different tip clearance sizes ("TC1" < "TC2" < "TC3") were applied simultaneously to the three rotors at four different rotational speeds (corresponding to 100%, 90%, 80% and 68% of design speed). Figures 1.5 and 1.6 plot the resulting variation in the speedlines in terms of total pressure ratio and efficiency, respectively. One can observe that as tip clearance increases at any particular rotating speed, the total pressure ratio, efficiency and stall margin decrease, with the drop in pressure ratio increasing with decreasing mass flow while the largest drop in efficiency occurring around the peak-efficiency point. The negative impact of tip clearance also increases with rotational speed.

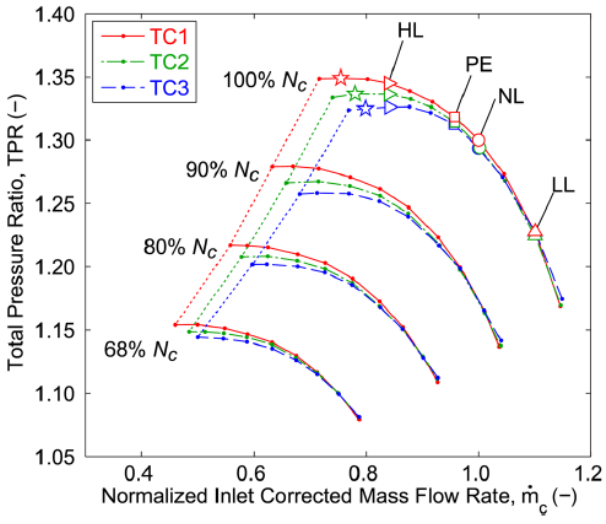

Figure 1.5: Effect of the tip clearance size on pressure ratio and stall margin [5]

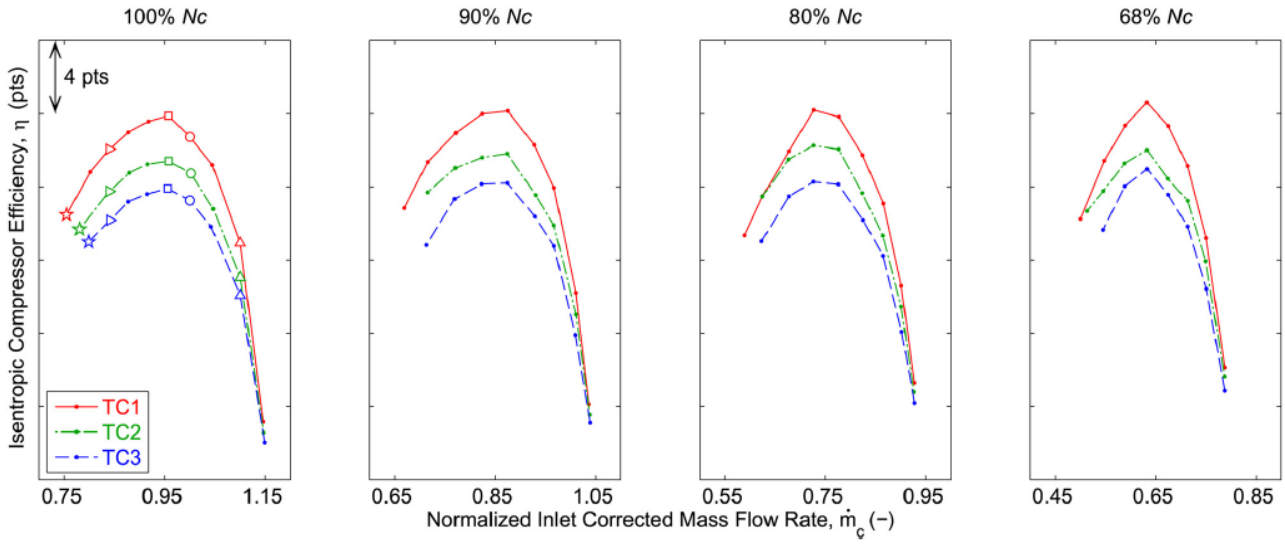

Figure 1.6: Effect of the tip clearance size on efficiency [5]

In fact, for a multi-stage compressor as is usually found in aero-engines, each compressor stage is designed to be operating at its optimum point, which is referred to as *stage matching*. Since the inlet conditions to each stage depends on the outlet conditions of the upstream stage, a change in performance of any stage has a cascading negative impact on all stages downstream as it moves each downstream stage further from its optimum operating point. As such, the negative impacts seen for a compressor is greatly amplified in a multi-stage compressor environment. More details can be found in reference [6].

At the aero-engine level, a drop of either the overall total pressure ratio and efficiency of the compressor due to tip clearance increase has to be compensated by an increase of the fuel mass flow injected in the combustion chamber in order to keep the same output power (and thrust). In terms of stability, a drop in stall margin is equivalent to a lower operational range making the engine more prone to surge. Thus, due to tip clearance increase, the aero-engine fuel consumption increases and its operating envelope decreases as the engine ages.

Moreover, as the minimum achievable tip clearance is a finite number due to manufacturing constraints, compressor stages with low rotor blade heights, for which the tip clearance represent a greater proportion of the span, are more affected by the negative effects related to tip clearance and its increase. This includes compressor stages in small engines and rear (downstream) stages in multi-stage compressors. Furthermore, as the bypass ratio of aero-engines increases to improve

propulsive efficiency [5], the engine core and its compressor is becoming smaller, thus making the impact of tip clearance increase an issue of rising importance.

1.3 Context of the current project

The current study is part of a long multi-phase program sponsored by Pratt & Whitney Canada that aims to reduce the drop in performance and stall margin of compressors due to tip clearance increase, henceforth referred to as the *sensitivity to tip clearance* or just *sensitivity*. If successful, this research program will lead to aero-engines that are more robust to degradation in performance and fuel consumption and better able to maintain their full operating envelope over their lifespan.

This research program started with two prior doctoral research projects. The first doctoral project by Erler [7] was a numerical investigation to find rotor blade design strategies to reduce the sensitivity of axial compressors to tip clearance. Using a theoretical transonic axial compressor rotor, Erler [7] identified two flow features responsible for sensitivity to tip clearance increase, namely double leakage and incoming meridional momentum in the rotor tip region. Double tip leakage refers to the part of the tip clearance flow that continues pitchwise in the blade passage to enter the tip clearance of the circumferentially adjacent rotor blade rather than convecting downstream out of the rotor blade passage. This study found that a reduction (or elimination) of double leakage and/or an increase in the incoming tip meridional momentum improve the sensitivity to tip clearance. Erler's study proposed and demonstrated computationally two axial rotor blade design strategies (presented in chapter 2) that exploited these two flow features to successfully reduce the sensitivity of the studied rotor. These strategies were full forward chordwise sweep and reduction in the blade stagger angle in the outer span.

In the second doctoral project carried out numerically, Cevik [8] proposed a novel casing treatment concept to reduce double leakage and reduce the sensitivity. This casing treatment, for which a patent application has been submitted [9], consisted of shallow negative saw-tooth shaped circumferential grooves placed over the rotor. He used a numerical parametric study to refine the proposed casing treatment for the theoretical rotor used by Erler [7] to successfully show through CFD simulations that it reduces double leakage and sensitivity of performance and stall margin to tip clearance.

The current phase of the research aims to experimentally demonstrate the findings of the above projects, namely the desensitizing blade design strategies and casing treatment, for a real aero-engine axial compressor rotor. For this phase of the research program, the compressor test rig at École Polytechnique de Montréal, as shown in Figure 1.7, has been built to accommodate one full-scale axial compressor stage of an aero-engine. As a first step, the blade design strategies and casing treatment concept must be applied for the rotor of this compressor stage in order to provide the production geometry of the casing treatment and a revised desensitized rotor for manufacturing and testing.

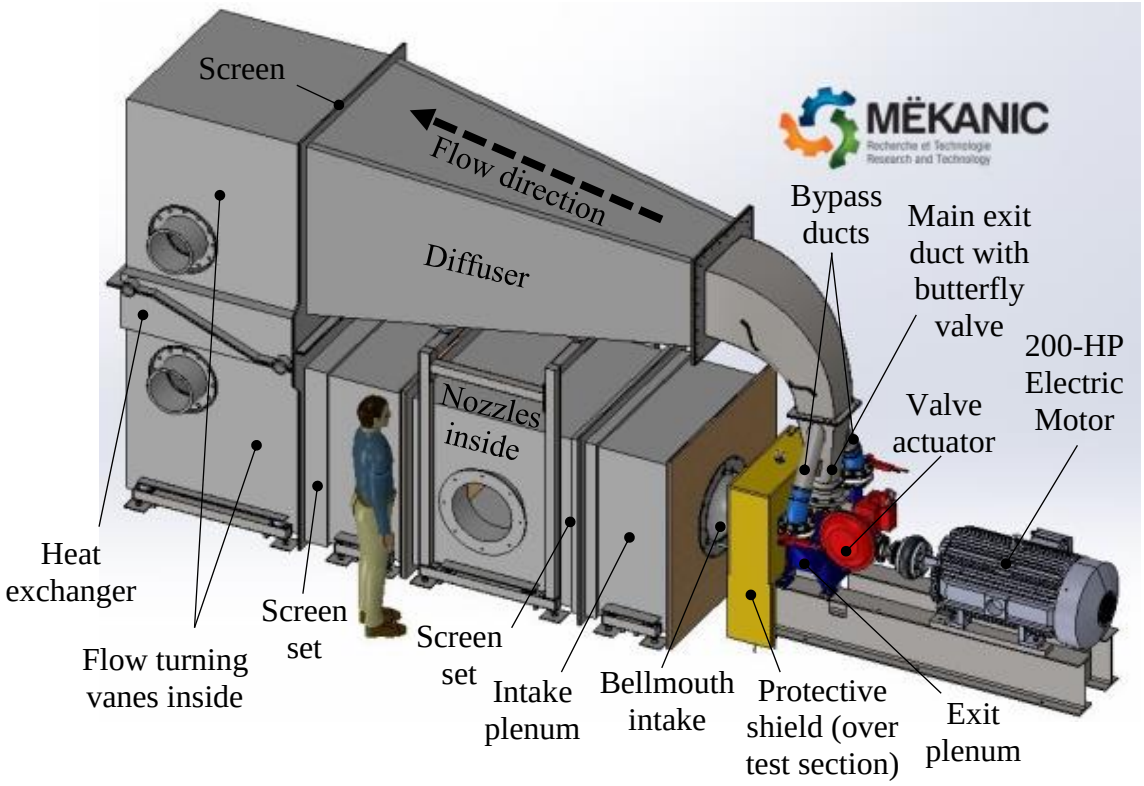

Figure 1.7: New compressor test rig at École Polytechnique de Montréal – © MËKANIC

1.4 Objectives

The objectives of this study are:

1. Design an optimal casing treatment for reducing the performance and stall margin sensitivity of the aero-engine transonic axial rotor in the compressor test rig.
2. Redesign the aero-engine transonic axial rotor in the compressor test rig to reduce the performance and stall margin sensitivity to tip clearance increase.

For the two above objectives, the resulting new designs are subject to the following constraints:

1. The tip clearance of the test rotor varies from a minimum value of 0.74% to a maximum value of 2.57% span.
2. Keep the nominal pressure ratio within ±0.25% of the baseline nominal pressure ratio.
3. Minimize penalty in nominal efficiency to within 0.25 points of the baseline nominal efficiency.
4. Maintain or improve the nominal stall margin.

First of all, the tip clearance relative values given above refer to the values measured on the rotor when it is operating at full-speed (a.k.a. *hot* tip clearance). The tip clearance at idle mode (a.k.a. *cold* tip clearance) is higher because of the spanwise expansion of the blade under rotation. Tip clearances presented throughout this thesis refer to *hot* tip clearances.

The lowest tip clearance considered (0.74% span), named the *nominal* (on design) tip clearance, refers to the design tip clearance for this rotor. The pressure ratio, efficiency and stall margin at nominal tip clearance would be qualified by the adjective “nominal” to differentiate them from performance and stability parameters corresponding to higher tip clearances.

The highest tip clearance considered (2.57% span) goes beyond the tip clearance reached by the rotor at the end of its lifespan. However, since the new designs will be tested experimentally, it was necessary to select a tip clearance that is high enough to measure easily the change in performance and stability during tests and therefore formulate compelling conclusions.

Finally, certain strategies that desensitize rotors to tip clearance increase come with a significant nominal performance and stability penalty. The purpose of the constraints imposed is to rule out

these strategies and to apply those enabling to have a desensitized rotor to tip clearance increase *while* keeping a high nominal performance and stability.

The deliverables of this project will be the geometries of the casing treatment and new rotor ready for production (including a prior structural analysis for the new rotor) and subsequent installation and testing in the compressor test rig.

1.5 Outline of the thesis

The present thesis is structured in seven chapters: following this introductory chapter, a literature review is presented in Chapter 2, which deals with tip clearance flow physics and strategies to desensitize rotors to tip clearance increase. The chapter 3 describes the methodology for the current project. The results and accompanying discussions for the baseline rotor, casing treatment and new rotor design are presented in chapters 4, 5 and 6, respectively. The conclusions and future work are given in chapter 7.

CHAPTER 2 LITERATURE REVIEW

Given the importance of tip leakage flow to compressor performance and stability and sensitivity to tip clearance, the literature review will start with the flow features associated with tip clearance flow and their impacts on nominal performance and stability (sections 2.1 through 2.3). Thereafter, section 2.4 covers the effects of tip clearance increase. Finally, the section 2.5 reviews past work on design strategies to reduce/eliminate the sensitivity of compressor performance and stability to tip clearance increase.

2.1 Primary flow features associated with tip clearance

Inoue et al. [10] carried out an experimental study on an axial compressor rotor with different tip clearance sizes. They showed that the tip leakage flow exiting the tip clearance on the blade tip suction side rolls up into a tip vortex, as illustrated in Figure 2.1 (taken from a different source [3]). Moreover, the intensity of the vortex roll-up increases with tip clearance size.

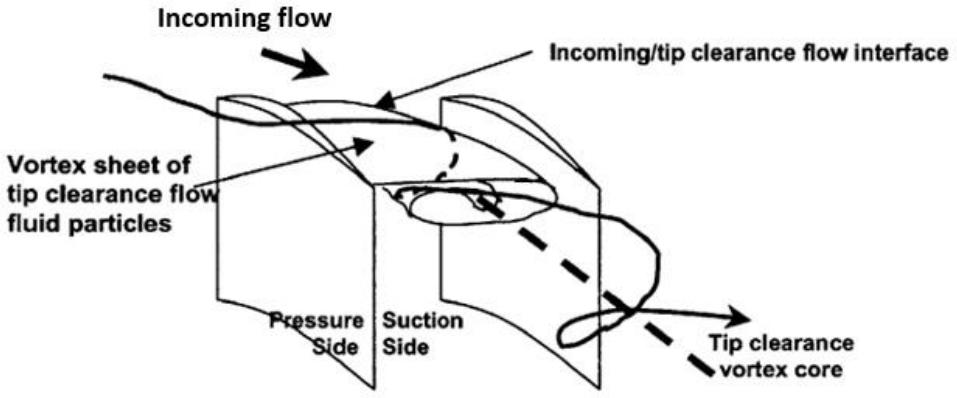

Figure 2.1: Tip clearance vortex representation - Adapted from [3]

Storer and Cumpsty [11] showed that tip leakage flow is essentially a pressure driven flow and its velocity as it exits the tip clearance on the suction side can be decomposed in two components. The streamwise component, parallel to the local blade camber, is the same as that of the local flow on the pressure side from where the tip leakage flow originates. This velocity component is thus directly related to the rotor inlet flow. The normal velocity component, perpendicular to the local blade camber, is the result of the acceleration of the flow through the tip clearance gap due to the local static pressure difference between pressure side and suction side at the blade tip. This pressure difference is referred to as blade tip loading and is linked to the flow turning (camber) by the blade.

These two velocity components combine to form the resulting local tip clearance flow velocity as illustrated in Figure 2.2.

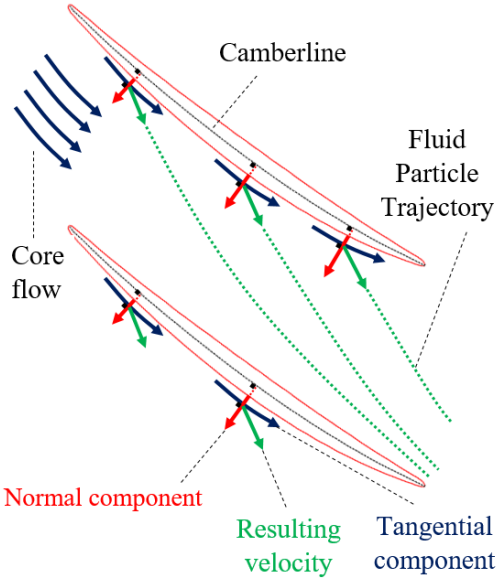

Figure 2.2: Velocity components linked to the tip clearance vortex at the tip section

This normal velocity component, which is perpendicular to the (streamwise) core flow, is responsible for the roll up that creates the tip vortex. A larger normal velocity component would lead to a larger and more intense tip vortex.

In the ideal case, depicted on Figure 2.2, the tip leakage flow would form the tip vortex and convect out of the rotor passage through the trailing edge plane. However, if the normal velocity component is high enough perhaps from high tip loading, the tip clearance fluid can reach the circumferential adjacent blade pressure side and enter its tip clearance, as illustrated in Figure 2.3. This phenomenon is called *double leakage* as discussed in reference [12] and is often associated with tip clearance fluid close to the shroud. While fluid exiting the tip clearance near the blade tip is often entrained downstream by shear/mixing interaction with the passage core flow underneath, the tip clearance fluid next to the shroud have much less interaction with the core flow while also being dragged circumferentially by the counter-rotating shroud in the relative frame of reference. This fluid thus tends to maintain a more circumferential flow path and is more prone to double leakage. Figure 2.3 also shows that double leakage fluid enters the second tip clearance with a non-zero normal velocity component and will thus exit this tip clearance with higher normal velocity, which will increase the likelihood of additional double leakage [7]. From this reasoning,

one can deduce that the factors which could generate or increase double leakage are: higher tip loading (larger normal velocity) [12], lower blade pitch (circumferential distance between blades) [7], lower incoming flow velocity (lower deflection of the tip clearance flow in the streamwise direction due to a weaker incoming flow) [7] or a higher tip clearance size (more fluid near shroud) [12].

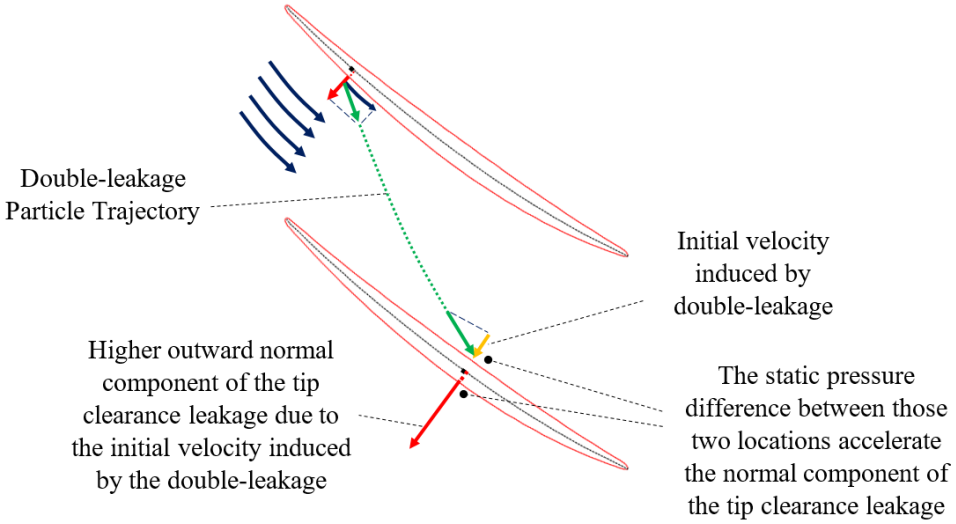

Figure 2.3: Effect of double-leakage in the tip section

2.2 Impact of the tip clearance on performance

Tip clearance flow affects both the efficiency and pressure ratio of the compressor.

Storer and Cumpsty [2] showed through simulations that the region in the rotor passage where the normal component of tip leakage flow mixed with the core flow is the locus of the highest dissipation rates in the entire blade passage. They concluded that the mixing loss between the tip leakage flow and core flow is the primary source of loss associated with the rotor efficiency degradation due to tip clearance.

In addition, the tip leakage flow and its mixing with the core flow also generates a region of low streamwise velocity, also known as *tip blockage*, essentially a 3D equivalent of a boundary layer displacement thickness in the tip region of the blade passage. The tip blockage was analyzed and quantified by Khalid et al. [13] who modeled its development through the blade passage as a 1D wake moving up a pressure gradient. The tip blockage effectively reduces the increase in normal flow area across the passage in the relative (rotating frame) frame (see Figure 2.4), thus reducing

the static pressure rise across the rotor blade passage. Figure 2.4 shows that the tip blockage also deflects the incoming flow toward the lower span region, thus increasing the streamwise velocity in the lower span region. At the same time, the fluid in the tip blockage region has a low streamwise velocity. According to the velocity triangles for these two regions presented in Figure 2.5, the change in relative streamwise velocity ("V_{rel}") at the rotor exit causes a reduction in the circumferential component of the absolute rotor exit velocity ("V_{abs}") (i.e. flow turning in the stationary frame) in both regions frame which translates to lower work and less kinetic energy/dynamic pressure transferred to the fluid. In decreasing both the rise in static pressure and dynamic pressure, the tip clearance flow thus reduces total pressure rise. These processes were demonstrated experimentally by the study made by Inoue et al. [10].

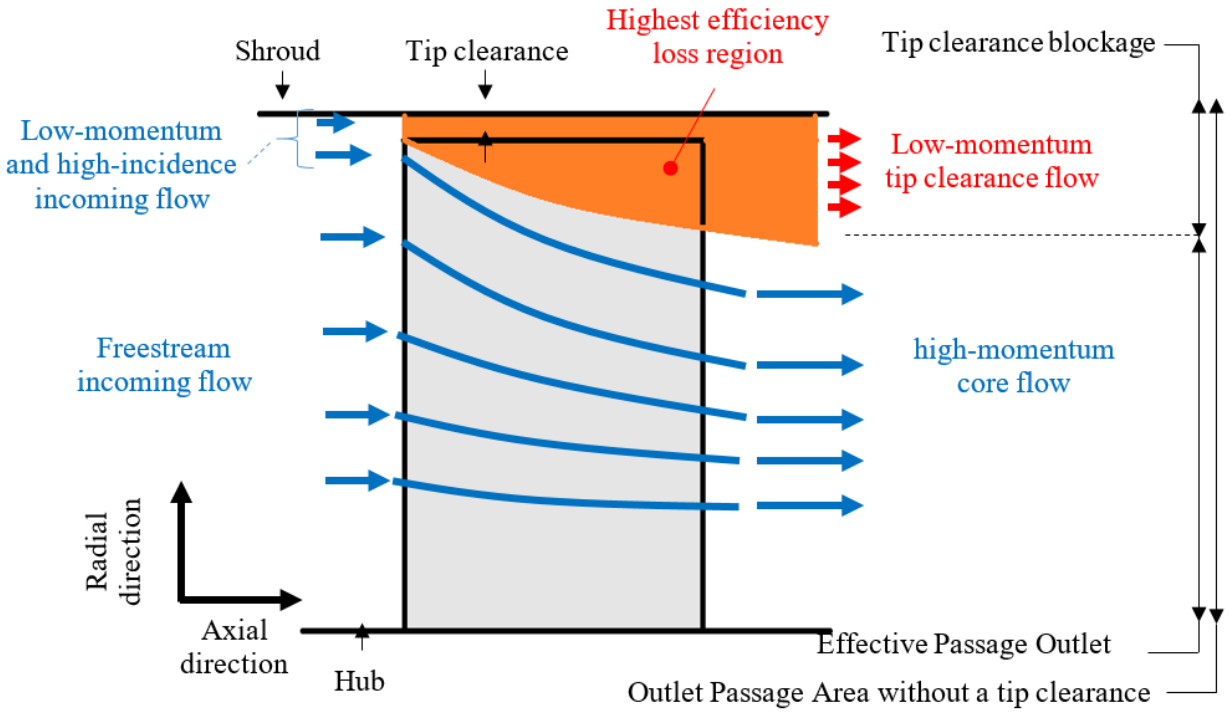

Figure 2.4: Blockage caused by the tip clearance flow in the rotor passage

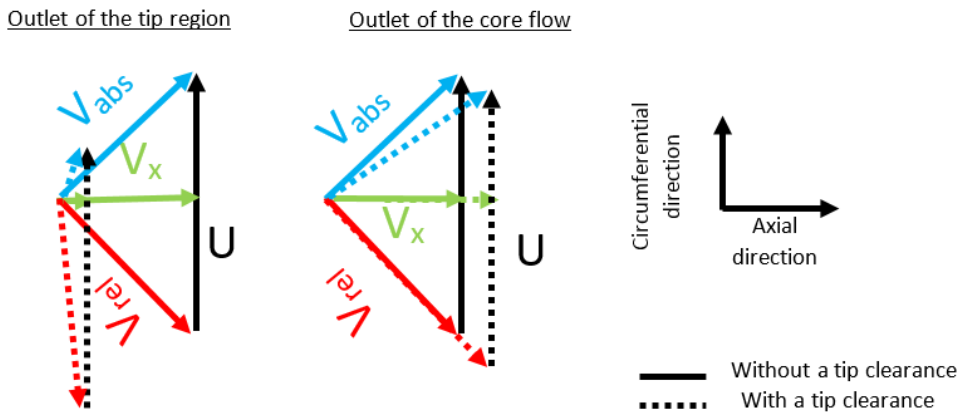

Figure 2.5: Impact of the tip clearance on the flow turning at the rotor outlet

Figure 2.6 summarizes the effects of tip clearance flow on rotor performance. The velocity triangles taken at the rotor inlet in figure 2.7 show that as the mass flow decreases along a speedline, the drop in axial velocity leads to increase in incidence and thus increase in flow turning across the blade and thus blade loading. Since the strength (normal velocity component) of the tip clearance flow depends on blade loading, the negative effects of the tip clearance on rotor performance rises as mass flow is decreased along a speedline.

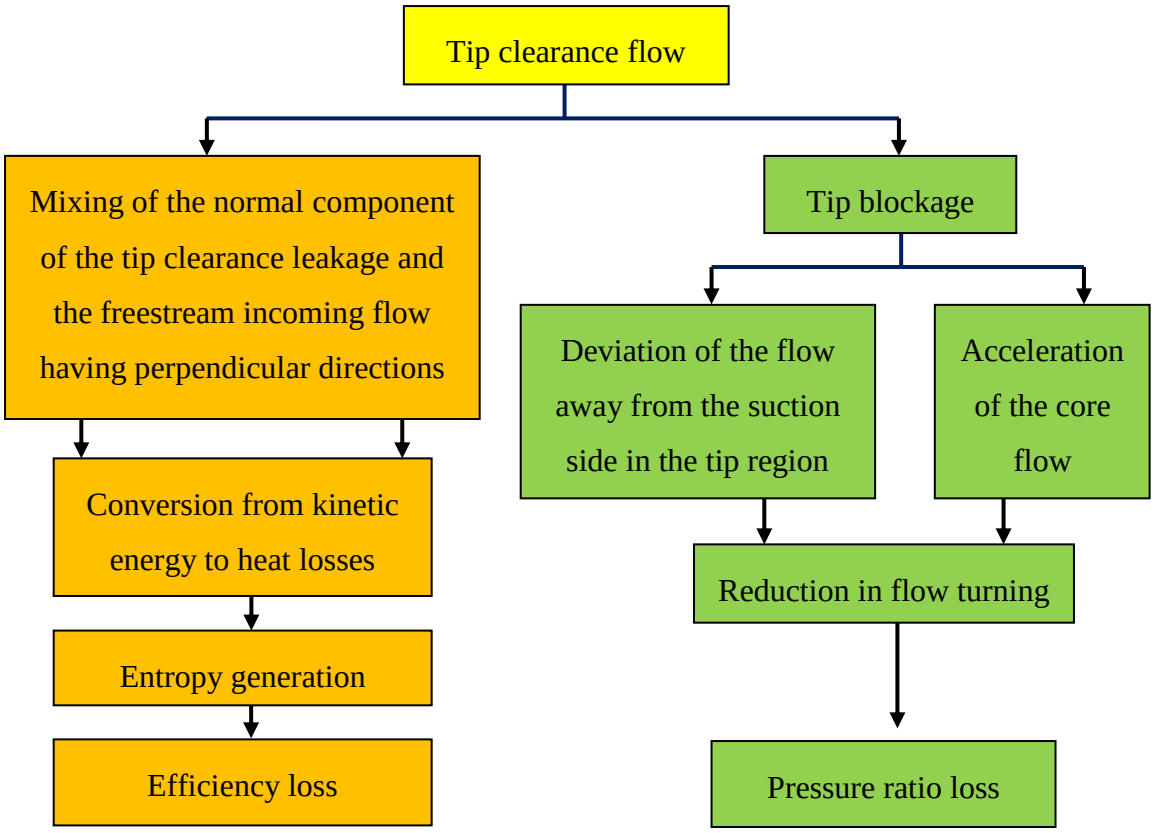

Figure 2.6: Impacts of the tip clearance flow on the performance of the rotor

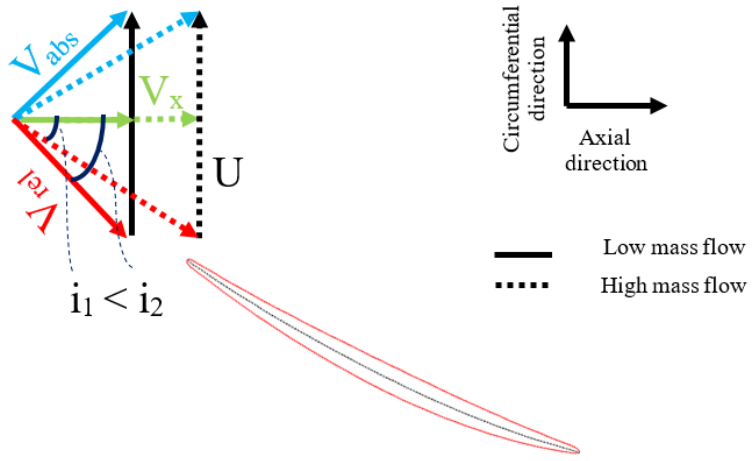

Figure 2.7: Impact of a change in mass flow on the incidence of a blade passage

2.3 Impact of the tip clearance on aerodynamic stability

Rotating stall, often abbreviated as “stall”, is the point in the speed line corresponding to a significant drop of pressure ratio and efficiency as the mass flow is decreased. From the flow perspective, it corresponds to a velocity deficiency cell (or stall cell) that moves circumferentially in the compressor at 15-50% of the rotational speed [3]. This is illustrated in figure 2.8.

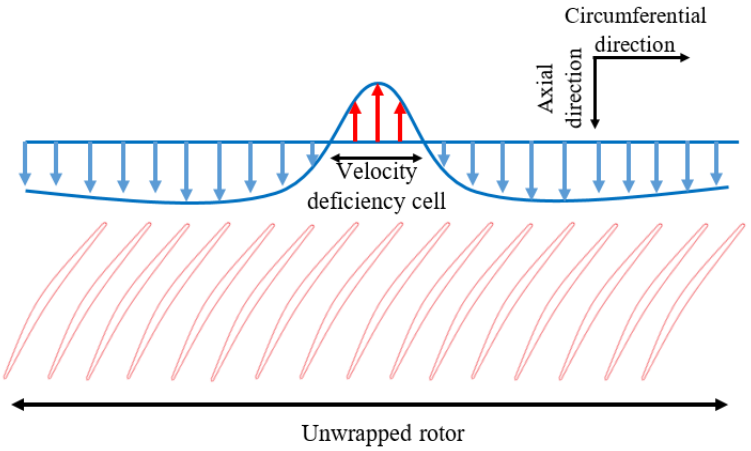

Figure 2.8: Representation of rotating stall

Two routes to rotating stall exist: modal stall inception and spike stall inception. According to Camp and Day [14], modal stall inception is characterized by the relatively slow growth of a long length-scale and low-amplitude velocity perturbation with circumferential wavelength on the order of the annulus, illustrated in Figure 2.9. This perturbation develops into a stall cell within 10 to 40 revolutions. Modal stall inception has been shown to occur when the slope of the speedline in terms of total-to-static pressure ratio[2] of the entire compression system is either zero or positive [14]. Moore and Greitzer [15] showed analytically that a positive slope in this speedline is equivalent to a negative damping (i.e. an amplification) of *natural* perturbations which grow into fully-developed rotating stall cells. The leveling-off of the total-to-static pressure rise speedline toward zero/positive slope can occur because of excessive losses in pressure rise due to strong tip clearance flow or blade boundary layer separation [16], both of which can occur as the incidence increases (from mass flow reduction) as previously shown in Figure 2.7.

[2] The compressor total-to-static pressure ratio is the ratio of the static outlet pressure over its total inlet pressure.

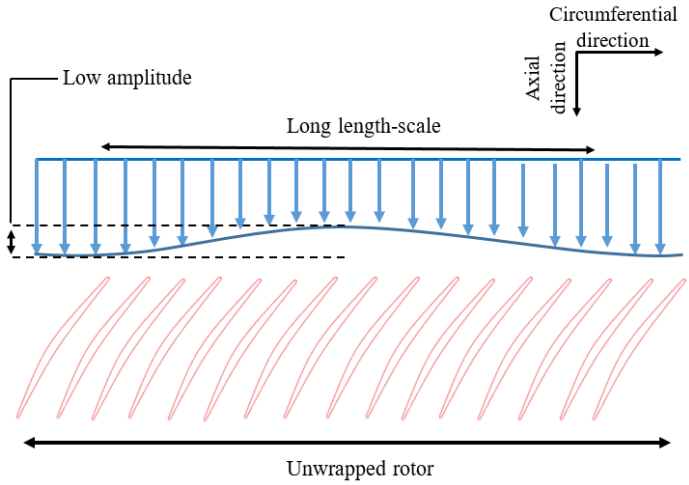

Figure 2.9: Long-length scale and low amplitude velocity perturbation leading to modal stall

On the other hand, spike stall inception is characterized by the sudden appearance of short length-scale and high-amplitude velocity perturbation in the rotor tip region, as illustrated in Figure 2.10, rotating at about 70% of the compressor speed [3]. It rapidly develops into a stall cell within 2 to 3 revolutions. Spike stall inception has been shown to occur when the slope of the total-to-static pressure ratio speedline is still negative (i.e. *before* reaching the zero-slope condition leading to the onset of modal stall). Vo et al. [16] proposed and explained two criteria for predicting spike stall inception that are associated with tip clearance flow. As the tip clearance leakage strengthens at lower mass flows, the interface at which the incoming flow meets the tip clearance leakage moves toward the leading edge of the rotor, as illustrated in Figure 2.11. The first criterion proposed for spike stall inception is the spillage of the tip clearance flow on the adjacent blade passage which occurs when the incoming flow/tip clearance leakage interface reaches the adjacent blade leading edge. The second criterion is the reversal of the tip clearance flow near the trailing edge which convects upstream (backflow) and impinges on the adjacent blade pressure side. In Figure 2.12, these two criteria are illustrated on the left plot and shown through CFD simulations of spike stall inception on the right. Vo et al. [16] proposed that both criteria must be present for spike stall inception to occur.

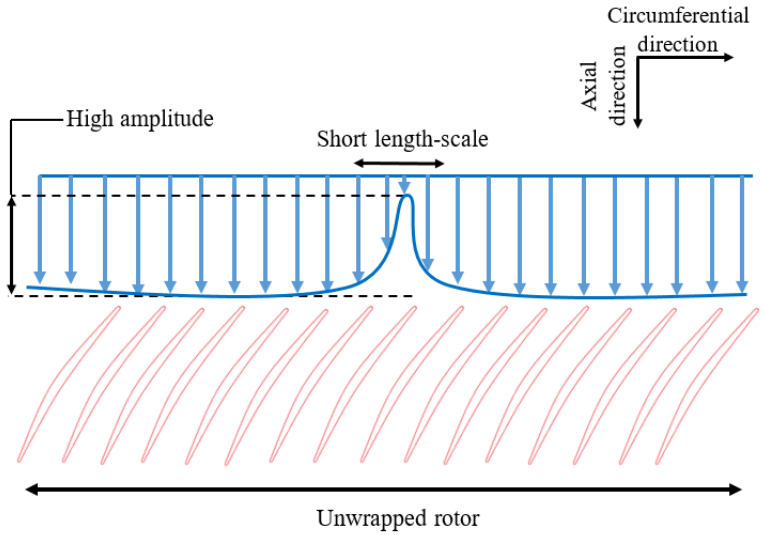

Figure 2.10: Short-length scale and high amplitude velocity perturbation leading to spike stall

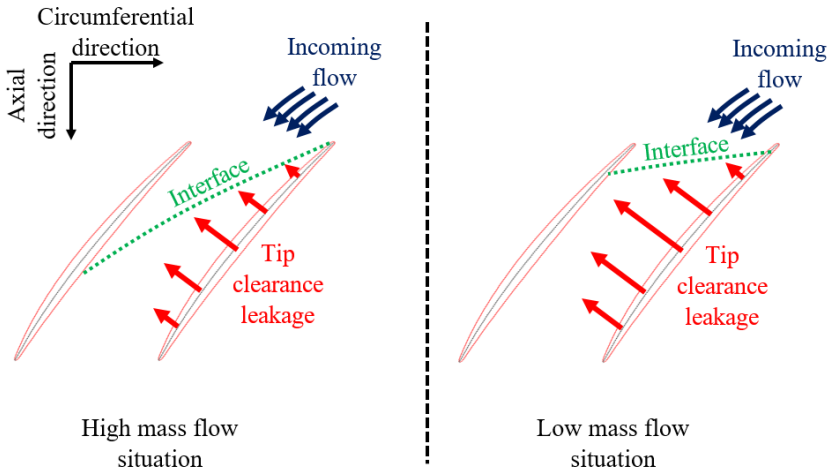

Figure 2.11: Interface between the incoming flow and the tip clearance leakage at the tip section

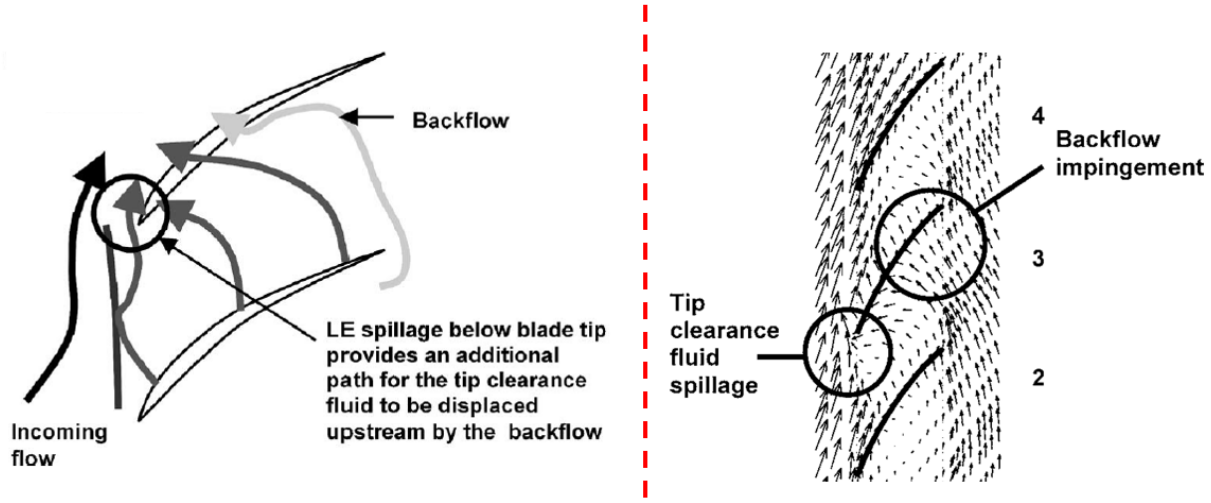

Figure 2.12: Criteria leading to the formation of the spike stall perturbation – Adapted from [16]

The routes to both types of stall inception are summarized below in Figure 2.13. It is noted that tip clearance flow can cause both modal stall inception due to the growth of the tip clearance blockage, leading to the turnover of the speedline, and spike stall inception through the stall criteria proposed by Vo et al. [16]. In this case, the rotor is called *tip-critical*. Otherwise, modal stall inception can occur due to blade or hub boundary layer separation leading to the turnover of the speedline.

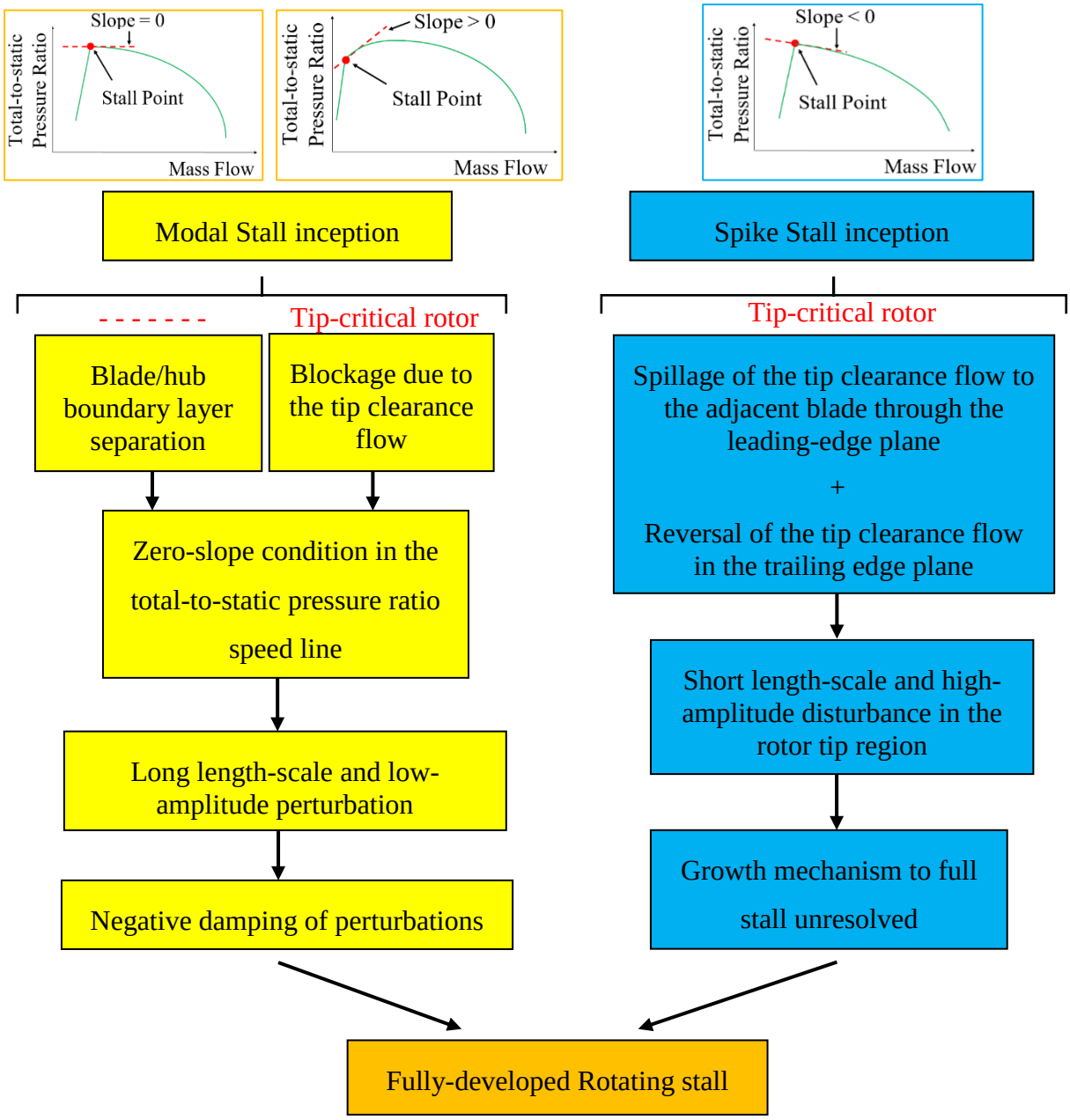

Figure 2.13: Routes leading to rotating stall in a compressor

2.4 Impact of tip clearance increase on performance and stability

From the three previous sections, one can infer that the negative impact of tip clearance flow on compressor performance and stability increases with tip clearance size. This is confirmed by several experimental work such as those of Berdanier and Key [5] previously shown in Figures 1.5 and 1.6 and Freeman [17] who carried out measurements on a multi-stage high-speed axial

compressor at three different tip clearances. The effect of tip clearance on the compressor map is illustrated in Figure 2.14 and shows similar trends as Berdanier and Key [5] with regard to the drop in performance and stall margin.

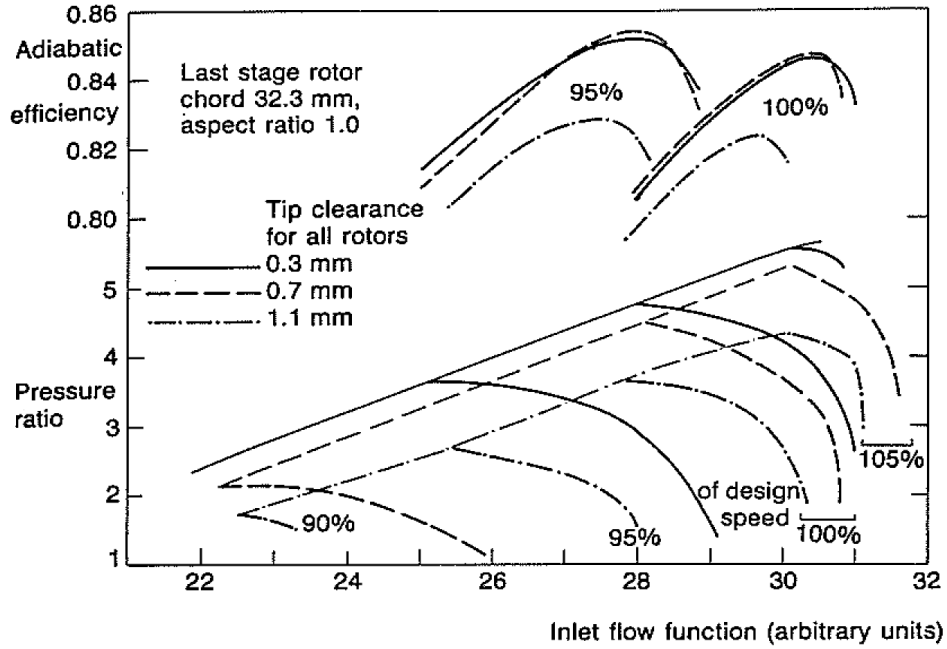

Figure 2.14: Effect of tip clearance increase on the compressor map of a multi-stage high-speed axial compressor [17]

In a numerical study made on a theoretical high-speed axial compressor rotor, Erler [7] showed, for this rotor and other variations of its design, that the mixing loss in the tip region and tip blockage increase with tip clearance leading to a drop in performance as shown in figure 2.15. Erler [7] went on to discover and explain two flow features that are responsible for the performance and stability sensitivity to tip clearance. The first is double leakage flow. As shown previously in figure 2.3, the suction of double leakage flow into the tip clearance greatly enhances the normal component of the resulting tip leakage flow, thus strengthening the tip clearance flow and greatly penalizing pressure ratio, efficiency and stall margin. Erler [7] carried out numerical experiments in which the blade number of the rotor was varied to change the blade pitch and the double leakage. The results in figure 2.16 showed that the higher the double leakage proportion (of total tip leakage flow) at nominal tip clearance, the larger and faster the double leakage proportion grows with increasing tip clearance, which leads to more sensitivity in performance and stability. The second flow feature affecting sensitivity was the meridional momentum in the tip region. Erler [7] explained through

the illustration in figure 2.17 that an increase in this parameter pushes the tip clearance flow downstream away from the pressure side, reducing the chordwise extent (and amount) of double leakage which thus contributes to improved sensitivity.

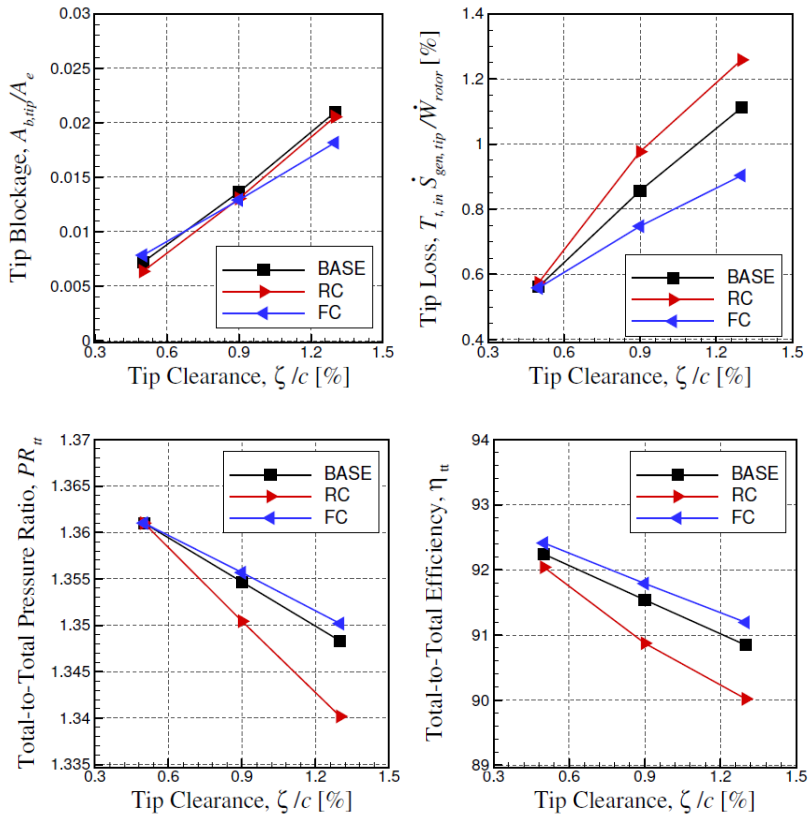

Figure 2.15: Variation of tip clearance blockage and mixing losses and performance with tip clearance for axial compressor rotors [7]

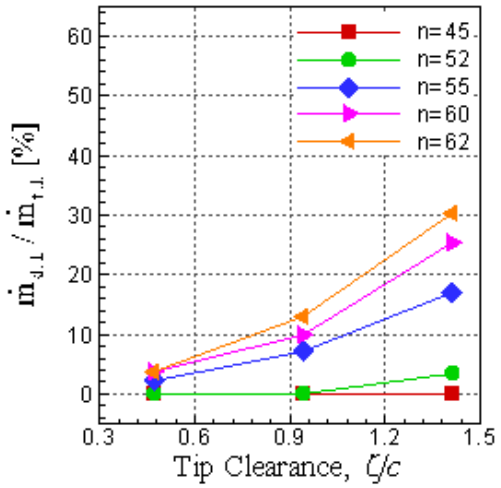

Figure 2.16: Variation of double leakage proportion with tip clearance for different blade numbers (*n*) (higher *n* means lower blade pitch) [7]

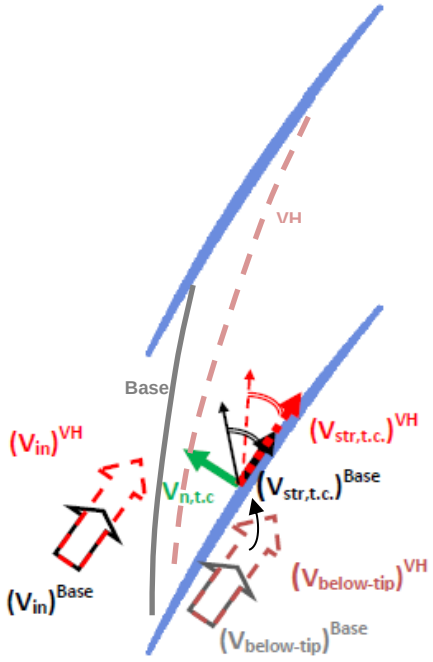

Figure 2.17: Effect of incoming tip meridional momentum on sensitivity (*Base*: reference, *VH*: high incoming meridional momentum in the tip) [7]

2.5 Design strategies desensitizing performance and stability to tip clearance increase

Most of the work found in the literature focuses on improving nominal performance and stability. Only a few studies cover directly or indirectly the reduction in the sensitivity to tip clearance of the performance and/or stability. As shown in Figure 2.18, the desensitizing strategies fall under two categories: blade design strategies and gas path design strategies. Blade design strategies mostly involve changes in the camber line/blade sections and stacking line. The stacking line refers to the spanwise line that goes through the centers of gravity of the blade sections making up the 3D blade. On the other hand, gas path design strategies involve casing treatments (slots or grooves over the rotor) or gas path contouring. The terminology used to describe stacking-line changes in this section is given in Appendix A.

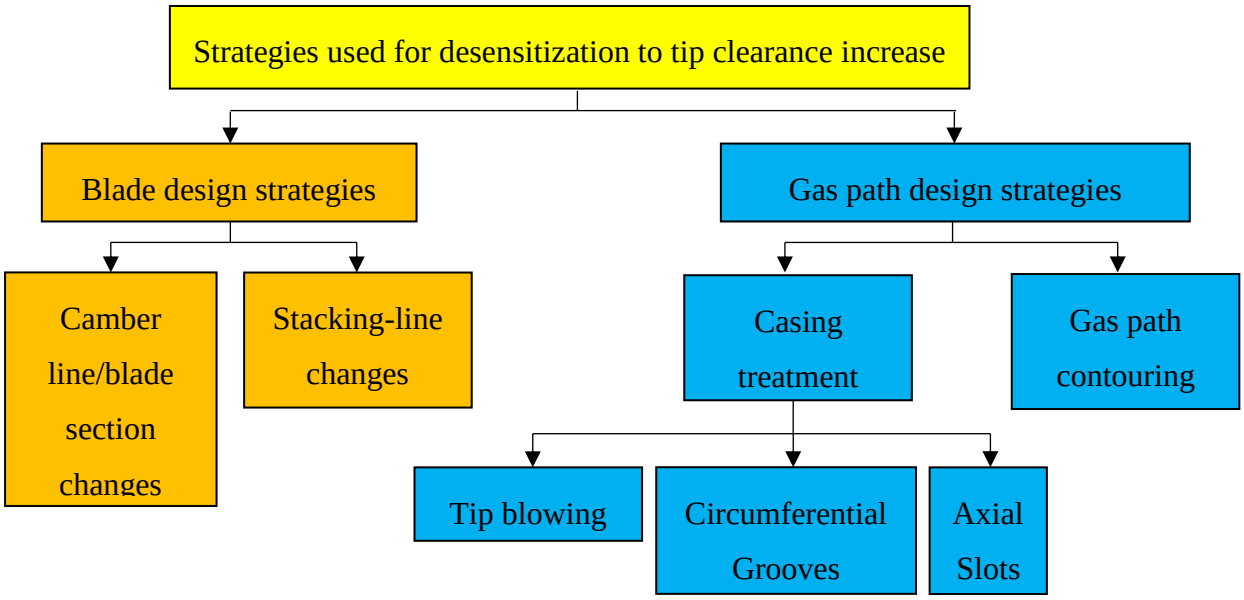

Figure 2.18: Types of strategies used to decrease sensitivity to tip clearance increase

2.5.1 Blade design strategies

An experimental and analytical study was carried out by McNulty et al. [18] on two different radially-stacked rotors. Configuration 1 was characterized by a moderate loading in the tip region while configuration 2 was highly loaded in this region. For both rotors, two different tip clearances were considered ranging from 1.41% to 2.64% of the rotor chord. These two configurations were swept in the forward chordwise direction by the amounts shown in Figure 2.19. The results

obtained are shown in Figure 2.20. For configuration 1, the nominal efficiency and throttle margin (equivalent to stall margin) were improved. However, the sensitivity to tip clearance of stall margin deteriorated while the sensitivity of efficiency improved. For configuration 2, the nominal efficiency and stall margin remained essentially the same while their sensitivities improved. The authors explained the findings by saying that forward sweep induced a movement of the flow toward the tip region which reduced the tip loading and thus tip blockage.

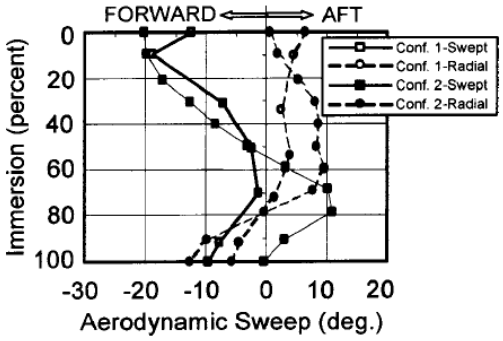

Figure 2.19: Amount of forward chordwise sweep applied to the baseline rotors of the study made by McNulty et al. [18]

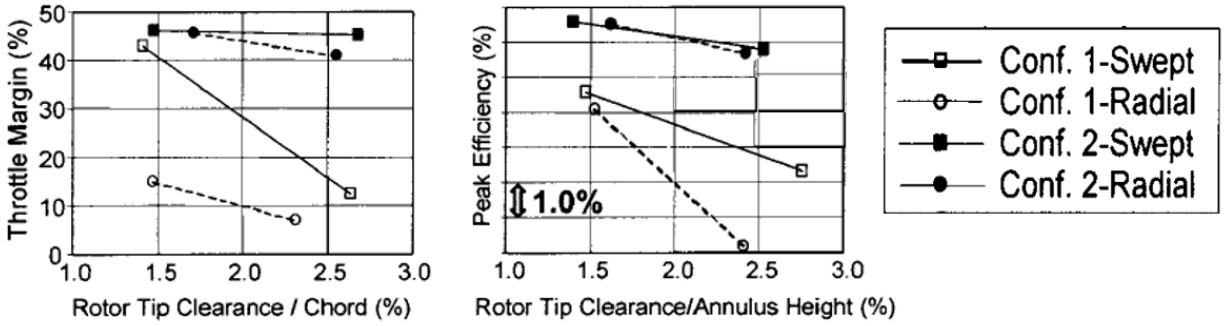

Figure 2.20: Results obtained from the study made by McNulty et al. – Adapted from [18]

Wadia et al. [19] carried out a numerical study on transonic axial compressors at three different tip clearance sizes (0.4%, 0.8% and 1.6% of the rotor mean span). A baseline radially-stacked rotor was swept in the forward direction to obtain a new rotor, as depicted in Figure 2.21. The corresponding simulations results in Figure 2.22 indicate that the swept version of the rotor has a higher efficiency and stall margin at all tip clearance sizes. Moreover, the stall margin sensitivity to tip clearance of the swept rotor improved between the lowest and moderate tip clearance size. According to the authors, the observed improvements stem from the fact that the sweep pulls the

flow toward the tip region, resulting in a lower loading in the tip region and a weaker tip clearance blockage, a reasoning similar to that of McNulty et al. [18].

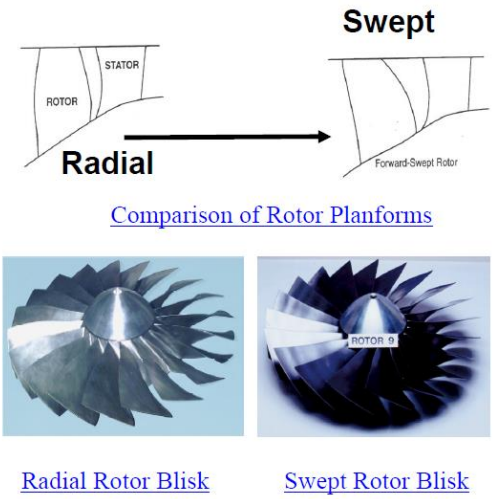

Figure 2.21: Comparison between the baseline rotor ("Radial") and the new rotor ("Swept") from the study of Wadia et al. [19]

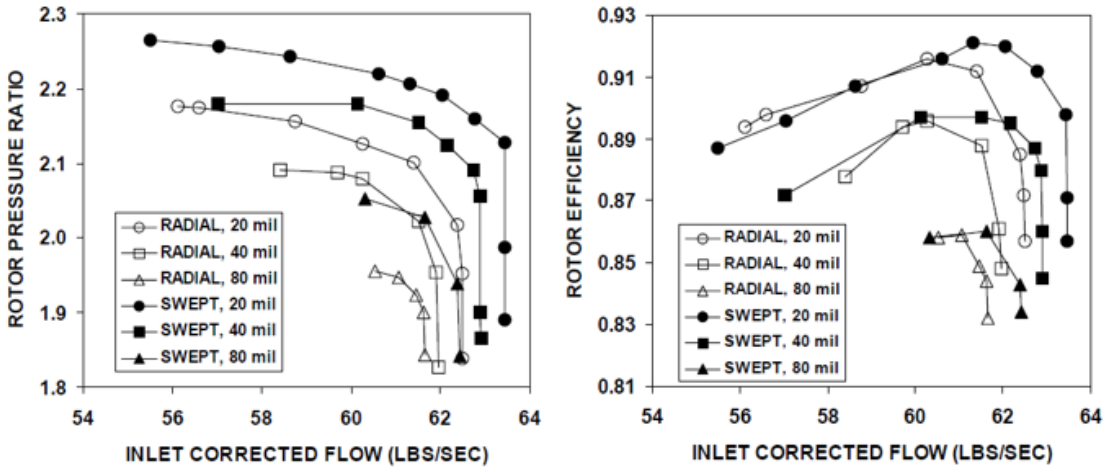

Figure 2.22: Results obtained from the study made by Wadia et al. [19]

Erler [7] performed the first systematic numerical parametric study of blade design strategies for reducing performance and stability sensitivity to tip clearance. Based on the two desensitizing flow features that were discovered and the observed effects of different blade design parameters on sensitivity, Erler [7] proposed and simulated two rotor designs, shown in Figure 2.23 against the baseline rotor ("BASE"), to exploit the desensitizing flow features. The constraints imposed upon the new designs consisted of maintaining the same tip loading and total pressure ratio at the design

point as the baseline rotor. The first new rotor (called “PLS”) involved linearly reducing the stagger angle of the rotor blade in the outer 50% span from 0 to 3 degrees. The intended purpose was to increase the effective tip clearance flow travel distance across the blade passage to reduce double-leakage. The second rotor (called “FFCS”) was obtained by sweeping the baseline rotor 20 degrees in the forward chordwise direction from hub to tip, with the aim of increasing the tip meridional momentum (with an accompanying reduction in double leakage). Simulations were carried out on the baseline rotor and the two new designs at three tip clearance sizes (0.4%, 0.9% and 1.8% of the rotor mean chord) and the results are shown in Figures 2.24. Both new rotors significantly improved the performance and stall margin sensitivity to tip clearance, with the “FFCS” design exhibiting a best nominal efficiency and stall margin. Figure 2.25 indicates that the intended effects on the two desensitizing flow features were achieved by the proposed rotor designs: the “PLS” design has a reduced double-leakage (without changing incoming tip meridional momentum) while the “FFCS” design increased the incoming meridional momentum in the tip region with a larger reduction in double leakage than the “PLS”. These observations were used to explain the slightly better sensitivity reduction of the “FFCS” design compared to the “PLS” design.

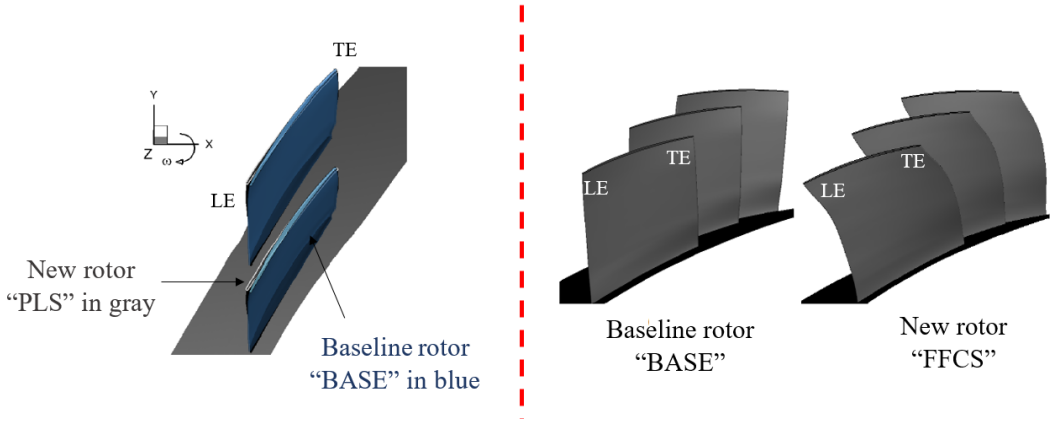

Figure 2.23: Comparison between the baseline rotor and new rotors designed in the study made by Erler – Adapted from [7]

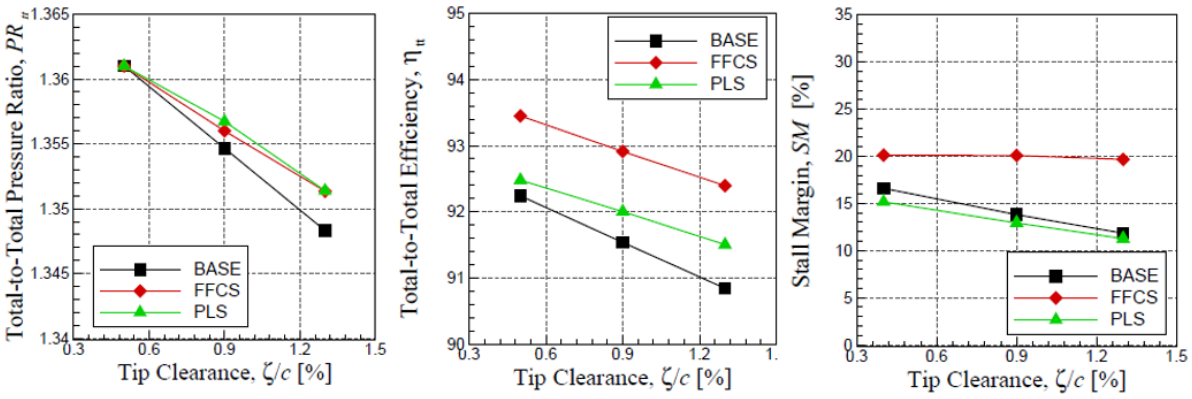

Figure 2.24: Results obtained from the study made by Erler [7]

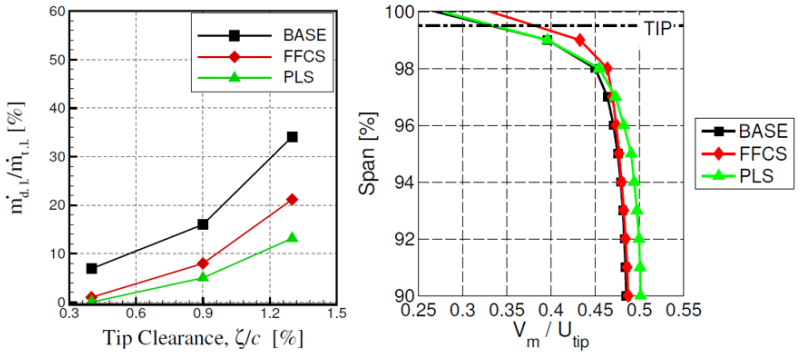

Figure 2.25: Flow features responsible for improvements in sensitivity to tip clearance in the study of Erler [7]

Seshadri et al. [4] used a multi-objective optimizer algorithm on an axial compressor rotor blade. Two tip clearance sizes were considered: 0.5% and 0.85% of the rotor mean span. The objectives imposed to the code were to maximize the mean efficiency (abbreviated by "μ(η)") between these two tip clearance sizes while minimizing its variance (or sensitivity abbreviated by "σ(η)"). Two different optimizations were made using the algorithm. In the first case, only stacking line changes were allowed to be applied on the baseline rotor (called "Datum"). The code used a combination of dihedrals and sweeps to modify rotor sections which led to the new design called "Robust A". In the second case, only camber line changes were allowed to be applied. The code ended up introducing bumps to the suction/pressure side of certain rotor sections at specific chord locations which led to the new design called "Robust B". Both new rotors are compared to the baseline rotor in figure 2.26. The improvements obtained at design point conditions are compared to the baseline rotor in figure 2.27. Although improvements were witnessed on both new rotors, the rotor "Robust

A" outperformed the rotor "Robust B" in terms of mean efficiency and its sensitivity to tip clearance. According to the authors, modifications brought to the baseline rotor are equivalent to off-loading tip sections close to the leading-edge and pushing the loading toward the trailing-edge. These modifications translated into a weaker tip clearance vortex, a lower amount of double-leakage and, by extension, lower mixing losses.

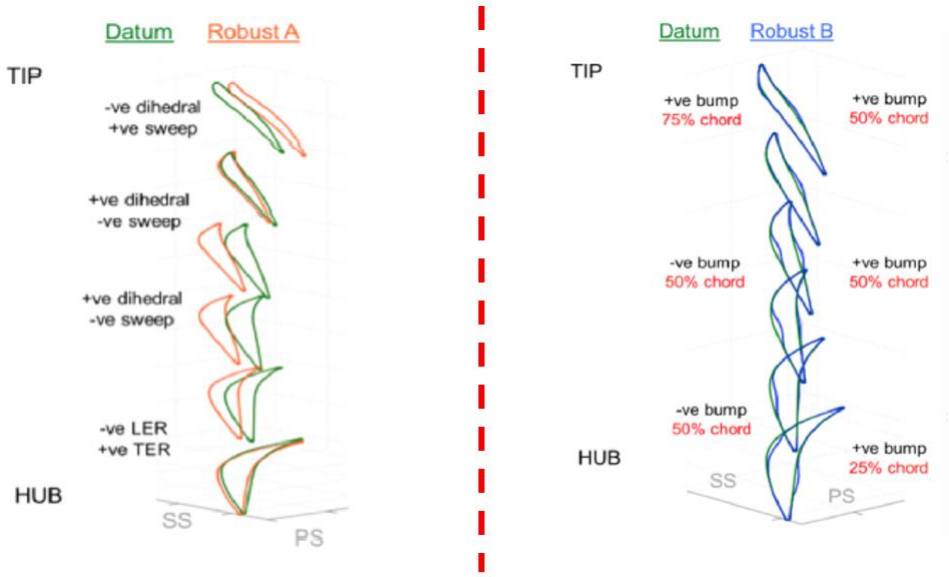

Figure 2.26: Comparison between the baseline rotor and new rotors in the study made by Seshadri et al. [4]

Blade	Normalized $\mu(\eta)$	$\sigma(\eta)$
Datum	0.0	0.1844259
Robust B	+0.6260%	0.1320597
Robust A	+1.1939%	0.1080598

Figure 2.27: Results obtained from the study made by Seshadri et al. [4]

The final study using blade design strategies for the purpose of desensitization to tip clearance is the one made by Halbe et al. [20]. Two tip clearance sizes were considered: 1% and 3% of the rotor mean span. The stagger angle of the baseline rotor tip section was increased to raise the incidence while the trailing edge was opened (i.e. the flow turning was reduced). The hub section did not experience any noticeable change. The comparison between the baseline rotor hub/tip sections with those of the new rotor (called "tip-tailored") is shown in figure 2.28. The improvements obtained

are shown in figure 2.29. According to the authors, the increase in stagger angle of the tip section realigned the blade with the flow. That is because the resulting increase in the tip incidence applied to the new rotor corresponded to the increase in incidence caused naturally by the low-momentum tip clearance blockage. Also, the reduction in loading in the tip section decreased the strength of the tip clearance flow. Both effects reduced tip region losses.

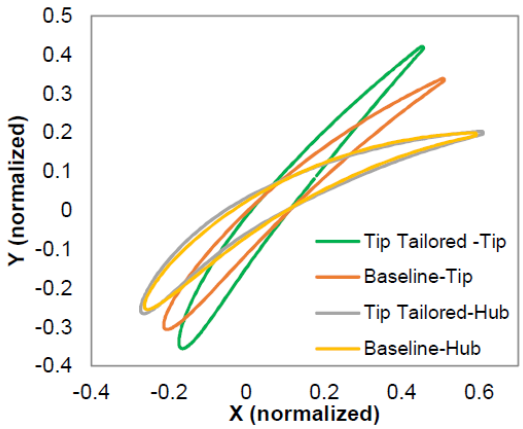

Figure 2.28: Comparison between the baseline rotor and the new rotor ("Tip-tailored") from the study of Halbe et al. [20]

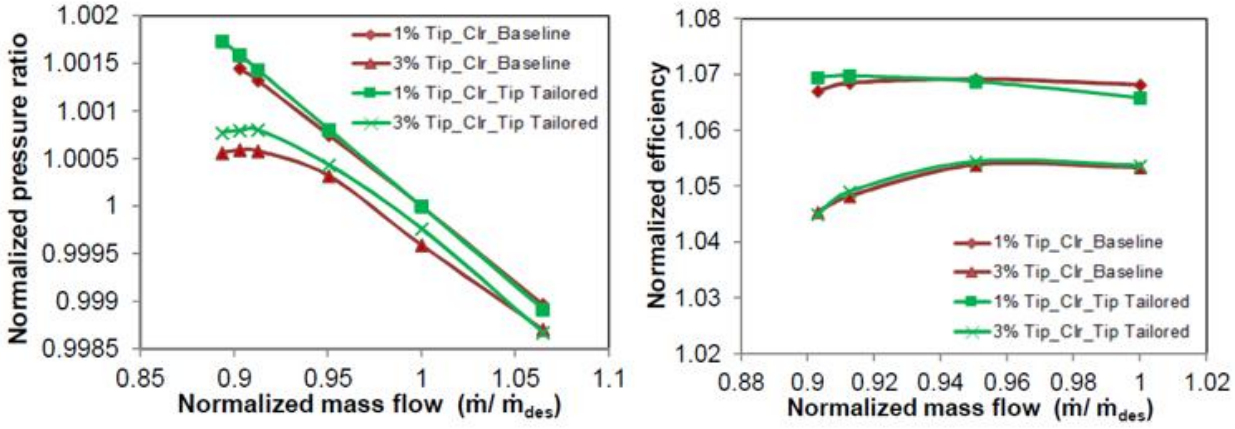

Figure 2.29: Results obtained from the study made by Halbe et al. [20]

2.5.2 Gas path design strategies

An experimental study carried out by Smith and Cumpsty [21] investigated the effect of a casing treatment made up of axial-skewed slots on a low-speed axial compressor rotor, as shown in Figure 2.30. The tests were carried out at four different tip clearance values (1%, 3.5%, 6% and 11% of the rotor chord). The experimental setup did not allow measurement of the rotor efficiency. Figure

2.31 plots the measured speedlines, in terms of static pressure rise coefficient versus flow coefficient (equivalent of mass flow), for the rotor with smooth shroud (“SW”) and with the casing treatment (“CT”). The results show that the casing treatment improves the stall margin at all tip clearances as well as reduces the pressure rise sensitivity to tip clearance at low mass flows.

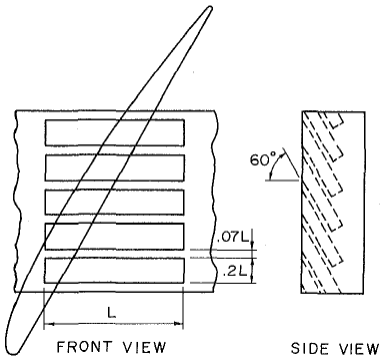

Figure 2.30: Casing treatment used in the study made by Smith and Cumpsty [21]

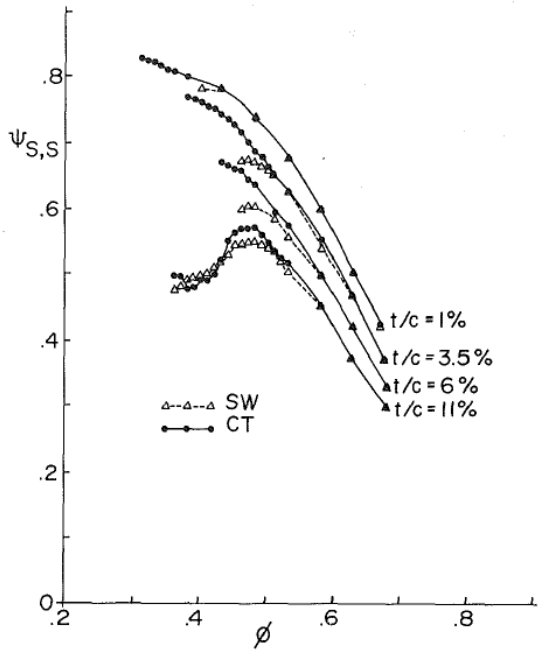

Figure 2.31: Results obtained from the study made by Smith and Cumpsty [21]

Beheshti et al. [22] numerically investigated the effect of a casing treatment consisting of a single circumferential rectangular groove (Figure 2.32) at two tip clearance sizes: 1% (“medium”) and 1.5% (“large”) of the rotor span. The results obtained with a smooth shroud (“Smooth”) and with a casing treatment (“Treatment”) are shown in Figure 2.33. They indicate that this casing treatment

improved the nominal efficiency and stall margin along with their sensitivities to tip clearance. According to the authors, the tip clearance leakage flow is suctioned into the groove which results in a weaker recirculation area associated with the tip clearance flow.

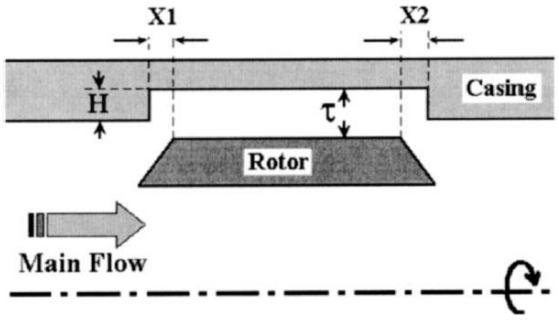

Figure 2.32: Casing treatment used in the study made by Beheshti et al. [22]

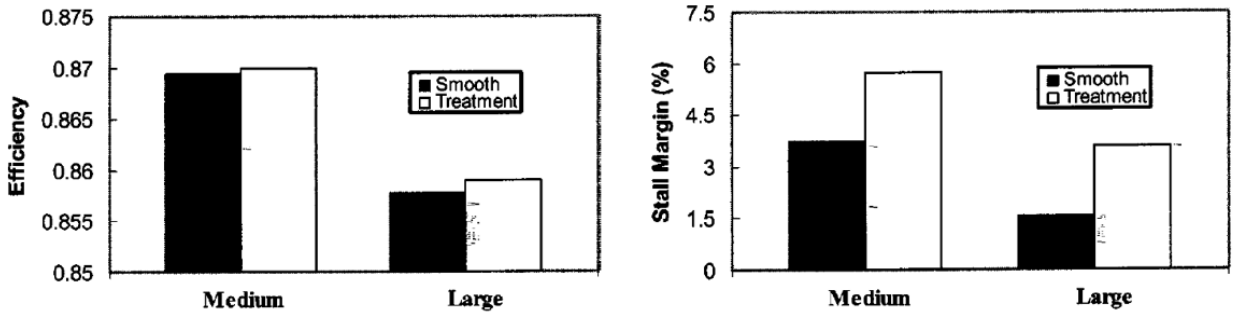

Figure 2.33: Results obtained from the study made by Beheshti et al. [22]

Cevik [8] proposed and investigated two gas path design strategies to exploit the desensitization flow features proposed by Erler [7] to desensitize the performance and stability sensitivity. This computational study used the same baseline transonic axial compressor rotor as Erler [7] with the same three tip clearance sizes (0.47%, 0.94% and 1.41% of the rotor tip chord). The first strategy consisted of changing the gas path to a concave shape, as shown in Figure 2.34, with the intent of increasing the meridional momentum in the tip region. The stall margin was estimated indirectly using the location of the interface between the incoming flow and tip clearance flow relative to the tip leading-edge plane at the design mass flow. This method is based on the criterion proposed by Vo et al. [16] for spike stall inception (as was shown to be the case for this rotor). The corresponding results shown in Figure 2.35 indicate that this gas path contouring technique caused a large penalty in nominal performance with negligible or no improvement in sensitivity, despite an increase in meridional momentum in the tip region and a reduction in double-leakage at nominal

tip clearance. These results suggest that the aggressiveness in the shape of the gas path may have an effect of the desensitization flow features proposed by Erler [7].

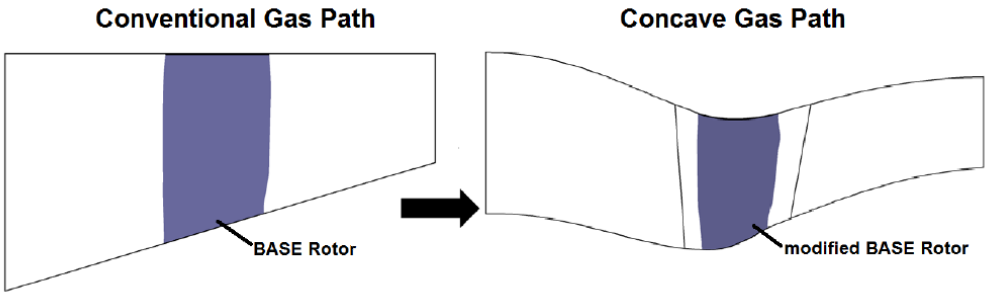

Figure 2.34: Gas paths used in the study made by Cevik [8]

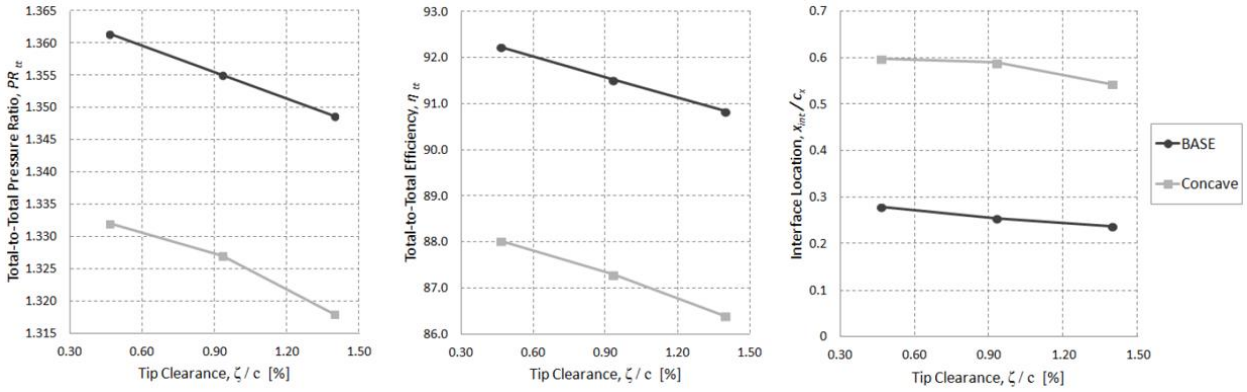

Figure 2.35: Results obtained from the study made by Cevik [8]

The second design strategy proposed by Cevik [8] is a novel casing treatment consisting of shallow circumferential negative sawtooth shape indentations (grooves) with a depth on the order of the tip clearance size, as illustrated in Figure 2.36. The intention is to reduce sensitivity through double leakage reduction. An extensive parametric study was carried out on the different design parameters, including indentation shape to provide some preliminary design trends. These trends were used to obtain a final design, which consists of the same indentation shape but with four shallower grooves starting closer to the rotor leading edge. Figure 2.37 compares the performance and stability predictions for the rotor with smooth casing, initial casing treatment and final casing treatment. The results show that proper optimization of this casing treatment can desensitize the pressure ratio to tip clearance completely with small nominal pressure ratio penalty, reduce the sensitivity of efficiency without any nominal efficiency loss and reverse the sensitivity in stall

margin with a net stall margin gain at nominal tip clearance. According to the author, improvements obtained stem from the important reduction of double leakage caused by the grooves.

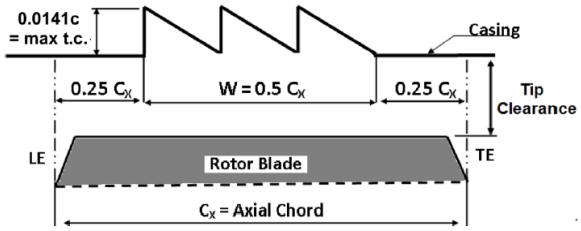

Figure 2.36: Casing treatment used in the study of Cevik et al. [23]

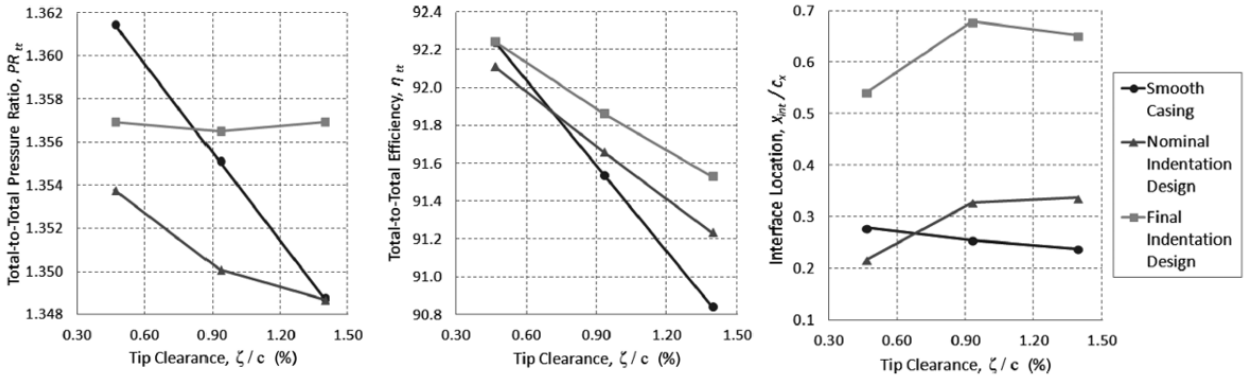

Figure 2.37: Results obtained from the study made by Cevik et al. [23]

Guinet et al. [24] numerically investigated tip blowing for desensitization to tip clearance. As illustrated in Figure 2.38, this technique consists of providing a non-axisymmetric recirculating duct that allows air to be extracted at a downstream chordwise location and re-injected from the shroud over the rotor at another location. The locations of duct extremities are chosen to provide enough pressure difference to drive the requested amount of air recirculation. Three different tip clearance sizes were considered in the current study: 0.5%, 1% and 1.5% of the rotor mean span. Contrary to previous studies presented, the nominal tip clearance size here was not the smallest value. It corresponded actually to 1% span. The flow suction location was at 90% chord downstream of the tip rotor leading-edge while the re-injection location was at 10% chord upstream of the rotor tip leading-edge. The results of the smooth casing (“SC”) and the tip blowing casing treatment (“TBCT”) are overlaid in Figure 2.39. The nominal performance was kept reasonably constant. The stall margin increased for the nominal and the highest tip clearance sizes where the rotor stalled through the spike stall inception. For the lowest tip clearance size, the rotor was no longer tip-critical because the stall was triggered by a blade boundary layer separation. This

separation is caused by the change in incidence which originates from the upward movement of the flow associated with the presence of the casing treatment. Otherwise, the sensitivity to tip clearance of the efficiency and stability were both reduced especially toward larger tip clearances. The reduction in tip clearance leakage and tip blockage by the casing treatment are amongst the proposed factors explaining the improvements achieved.

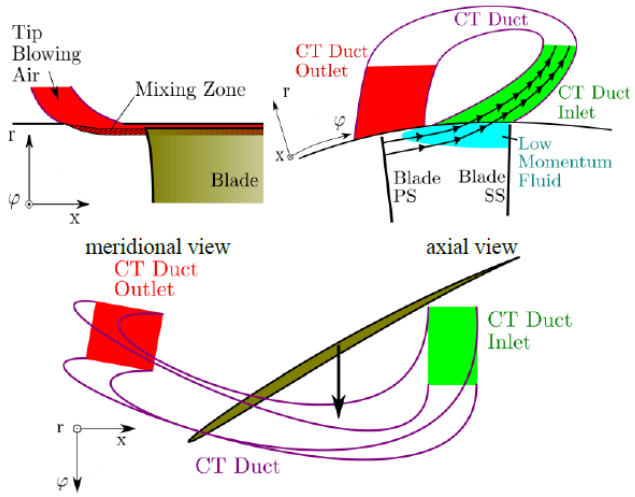

Figure 2.38: Casing treatment used in the study made by Guinet et al. [24]

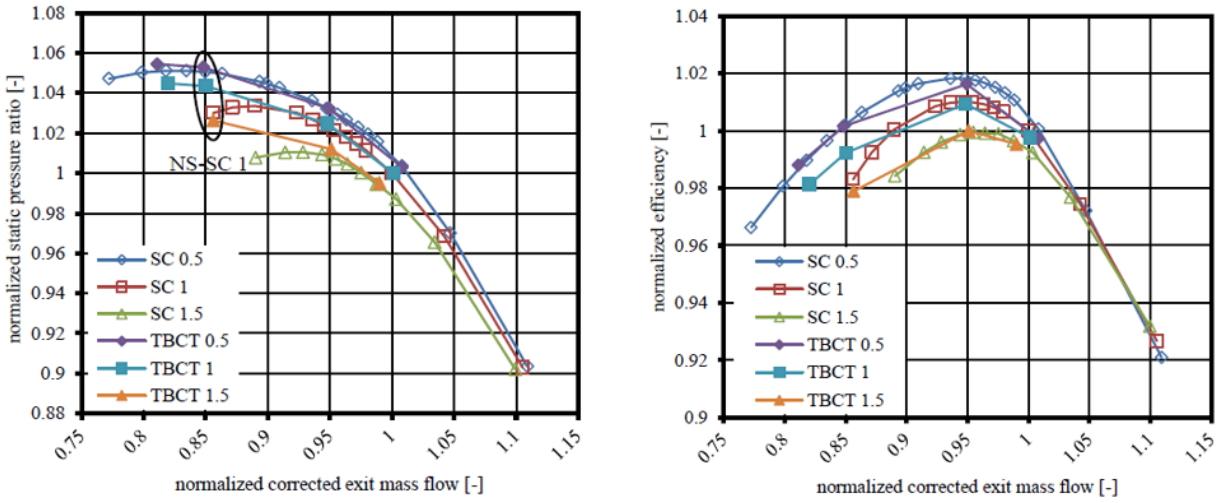

Figure 2.39: Results obtained from the study made by Guinet et al. [24]

CHAPTER 3 METHODOLOGY

3.1 General Methodology

The objective of this study is to reduce the sensitivity to tip clearance of a real aero-engine axial compressor rotor through the adaptation of a novel casing treatment and the redesign of the rotor blade geometry. Since numerous design iterations are required for each task, a computational approach is chosen as it allows for rapid evaluation of each configuration. Moreover, this approach allows for an in-depth analysis of the flow field to understand the effects of the casing treatment and rotor design features on the rotor nominal performance and stability and their sensitivities to tip clearance increase.

This study will carry out CFD simulations on the rotor under study using a numerical setup that reproduces adequately the compressor test rig setup in which it will be tested. Three rotor tip clearances will be simulated through displacement of the shroud above the rotor (as will be done in the rig), namely nominal (minimum), medium and large tip clearance corresponding to 0.74%, 1.65% and 2.57% of the rotor mean span, respectively. Most of the detailed analysis will concentrate on the nominal and large tip clearances to accentuate the differences in the flow field. Moreover, a stall margin assessment for this rotor, which can stall through modal or spike stall inception, requires the CFD simulations of a full speedline up to the stall point, which is prohibitively expensive given the number of configurations to be simulated during the design process of the casing treatment and the revised (new) rotor. Thus, the chosen approach is to carry out the design process based on performance at design mass flow only and to verify stall margin and its sensitivity only for the final design.

The methodology starts with an assessment of the baseline rotor with a smooth casing (Chapter 4) in terms of the variation of the design point performance (total pressure ratio and efficiency) and stall margin with tip clearance. This general overview of the nominal performance and sensitivity is followed by an analysis of the flow field to investigate the source of the variation of performance and stability with tip clearance.

Thereafter, in Chapter 5, the casing treatment geometry previously proposed by Cevik [8] on a theoretical axial compressor rotor will be adapted to the baseline rotor under study, taking into account the geometrical and manufacturing constraints in the context of the test rig. From an initial

casing treatment configuration, a parametric study would be carried out on the main casing treatment geometrical design parameters to obtain the variation of nominal performance and sensitivity with respect to each design parameter. These trends will be used to obtain a final casing treatment design offering the lowest nominal performance penalty and the best reduction (improvement) in performance sensitivity to tip clearance. After plotting the variation of design point performance and stall margin with tip clearance for baseline rotor without and with the final casing treatment configuration, an analysis of the flow field will be carried out to investigate the source of observed changes in nominal performance and stall margin and their sensitivities brought about by the casing treatment.

In Chapter 6, the design process of the new (revised) rotor will start with the application of the two desensitizing rotor design strategies proposed by Erler [7] on the baseline rotor geometry (while keeping a smooth shroud, i.e. no casing treatment). An assessment of the nominal performance and stall margin as well as their sensitivities to tip clearance will be made to see if these strategies work for the current rotor. If the strategies do not work, a new design strategy will be established based on the findings with regard to the desensitization mechanism of the casing treatment and design trends from new parametric studies. The final rotor design will be assessed in terms of nominal performance and stall margin and their sensitivities to tip clearance in comparison to the baseline rotor with a smooth shroud (Chapter 4) and with the final casing treatment (Chapter 5). Finally, an analysis of the flow field will be performed to explain the difference in nominal performance and stall margin and their sensitivities between the new rotor design and the baseline rotor design.

3.2 Computational setup

The simulation tool used for this project is ANSYS CFX R16.1. It is a commercial Reynolds-averaged Navier-Stokes (RANS) node-centered and pressure-based implicit CFD code widely used for simulations in turbomachinery. Turbomachinery components are meshed with ANSYS TURBOGRID R16.1 while the casing treatment grooves are meshed using ANSYS ICEM CFD R16.1.

3.2.1 Computational domain

Since the casing treatment and new rotor resulting from this study will be tested and compared experimentally to the baseline rotor in a compressor rig, experimental conditions would be reproduced as faithfully as possible in the computational setup in order to obtain comparable numerical and experimental results.

Figure 3.1 presents the cross section of this compressor test rig. In this environment, the rotor is preceded by an inlet guide vane (IGV) and a row of fingers. The two latter components were designed independently prior to this project to reproduce the inlet conditions to this rotor, in terms of spanwise distributions of total pressure and flow angle, that best replicate its operating environment in an aero-engine. A stator without hub clearance is placed downstream of the rotor. Figure 3.2 provides a front view of the main elements shown in figure 3.1.

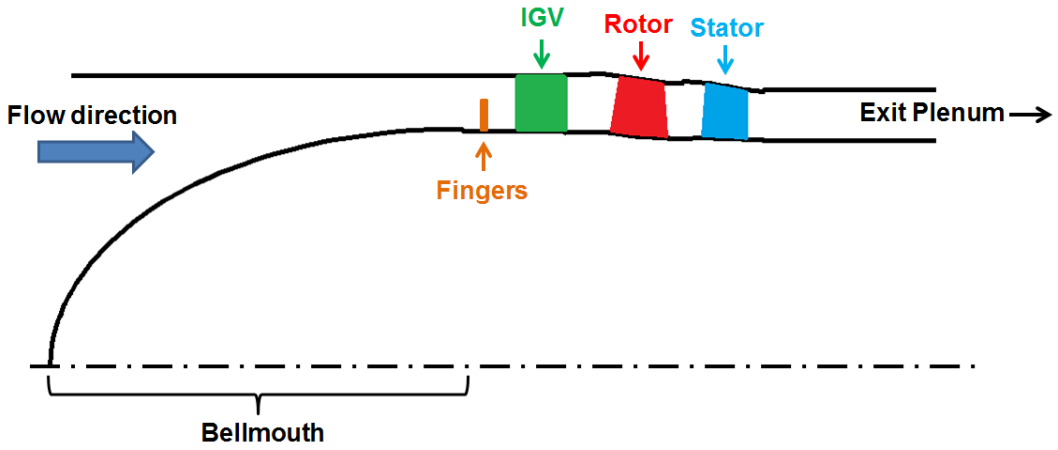

Figure 3.1: Compressor rig test section

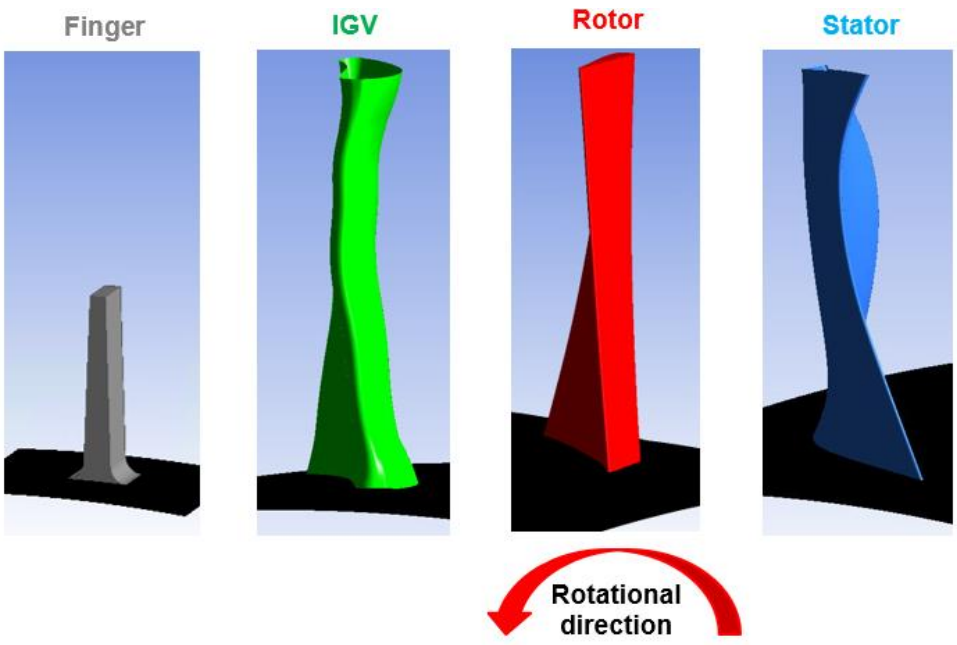

Figure 3.2: Fingers, IGV, rotor and stator of the compressor rig (looking downstream)

As depicted in Figure 3.1, the rotor shroud in this rig is tapered which means that its radius is decreasing as the flow moves downstream. As is the case in the test rig, the increase in tip clearance is modeled as a downstream translation of the rotor shroud as illustrated in Figure 3.3.

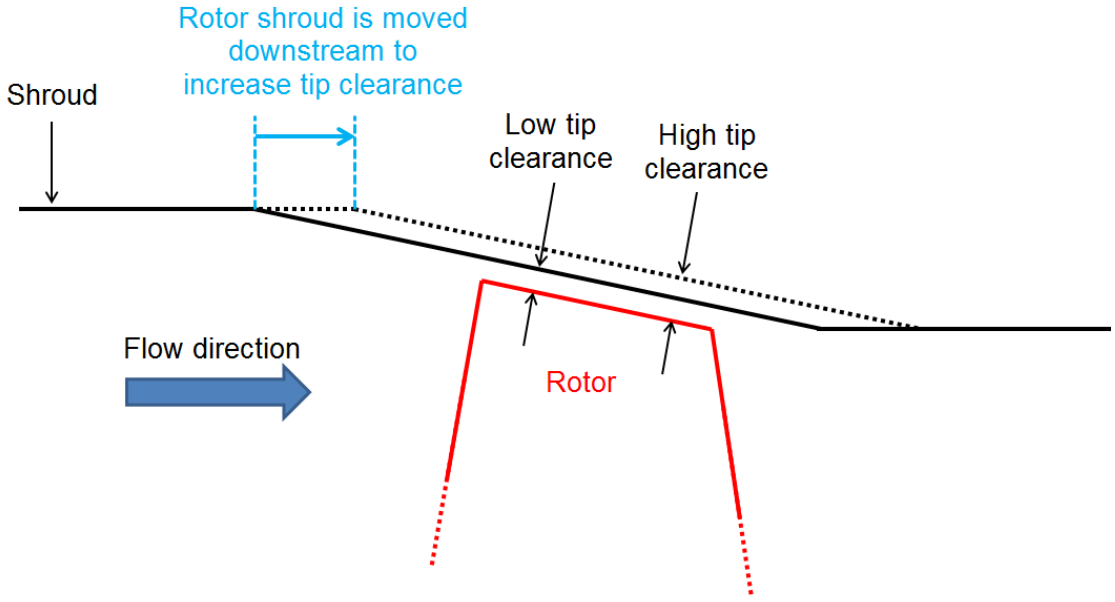

Figure 3.3: Modelling of the shroud for tip clearance increase

Three important considerations are made when modelling the gas path for CFD simulations in this project. The first is the extent of the computational domain. To keep the computational time and resources reasonable while retaining as closely as possible the effect of the blade rows adjacent to the rotor, the computational domain is chosen to include only the IGV, rotor and stator as shown in Figure 3.4, each modeled as a single-blade passage computational subdomain. All subdomains are set as stationary, except for the rotor subdomain which is solved in the rotating reference frame. According to best practices in CFD simulations in turbomachinery, ducts with a length corresponding to the circumferential size of the computational domain are added upstream of the IGV subdomain and downstream of the stator subdomain, respectively. This is to allow for the circumferential perturbations of up to one blade pitch in circumferential wavelength to attenuate to zero at the computational domain inlet and exit. The radial distribution of total pressure at the inlet of the computational domain is iterated upon to reproduce the same rotor inlet conditions as obtained from previous simulations of the compressor rig intake up to the rotor inlet (including the fingers).

The second consideration is the presence of small waterfalls in the gas path. Waterfalls are 0.01-0.02 inch backward facing steps at the junction of two components in the gas path. They are standard features in turbomachinery to allow for assembly tolerance while avoiding any forward facing step in the gas path (protrusion in the flow) that are aerodynamically much more damaging than the small recirculation zone associated with a backward facing step. Singh et al. [25] carried out a numerical study investigating the length of the recirculation zone resulting from a backward step having different angles and placed in a channel. The recirculation length was found to be independent of step angles ranging from 45 degrees to 90 degrees. The waterfalls are thus modeled as 45-degree ramps, as shown in Figure 3.5, to provide a smooth mesh while capturing their effect of the effective gas path.

The third consideration involves the modelling of the negative saw-tooth shaped indentations associated with the casing treatment proposed by Cevik [8] (see Figure 2.36). Manufacturing constraints require that a distance of 0.020 inch be placed between the grooves. In addition, the pointed shape of the indentations must be changed to allow for ease of meshing (using a structured grid). The resulting casing treatment is depicted in Figure 3.6. With the space between the grooves and *fracture* (cut at indentation extremity, set at 5% of the total groove width) fixed, the other geometrical parameters shown in Figure 3.6, along with the number of grooves, can be varied to

obtain an optimal design. It is noted that the compressor test rig is designed with a changeable shroud insert over the rotor, each insert specifically made for each tip clearance size, such that the axial location of the grooves with respect to the rotor remains constant for different tip clearances. This is implemented in the simulation domain. The casing treatment is modeled as a separate computational subdomain that is placed on top of the rotor computational subdomain.

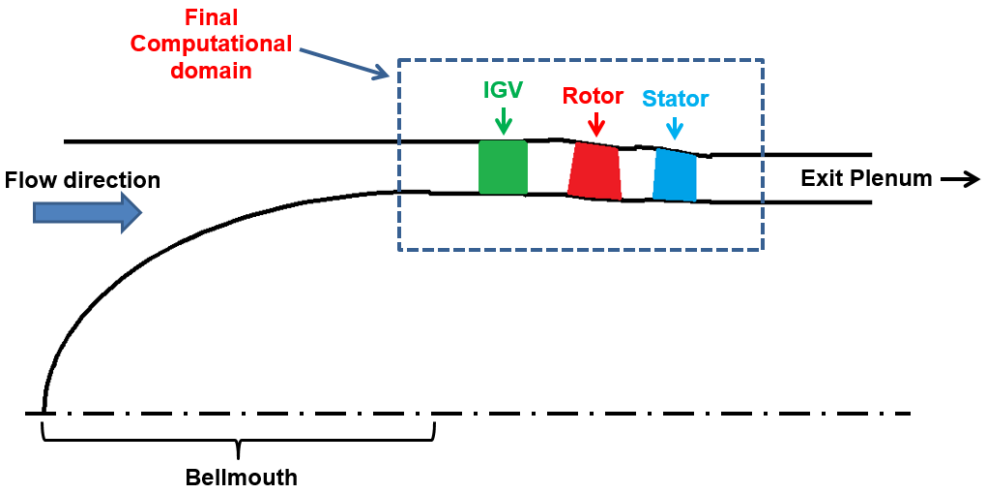

Figure 3.4: Extent of the final computational domain

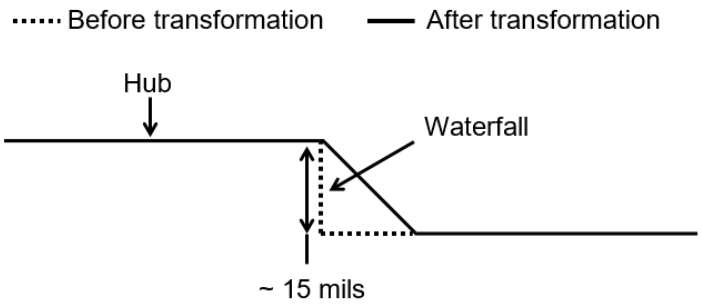

Figure 3.5: Modeling of waterfalls in the computational setup

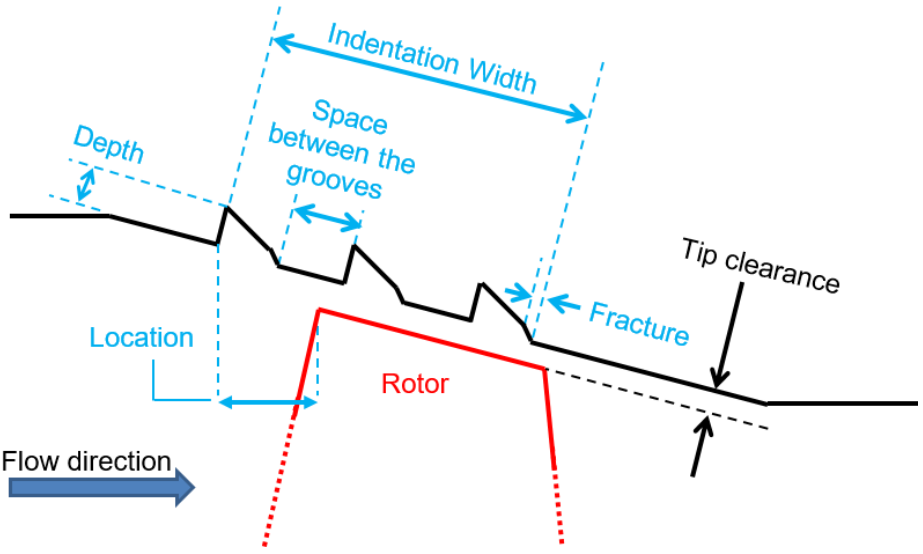

Figure 3.6: Design iteration of the casing treatment geometry used in this study

3.2.2 Mesh selection

The IGV, rotor and stator are meshed separately using ANSYS TURBOGRID R16.1. A structured mesh using the topology ATM Optimized of ANSYS is applied to the three components.

A mesh convergence study was carried out by refining simultaneously the meshes of the IGV, the rotor and the stator. Since these three components are of similar overall dimensions, mesh parameters are kept approximately the same for all of them except for the rotor tip clearance region which has a higher mesh density. The details of this mesh study appear in Appendix B. The final IGV, rotor and stator meshes have a total number of nodes of 8.4 million. Table 3.1 lists the number of nodes in the spanwise direction for each component. The (y+) values for the surface nodes is around 2 in the three components subdomains. The number of nodes in hub/shroud boundary layers is higher than the minimum value of 10 recommended by ANSYS [26] for accurate results with the SST turbulence model (see next section). In the tip clearance region, 30 non-uniformly spaced nodes are applied in the spanwise direction for the nominal tip clearance size (about 0.75% of the chord). This is higher than the number of nodes recommended by Van Zante et al. [27] to capture accurately the physics of the flow in this region for an axial compressor (12 elements for a tip clearance size of 1.3% chord). For tip clearance sizes of 1.65% and 2.57% span, the number of nodes in the spanwise direction is increased to 65 and 100 respectively. Therefore, a similar spanwise mesh density is kept in this region regardless of the tip clearance size. The final meshes

for the IGV, the rotor and the stator are shown in Figures 3.7, 3.8 and 3.9, respectively, while the tip clearance mesh for the rotor at the three simulated tip clearances is presented in Figure 3.10.

Table 3.1: Number of nodes in the spanwise direction for each component

	IGV	Rotor	Stator
Hub boundary layer	149 in total	45	45
Between boundary layers		45	50
Shroud boundary layer		45	48

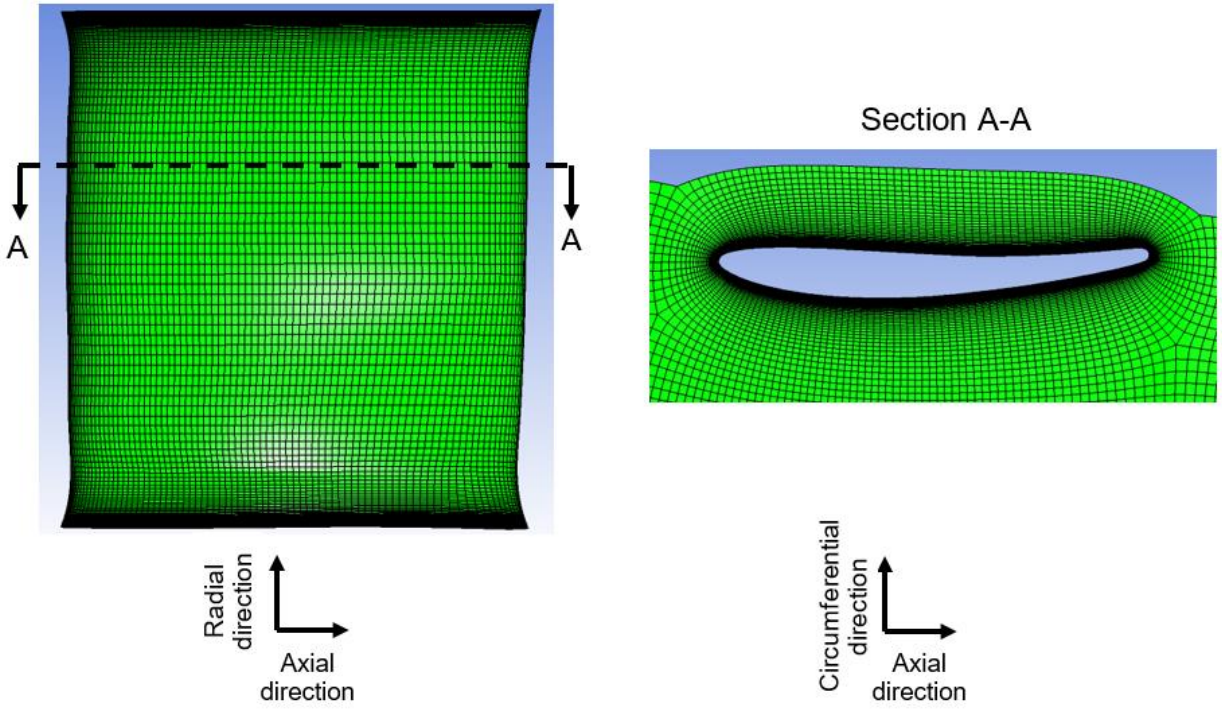

Figure 3.7: Mesh of the IGV

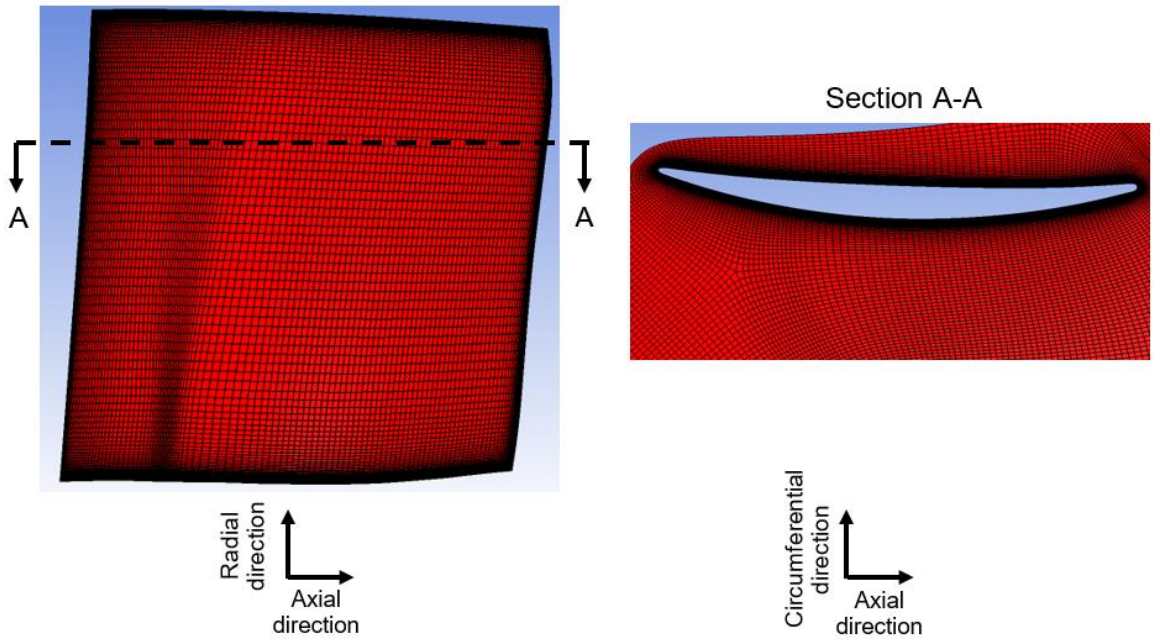

Figure 3.8: Mesh of the rotor

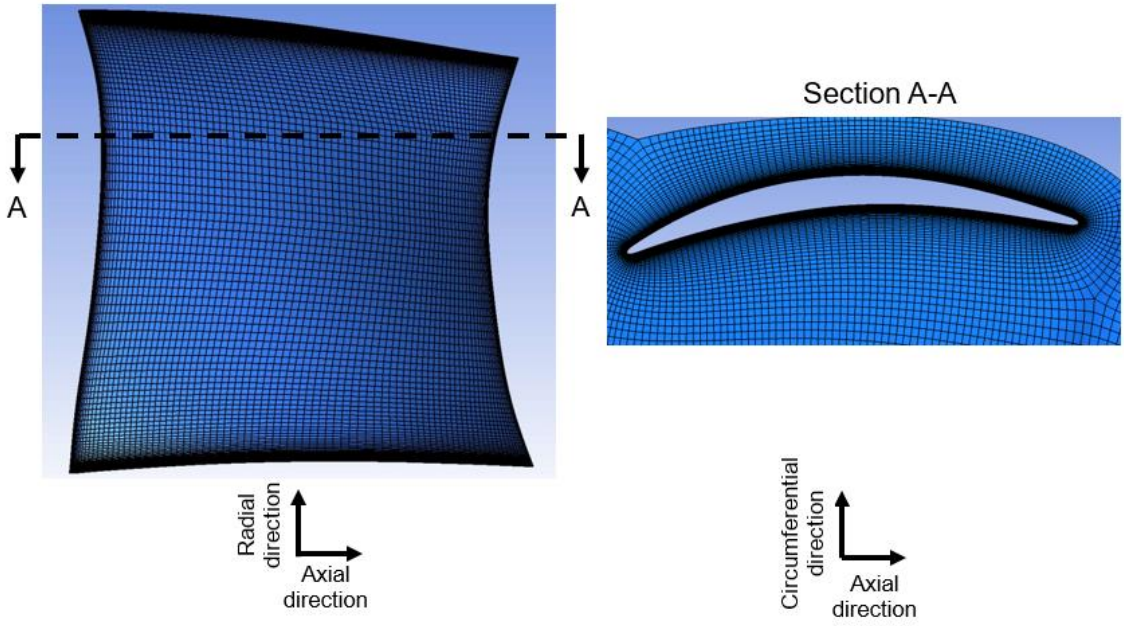

Figure 3.9: Mesh of the stator

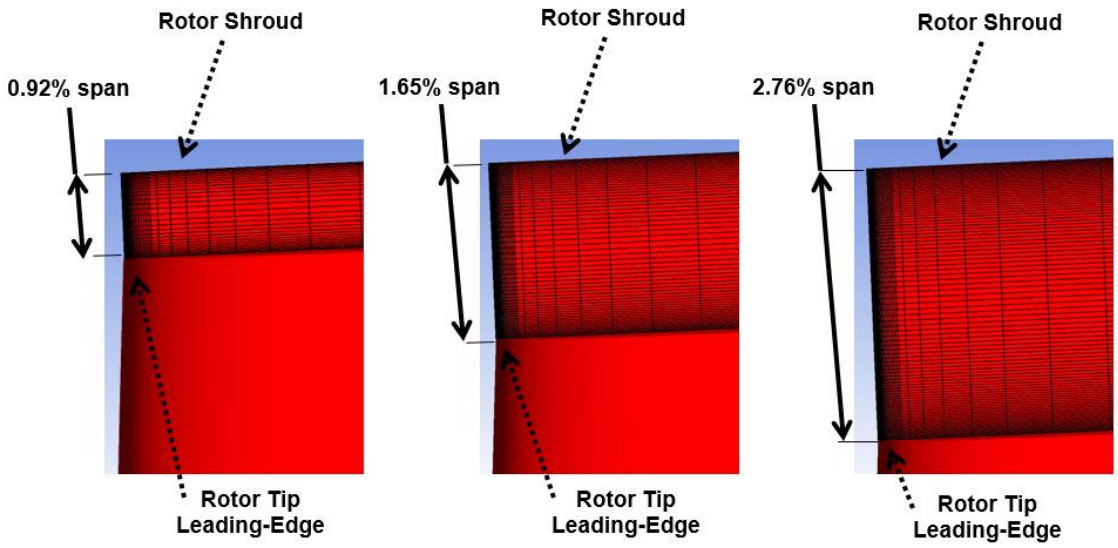

Figure 3.10: Spanwise mesh density in the tip clearance region

The casing treatment is meshed separately with ANSYS ICEM using a structured mesh. The mesh convergence study which was carried out on the casing treatment geometry is presented in Appendix B. The final mesh, shown in figure 3.11, has 128,000 nodes per groove with 40, 80 and 40 nodes in the streamwise, pitchwise and spanwise directions, respectively.

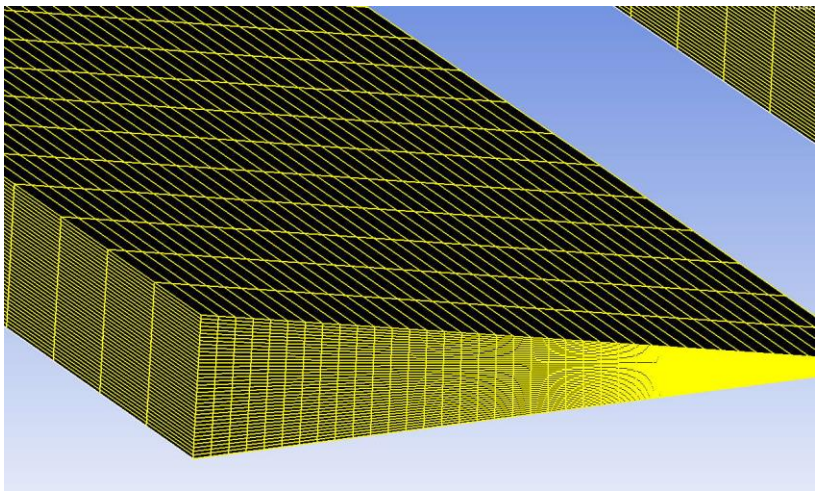

Figure 3.11: Mesh of one casing treatment groove

Since the casing treatment computational subdomain is adjacent to and interacts with the rotor computational subdomain, their mesh densities are kept similar in all directions at the interface for accurate transfer of flow properties, as shown in Figure 3.12.

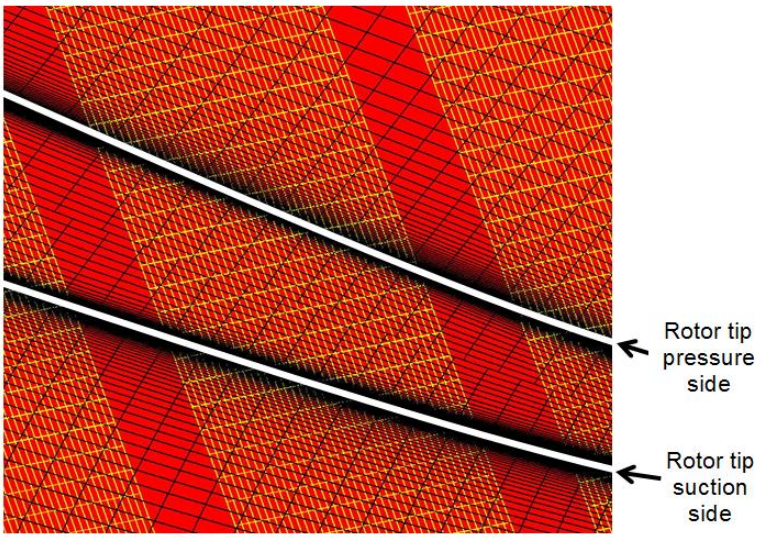

Figure 3.12: Meshes of the casing treatment (in yellow) and the rotor (in black) at interface between their respective computational subdomains

3.2.3 Boundary conditions and turbulence model

With the turbulence generated by the fingers in the rig and a generally positive pressure gradient across the compressor, the flow is assumed fully turbulent and thus a boundary layer transition model is not used in the simulations. The turbulence model used in this study is the Shear Stress Transport (SST) turbulence model. Yin et al. [28] compared results from CFD simulations using two different turbulence models on two transonic axial compressor rotors with experimental measurements. They found that the SST turbulence model adequately captured the flow in the endwalls, including the tip clearance flow and its interaction with the main flow. Liu et al. [29] carried out a similar type of study with six different turbulence models on a low-speed axial compressor. They found that the SST turbulence model best predicted the experimental circumferential motion of the tip clearance vortex. Therefore, the SST turbulence model was applied throughout the current study.

Throughout the rotor design process, the computational setup is made up of three subdomains corresponding to the IGV, Rotor and Stator. In the casing treatment design process, the computational setup is made up of the three previous subdomains in addition to the casing treatment subdomain. All subdomains are set to be stationary except the rotor subdomain which is set to be rotating.

Figure 3.13 shows the inlet/exit boundary conditions and interface type between the computational subdomains. The inlet conditions to the computational domain consist of specifying a spanwise total pressure profile, a uniform temperature, a flow direction/swirl angle (zero-degree), a turbulent kinetic energy profile and a turbulent eddy frequency profile. At the outlet of the computational domain, a mass flow rate is specified. Rotational periodicity conditions are imposed to all lateral surfaces. A mixing plane (*stage*) interface is imposed between adjacent blade row subdomains, for which flow properties are circumferentially averaged before being transferred to the downstream subdomain [26]. No-slip wall conditions are imposed to all solid surfaces. Since the rotor subdomain is in the rotating frame of reference, the shroud as well as the hub portions away from the rotor blade passage are set as counter-rotating no-slip walls to cancel the rotation effect on these surfaces.

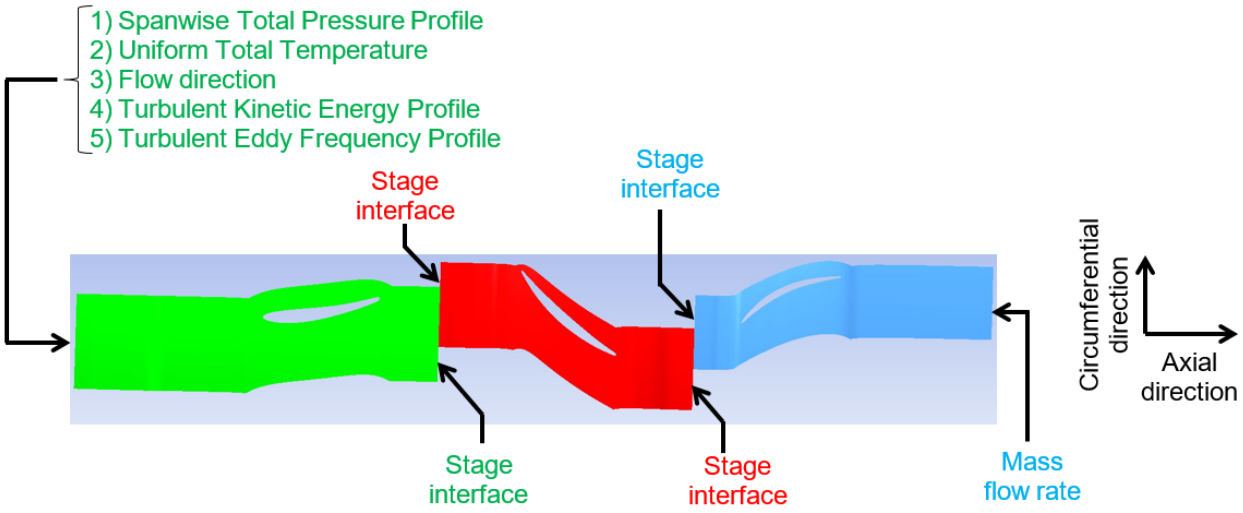

Figure 3.13: Boundary conditions imposed to the IGV, rotor and stator subdomains

Figure 3.14 summarizes the boundary conditions for the casing treatment subdomain. A no-slip wall is applied to the solid surfaces while a rotational periodicity condition is imposed on lateral surfaces. A *frozen rotor* interface is used at the interface between the rotor and casing treatment subdomains. This is a standard interface for simulating circumferential grooves, which allows for transferring the circumferential variation in flow properties across the interface while maintaining the casing treatment domain stationary.

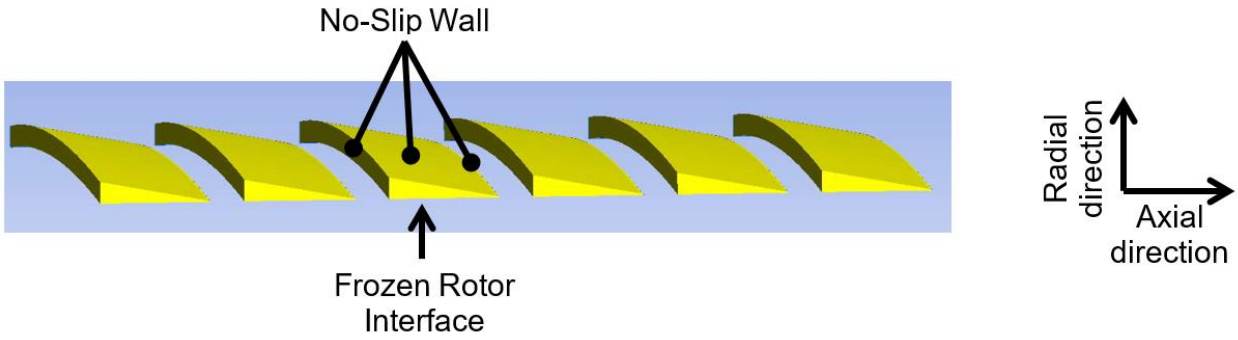

Figure 3.14: Boundary conditions imposed on the casing treatment subdomain

3.2.4 Simulation and post processing procedure

Steady-state simulations are used to obtain results at design point conditions. For stall margin calculations, steady-state simulations are first carried out to find stable operating points left of the design point on the speedline by reducing the specified exit mass flow. This procedure is basically the simulation of the speedline. The *stall point* is the point after which a decrease in mass flow results in a sudden drop in pressure ratio (discontinuity in speedline). Since the flow usually exhibits unsteadiness near the stall point, simulations on the stall point and the two adjacent points at higher and lower mass flow are repeated in transient mode to validate the stall point. Post-processing for these points is done on a time-averaged flow field.

In terms of the post-processing, all parameters are calculated for the rotor, which is the focus in this study. Thus, the inlet plane for calculating the flow properties is located at 10% axial chord upstream of the rotor leading edge while the outlet is located at 10% axial chord downstream of the rotor trailing edge. The fundamental stagnation flow properties, namely total pressure (P_T), total temperature (T_T) and total enthalpy (h_T) are mass-averaged at these planes while the static pressure (P_S) as well as the static entropy (s) are area-averaged. The fundamental parameters used in this study are defined as:

- Corrected Mass Flow ($\dot{m}_{COR}$) = $\dot{m}\sqrt{\theta}/\ \delta$
- Total-to-total pressure ratio (PR_{TT}) = $P_{T,\ OUTLET}$ / $P_{T,\ INLET}$
- Total-to-total efficiency (η_{TT}) = $[(P_{T,\ OUTLET}/P_{T,\ INLET})^{(\gamma-1)/\gamma} - 1]/\ [(T_{T,\ OUTLET}/T_{T,\ INLET}) - 1]$
- Stall margin (SM) = $(\dot{m}_{COR,\ DESIGN\ POINT} - \dot{m}_{COR,\ STALL\ POINT})/\ \dot{m}_{COR,\ DESIGN\ POINT}$

- Aerodynamic loading = $(h_{T,\,OUTLET} - h_{T,\,INLET})/U^2$
- Sensitivity to tip clearance of a parameter $X = X_{\,LOW\ TIP\ CLEARANCE} - X_{\,HIGH\ TIP\ CLEARANCE}$

where θ refers to the rotor inlet total temperature normalized by the standard sea level temperature (288.15 K), δ the rotor inlet total pressure normalized by the standard sea level pressure (101325 Pa), γ the ratio of specific heats (which is assumed constant for this efficiency relation to apply) and U the rotational velocity (which varies along the span position).

Due to confidentiality, most parameters shown in the current thesis are normalized by reference values. For performance, the corrected mass flow, pressure ratio and efficiency are normalized by their respective values from simulation results for the baseline rotor with a smooth casing at nominal (minimum) tip clearance and design point conditions. On the stability side, calculated stall margins would be normalized by the stall margin for the baseline rotor with a smooth casing at nominal tip clearance.

CHAPTER 4 BASELINE ROTOR WITH A SMOOTH CASING

As illustrated in Figure 4.1, the baseline rotor is a high-pressure transonic axial rotor with a radial stacking line. It has a tapered shroud and a diverging hub. In other words, both hub and shroud radii decrease in the streamwise direction.

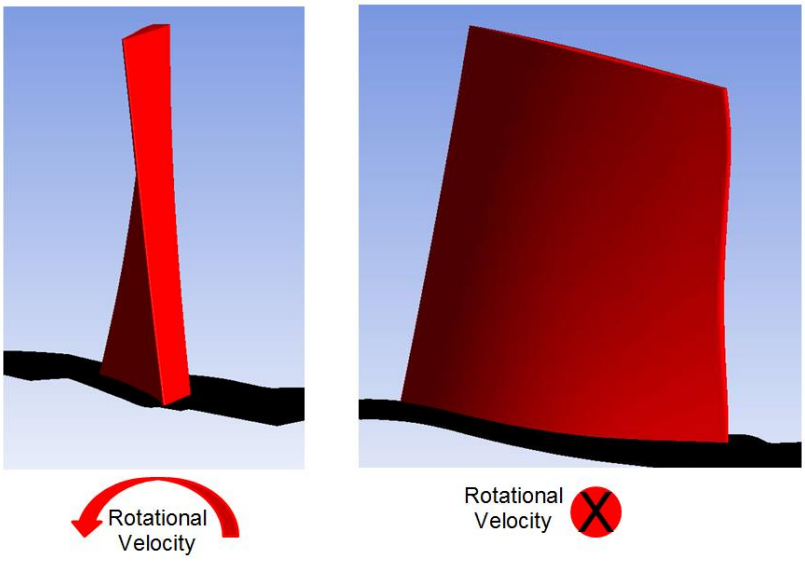

Figure 4.1: Baseline rotor geometry

4.1 General performance and sensitivity results

The variations of total-to-total pressure ratio, total-to-total efficiency and stall margin with tip clearance for the baseline rotor alone are shown in Figures 4.2, 4.3 and 4.4, respectively.

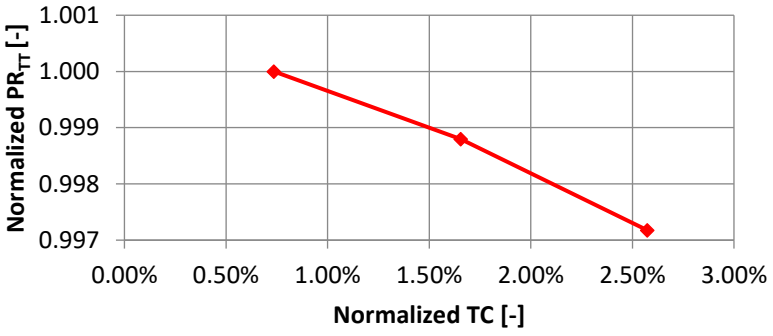

Figure 4.2: Design point total-to-total pressure ratio VS tip clearance

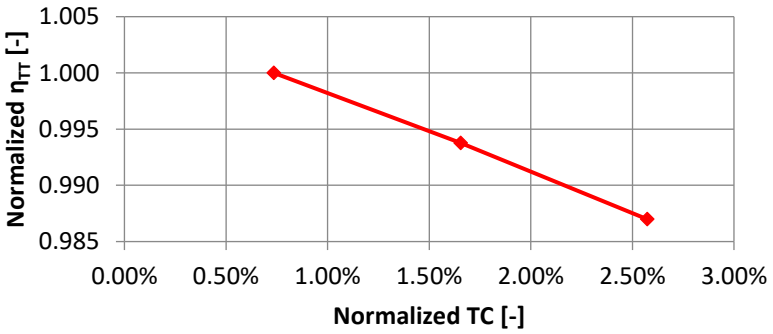

Figure 4.3: Design point total-to-total efficiency VS tip clearance

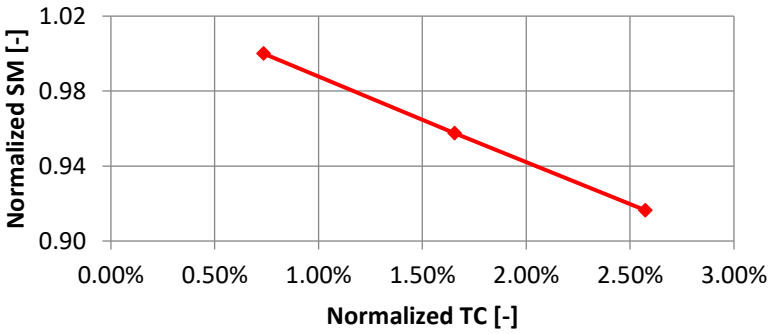

Figure 4.4: Stall margin VS tip clearance

From the perspective of design point performance, the pressure ratio drops by 0.28% while the efficiency drops by 1.30% from nominal (minimum) to high tip clearance size. The efficiency variation with tip clearance is more linear than the pressure ratio variation as indicated by the data on figures 4.2 and 4.3. On the stability side, the stall margin varies linearly with tip clearance and it drops by 8.4% from nominal to high tip clearance.

Henceforth, the text will often refer to two distinct flow regions in the blade passage: the tip region and the lower span region. The tip region is the region of low streamwise momentum flow located in the vicinity of the shroud, associated with the tip clearance fluid. This region includes the tip clearance vortex and tip clearance fluid that did not roll up into the vortex and nearby core flow layers slowed through mixing with the tip clearance fluid. In contrast, the lower span region covers the reminder of the blade passage and includes the core flow with high streamwise momentum and the boundary layers on the blade surfaces and hub.

4.2 Variation of pressure ratio with tip clearance

While the rotor total-to-total pressure ratio depends on inlet and exit total pressures (taken in the stationary reference frame), Appendix C shows that the inlet total pressure remains virtually unchanged with increasing tip clearance. As such, the variation with tip clearance of the rotor exit total pressure corresponds essentially to the sensitivity of pressure ratio and thus can be used to investigate the source of pressure ratio sensitivity. Figure 4.5 presents the contour plot of the difference in total pressure between nominal and high tip clearance taken at the rotor trailing edge plane. Small ellipses on the figure highlight regions with total pressure gain (+) or loss (-) as the tip clearance increases. The data indicates that the tip region experiences high-magnitude total pressure changes while the core flow undergoes low-magnitude total pressure changes.

In the tip region, although a small zone near the blade pressure side sees a total pressure gain (+) when the tip clearance increases, the extent and magnitude of total pressure losses (-) prevail. Therefore, net total pressure changes in the tip region correspond to losses. In the lower span region, certain zones show also low-magnitude total pressure gains. However, the bulk of this region experiences net low-magnitude total pressure losses. Therefore, net changes in total pressure in the lower span region correspond also to losses.

According to Figure 4.5, the total pressure loss in the tip region is about one order of magnitude greater than that in the lower span region. However, the mass flow in the lower span region is one order of magnitude greater than that in the tip region (the mass flow ratio being 21.9 and 13.4 for nominal and high tip clearance, respectively). Thus, at least for this rotor, *the contribution of the lower span region flow to the sensitivity to tip clearance of the total-to-total pressure ratio is on the same order of magnitude as that of the tip region*.

In terms of the general sources of the exit total pressure loss in both regions, the larger tip clearance flow with increased tip clearance leads to reduced axial flow velocity and increased relative flow angle in the tip region while the relative velocity increases in the lower span region (from the increased tip blockage diverting more flow toward the lower span region). The corresponding velocity triangles for these two regions, as illustrated in figure 4.6, both show a decrease in the rotor exit tangential velocity in the stationary frame, which is directly linked to the work on the flow and by extension the total pressure rise. This explains the general drop in exit total pressure in both regions.

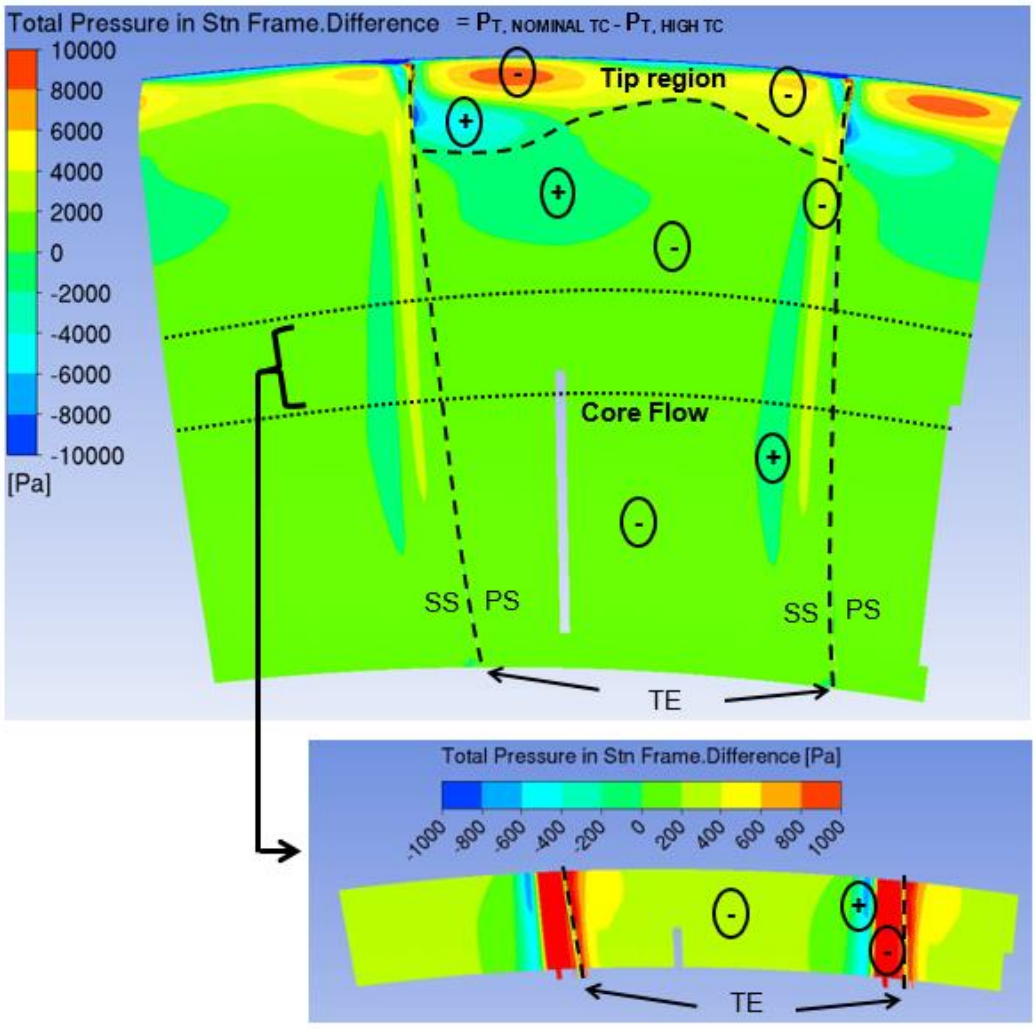

Figure 4.5: Difference in total pressure between nominal and high tip clearance at the rotor trailing edge plane

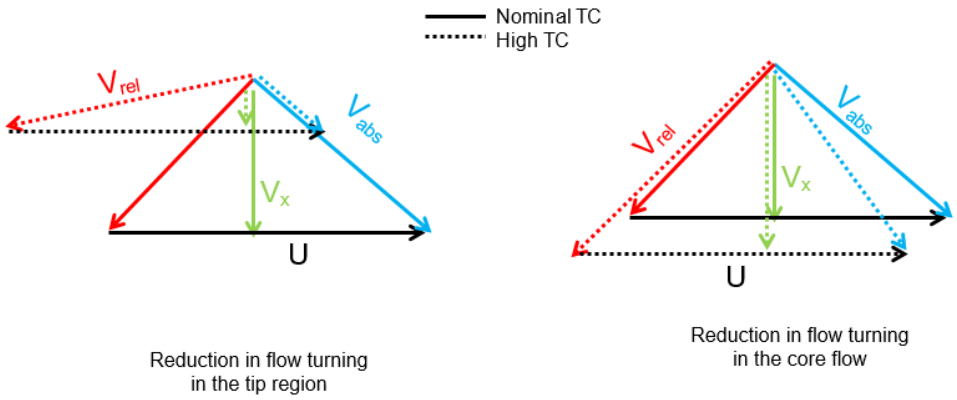

Figure 4.6: Velocity triangles for tip and lower span regions at nominal and high tip clearance

4.3 Variation of efficiency with tip clearance

The adiabatic efficiency of the rotor is directly linked to the aerodynamic losses generated in the rotor blade passage, namely viscous boundary layer losses and mixing losses associated with the tip clearance flow. These losses can be detected as entropy increases between the flow at the rotor inlet and exit. With the entropy of the inlet flow unaffected by the increase in tip clearance (see Appendix C), the change in entropy distribution at the rotor exit with tip clearance increase would help locate the regions of increased losses leading to a drop in adiabatic efficiency. Figure 4.7 is a contour plot of the difference in static entropy between nominal and high tip clearance at the rotor trailing edge plane. Small ellipses on the figure highlight regions with entropy increase (+) or decrease (-) as the tip clearance increases.

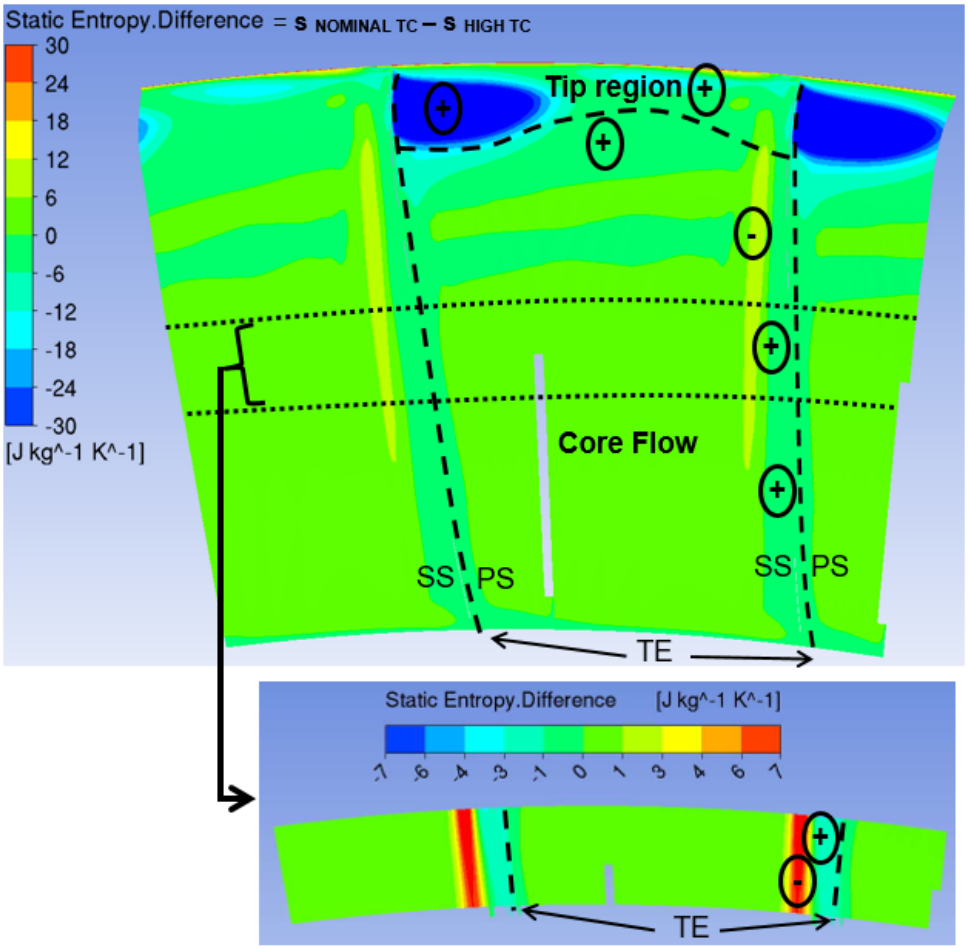

Figure 4.7: Difference in static entropy between nominal and high tip clearance at the rotor trailing edge plane

In the tip region, there is a significant entropy rise with tip clearance increase. In the lower span region, while there is naturally no change in the entropy of the core flow, the region in the vicinity of the blade suction side is characterized by a thin zone of entropy gain next to another thinner region of entropy loss, with the magnitude of entropy variation an order of magnitude below that in the tip region. With the tip region dominating in both size (mass flow) and entropy gain magnitude over the thin region of entropy loss in the lower span, there is a net entropy gain. It can thus be concluded that *the sensitivity to tip clearance of the total-to-total efficiency is mainly driven by the tip region.*

The source of the large entropy gain in the tip region with tip clearance increase can be explained by the presence of extensive double leakage as shown by the tip clearance streamlines at one span in Figure 4.8. As the tip clearance increases, the amount of double leakage inevitably rises, leading to larger tip clearance mass flow with a more perpendicular velocity relative to the core flow [7]. The result is a larger tip clearance flow region/tip vortex as evidenced in Figure 4.9 by the change in the extent of the high entropy region in the tip at the rotor trailing edge between the nominal and large tip clearance.

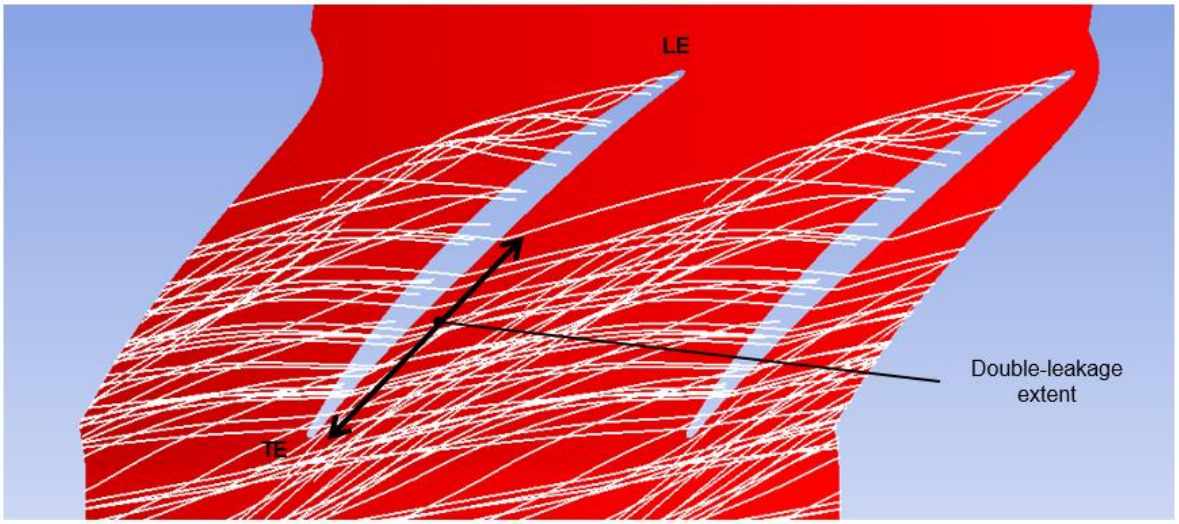

Figure 4.8: Double-leakage extent at the rotor tip plane at nominal tip clearance

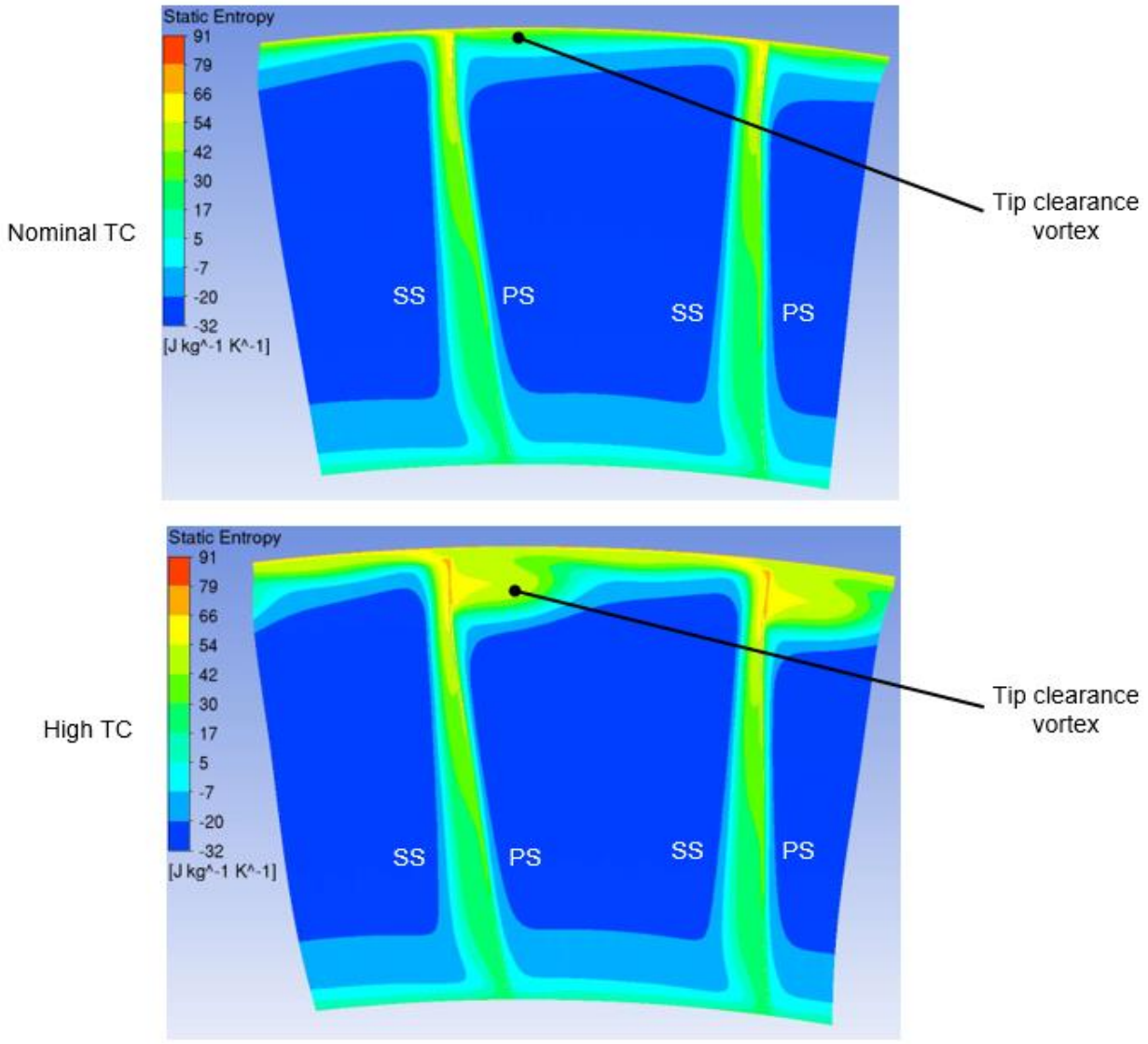

Figure 4.9: Tip clearance vortex growth at the rotor trailing-edge plane as the tip clearance increases

As for the entropy loss/gain region near the blade suction side in Figure 4.7, it is associated with the change in boundary layer thickness on the suction side. As the tip blockage region expands with increased tip clearance, more flow is diverted toward the lower span resulting in a streamwise velocity increase in the core flow. This velocity increase (which is shown by the relative Mach number contours in Figure 4.10 to be more prominent near the suction side) reduces the size of the suction side boundary layer, leading to lower entropy in the zone where the outer part of the boundary layer was located at lower tip clearance. At the same time, the larger velocity gradient

near the blade surface results in larger viscous losses, explaining the parallel layer of increased entropy.

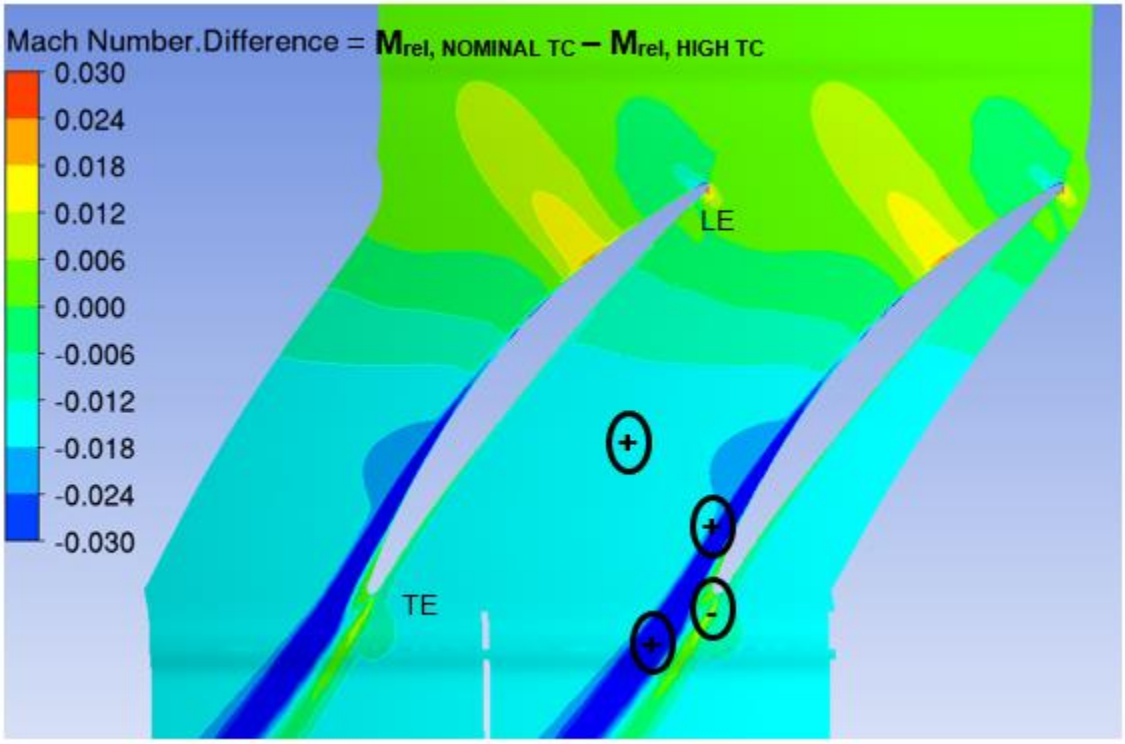

Figure 4.10: Variation in relative Mach number between nominal and high tip clearance at mid-span plane

4.4 Variation of stall margin with tip clearance

This section will infer the stall inception mechanisms associated with the baseline rotor at the three tip clearances by looking at tip flow characteristics. This exercise will provide some insights into the mechanisms behind the degradation of the stall margin with increasing tip clearance. In principle, an extremely costly transient full-annulus simulation at the stall point is required to determine with certainty the stall inception mechanism for each case. As this is very much beyond the computational capability of most organizations in terms of computational time and resources, the stall inception type will be inferred through the procedure proposed by Vo et al. [16]. This method consists of monitoring the position of the interface between the incoming and tip clearance flow at the blade tip section (as illustrated in Figure 2.11). This incoming/tip clearance flow interface (sometimes simply referred to in the current thesis as *interface*) can be easily identified

through entropy contours at the blade tip plane as the line of very high entropy gradient delimiting the low-entropy incoming flow region from the high entropy tip clearance flow region. Its position is determined by the momentum balance between the incoming and tip clearance flows. At the design point, the interface is still inside the blade passage. As the mass flow decreases, the momentum of the incoming flow decreases while that of the tip clearance flow increases (due to increased blade tip loading from increased incidence) such that the interface moves upstream toward the leading edge plane. When this incoming/tip clearance flow interface reaches the blade tip leading edge plane, tip clearance fluid spills below the blade tip leading edge into the adjacent blade passage (as shown in Figure 2.12). If this criterion is satisfied at the simulated *stall point* (i.e. the point at a mass flow below which a drastic fall of the total-to-total pressure ratio occurs on the simulated speedline), then spike stall inception occurs, if not (i.e. the interface is still inside the blade passage), it is modal stall inception.

While Vo et al. [16] stated that both of the proposed stall criteria need to be present for spike stall inception to occur, their work also showed that unless the tip clearance is unusually small, the other criterion (trailing edge backflow) usually occurs at a larger mass flow than the leading edge spillage criterion. Consequently, in most cases, the leading edge spillage criterion is the limiting criterion for spike stall inception.

Figure 4.11 plots the entropy contours at the blade tip plane of the baseline rotor at the stall point for each of the three simulated tip clearances. At nominal and medium tip clearances, the interface between the incoming flow and tip clearance flow is still inside the blade passage, from which one can infer modal stall inception. However, one can observe that the interface is closer to the leading edge plane at medium tip clearance even though the mass flow is higher (lower stall margin, as indicated in Figure 4.4) than that at nominal tip clearance. This fact indicates that the strength of the tip clearance flow has grown with increasing tip clearance to produce higher tip blockage. This rise in tip blockage causes the leveling-off (reaching zero slope) of the total-to-static pressure rise speedline to occur at a higher mass flow, leading to an earlier modal stall and thus reducing stall margin.

At the stall point for large tip clearance, which occurs at an even higher mass flow (lowest stall margin according to Figure 4.4), the interface is at the leading edge plane, signaling a spike stall inception. This indicates that the strength of the tip vortex has grown further between the medium

and large tip clearance, causing spike inception to occur even before the leveling-off of the total-to-static pressure rise speedline and modal stall inception.

In summary, the growth in the strength of the tip clearance flow that results from an increase in tip clearance is responsible for the decrease in stall margin of the baseline rotor.

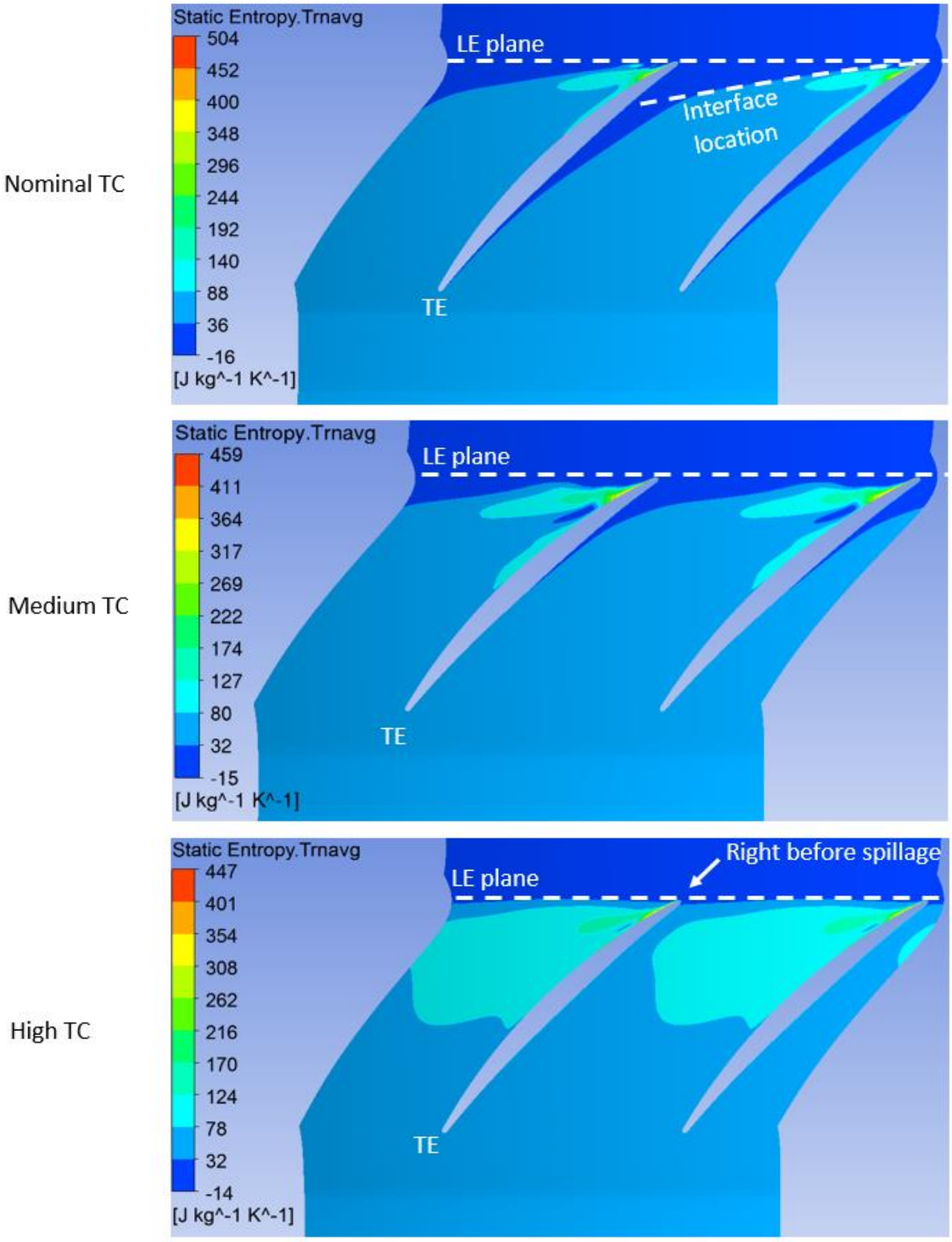

Figure 4.11: Entropy contours in blade tip plane of the baseline rotor at the simulated stall points for the three tip clearances

CHAPTER 5 DESENSITIZING CASING TREATMENT

5.1 Casing treatment design

In order to design the desensitizing casing treatment for the baseline rotor, the negative saw-tooth shaped grooves configuration proposed by Cevik et al. [23] is used and refined for this rotor through a parametric study with respect to the four geometric parameters associated with this casing treatment. As illustrated in Figure 5.1, these geometric parameters are the indentation width, grooves number, groove depth and indentation location (of the first groove with respect to the rotor tip leading edge).

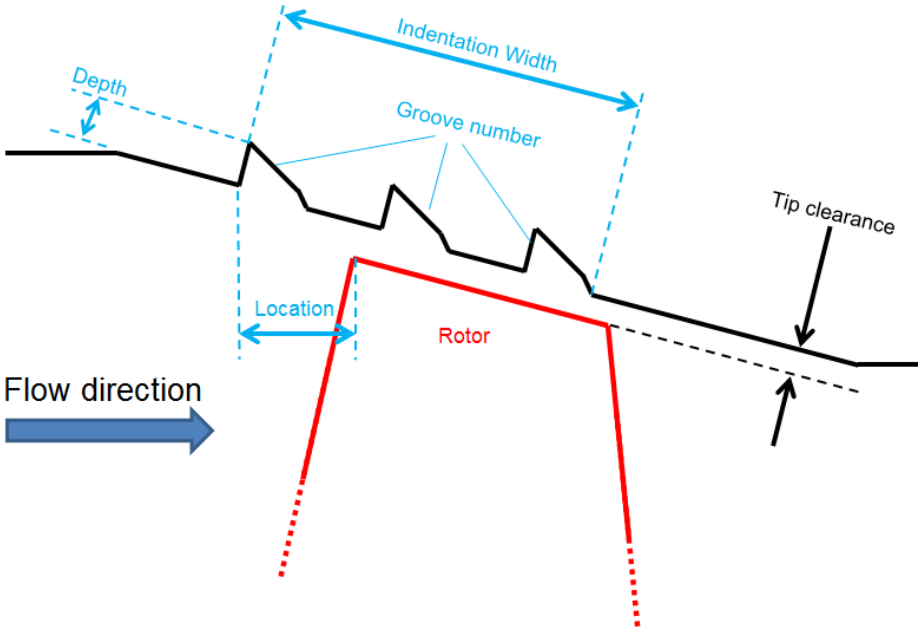

Figure 5.1: Geometric elements iterated in the parametric study used to design the casing treatment

For each geometric parameter, the variations of nominal total-to-total pressure ratio and efficiency and their sensitivities to tip clearance size, are obtained from CFD simulations at design mass flow. The sensitivity of total-to-total pressure ratio and efficiency is taken as the change in their respective values from nominal (minimum) tip clearance (0.74% span) to high tip clearance (2.57% span). From the trends observed, a final casing treatment configuration is obtained that takes into account the geometrical manufacturing constraints for this compressor rig. The stability would be checked for the final design only.

In the plots presented in this section, the four geometric parameters of the casing treatment are normalized by the rotor mean chord and only the performance and sensitivity parameters of the rotor are presented. The total-to-total pressure ratio and efficiency of the rotor are normalized by their respective design values (i.e. values for the rotor without casing treatment at nominal tip clearance). For reference, the sensitivity of the normalized total-to-total pressure ratio and efficiency for the baseline rotor without casing treatment are -0.003 and -0.013, respectively. Finally, homologous graphs related to the same performance parameter are placed on the same scale, so as to easily compare the dependency of the same performance parameter on different geometric elements.

Effect of indentation width

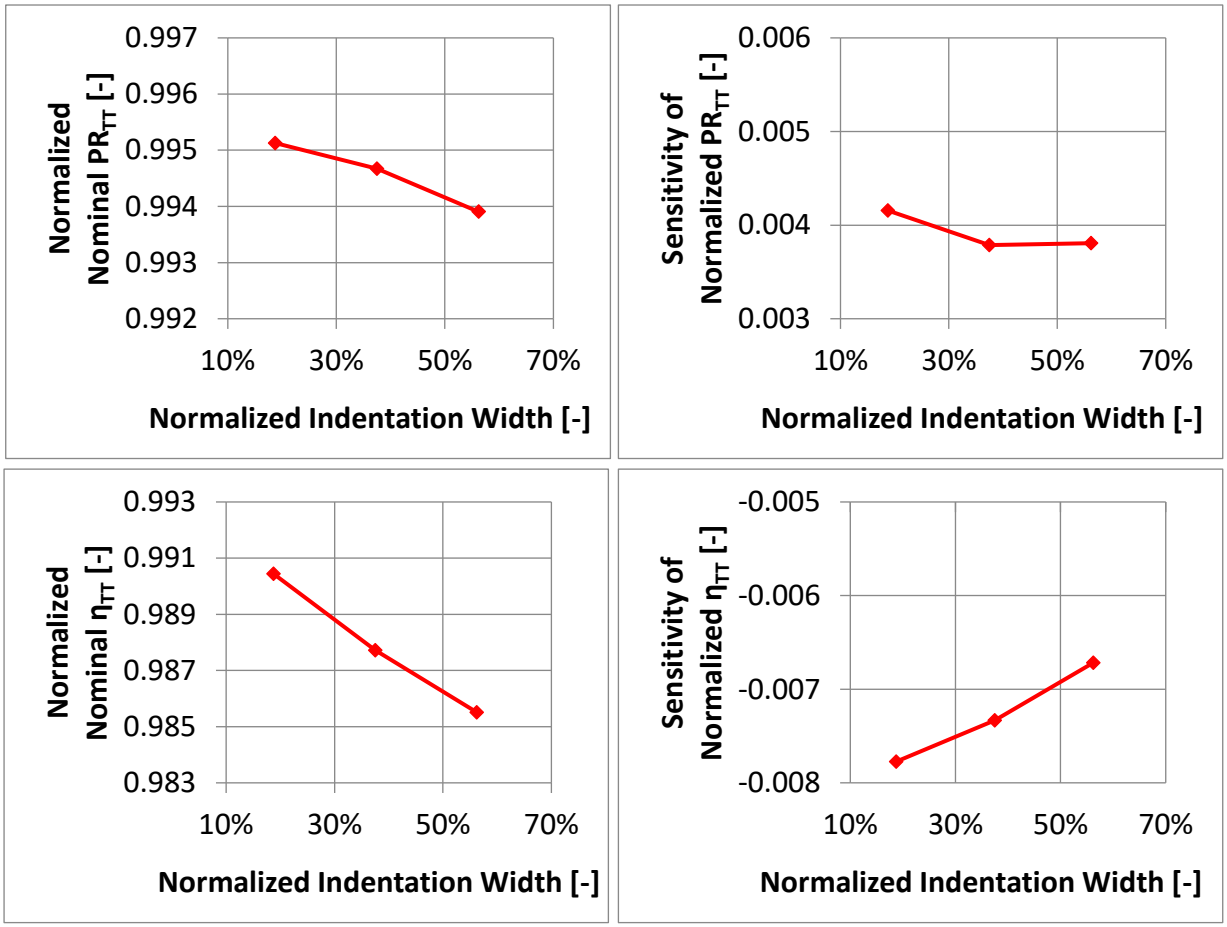

Figure 5.2: Parametric study on the indentation width

Figure 5.2 presents the variation of the performance and sensitivity parameters with the indentation width. The results indicate that a penalty for both the pressure ratio and the efficiency is present

regardless of the indentation width chosen. However, this penalty increases with the indentation width. In terms of the sensitivity parameters, the pressure ratio sensitivity is positive (pressure ratio rises with tip clearance) in the presence of this casing treatment, which is somewhat counter-intuitive, and drops very slightly with increasing indentation width. On the other hand, efficiency sensitivity is always negative but improves as the indentation width increases.

In summary, a low indentation width minimizes the nominal performance penalty while a high indentation width improves the efficiency sensitivity.

Effect of grooves number

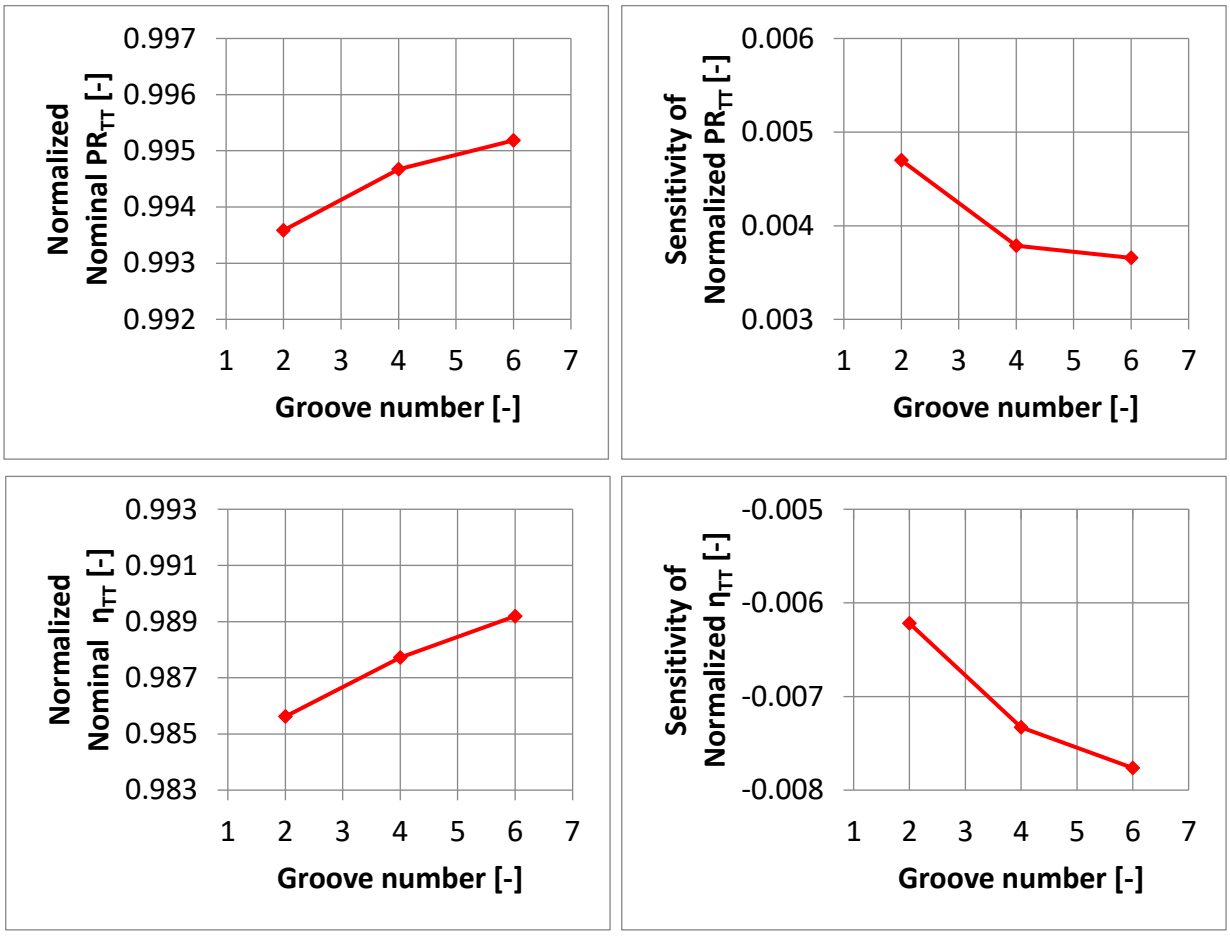

Figure 5.3: Parametric study on the grooves number

The results of the parametric study made on the grooves number are shown in Figure 5.3. Based on the left plots, the presence of the casing treatment introduces a nominal performance penalty that can be reduced by increasing the number of grooves. The right graphs show that the pressure

ratio sensitivity is once again positive while the efficiency sensitivity is negative regardless of the grooves number. Both sensitivities improve as the number of grooves decreases.

In summary, while a high number of grooves helps to reduce nominal performance penalty, better sensitivities are achieved with less grooves.

Effect of groove depth

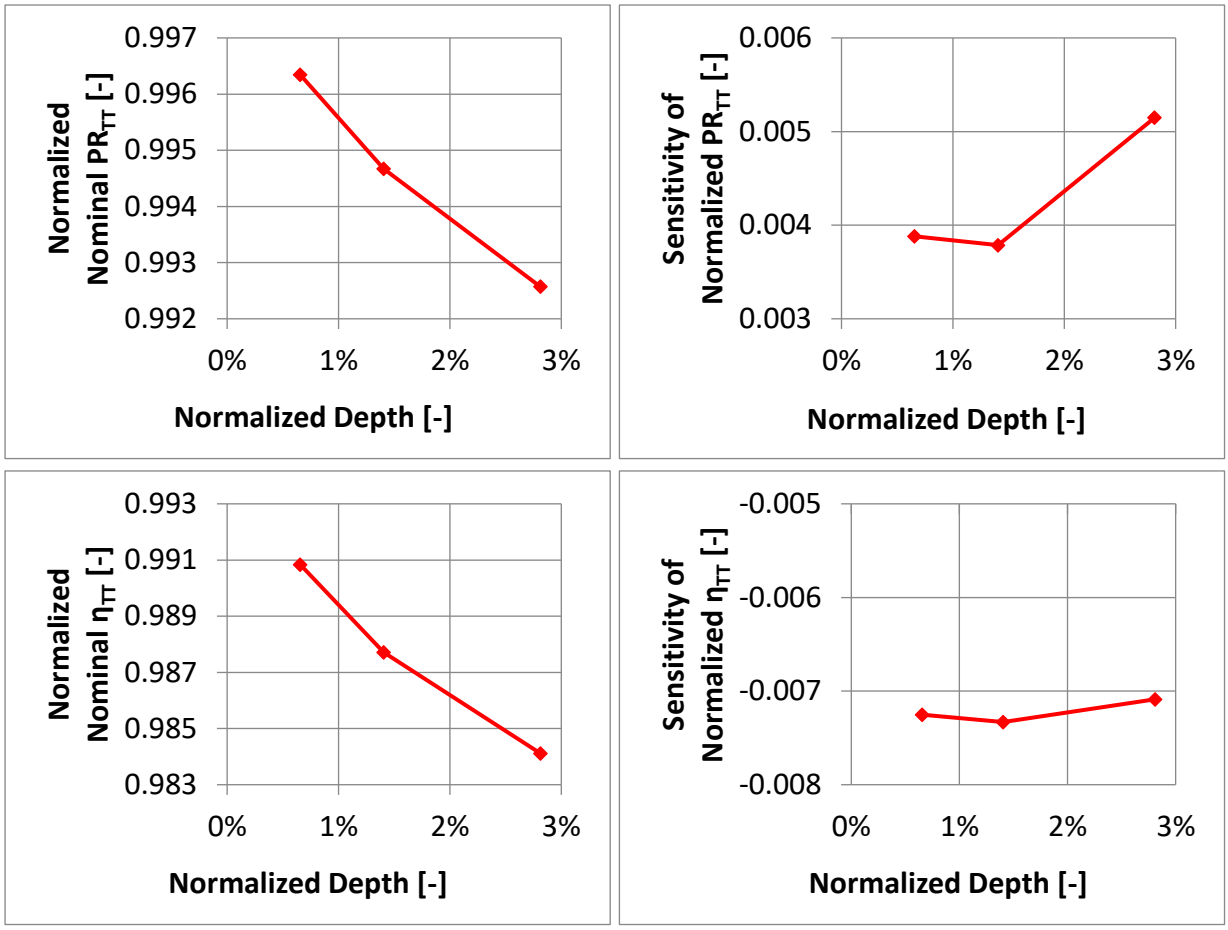

Figure 5.4: Parametric study on the grooves depth

Figure 5.4 shows the variation of the performance and sensitivity parameters with the grooves depth. While a nominal performance penalty and positive pressure ratio sensitivity is observed as before, the results indicate that this parameter has a very high impact on nominal performance penalty, only modest impact on pressure ratio sensitivity and negligible impact on efficiency sensitivity. Based on the trends observed, shallow grooves are desirable to achieve the lowest nominal performance penalty without affecting sensitivity (considering that the pressure ratio sensitivity is already positive and does not require further modest improvements).

Effect of indentation location

The results of the parametric study made on the grooves location are illustrated in figure 5.5. The convention for this parameter is that a positive location refers to the start of the first groove being placed upstream of the rotor tip leading edge while a negative location indicates its location being downstream of the rotor tip leading edge. The data indicates that the nominal performance penalty is not affected by the indentation location but that a more upstream location improves pressure ratio and efficiency sensitivity.

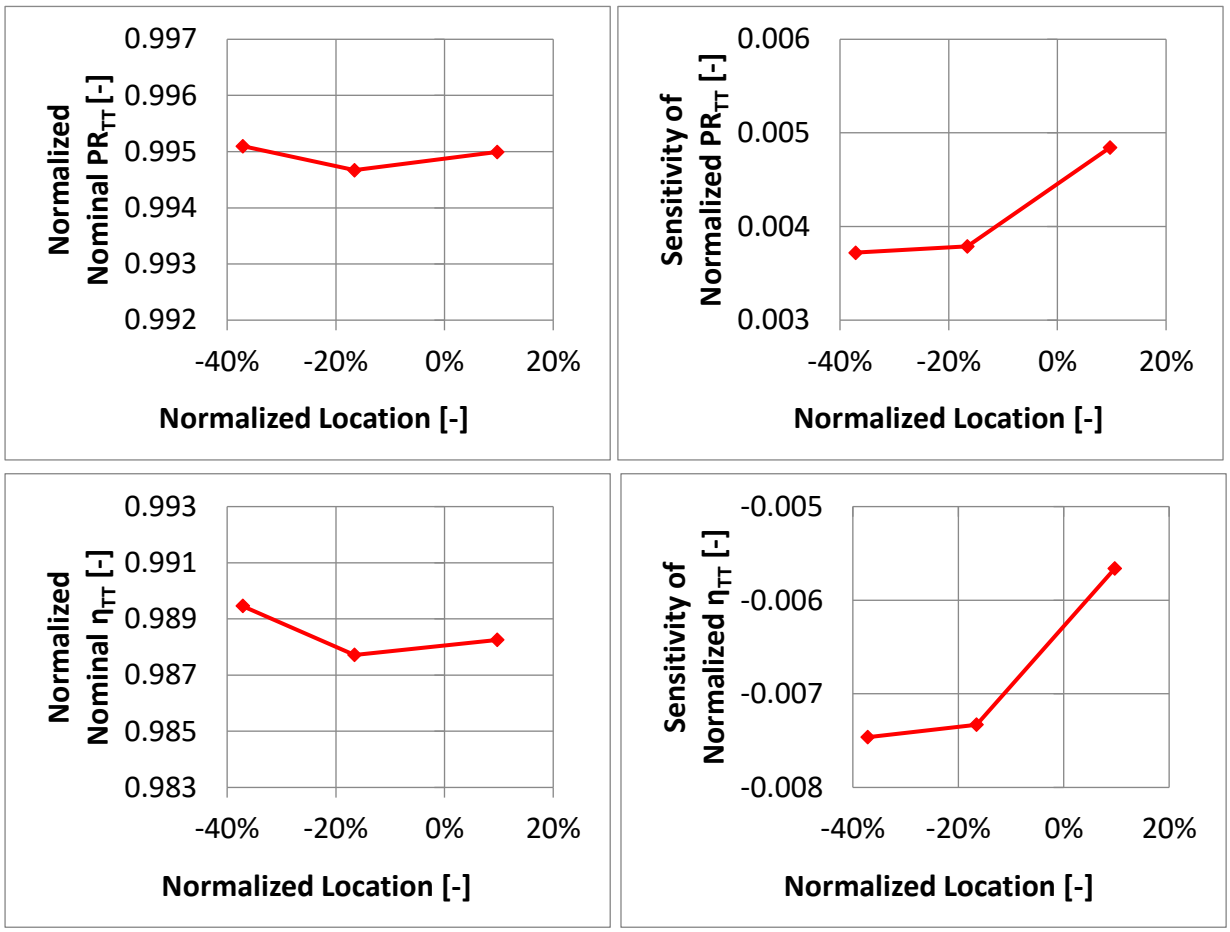

Figure 5.5: Parametric study on the location

Final casing treatment design

The above parametric study for the baseline rotor indicates that the proposed negative saw-tooth circumferential grooves casing treatment will always incur a nominal performance penalty,

produce a positive (reversed) total-to-total pressure ratio sensitivity and can reduce but not desensitize efficiency to tip clearance increase. Furthermore, there is usually a trade-off between nominal performance penalty and improvement in sensitivity.

While all the casing treatment configurations from the above parametric study reduce performance sensitivity, none of them respects nominal performance constraints of 0.25% penalty in total pressure ratio and efficiency. Consequently, the observed trends are used to combine the variations in geometrical parameters to obtain a suitable casing treatment design with the lowest possible nominal performance penalty. This exercise yields a negative saw-tooth circumferential grooves casing treatment with a low indentation width (18.7% chord), a high number of grooves (6) and a low depth (0.7% chord). For the grooves location, since the impact on the nominal performance is marginal while the possible improvements in sensitivity to tip clearance are significant, a location upstream of the rotor tip leading edge (9.7% chord) is selected. This design is called "Optimized" and its performance and sensitivity to tip clearance are summarized in table 5.1. This design achieves the highest nominal performance of all configurations simulated so far, with good sensitivity improvement (not the best achievable sensitivity given the compromise between sensitivity and nominal performance). Due to manufacturing constraints, the indentation width is increased from 18.7% to 37.5% chord to form the final design. This final design is shown in Figure 5.6 and its nominal performance and sensitivity are also shown on Table 5.1.

Table 5.1: Results obtained for the optimized and final designs of the casing treatment

Design name	Normalized nominal PR_{TT}	Normalized nominal η_{TT}	Normalized sensitivity of PR_{TT}	Normalized sensitivity of η_{TT}
Optimized	0.996	0.993	0.004	-0.008
Final design	0.997	0.993	0.004	-0.007

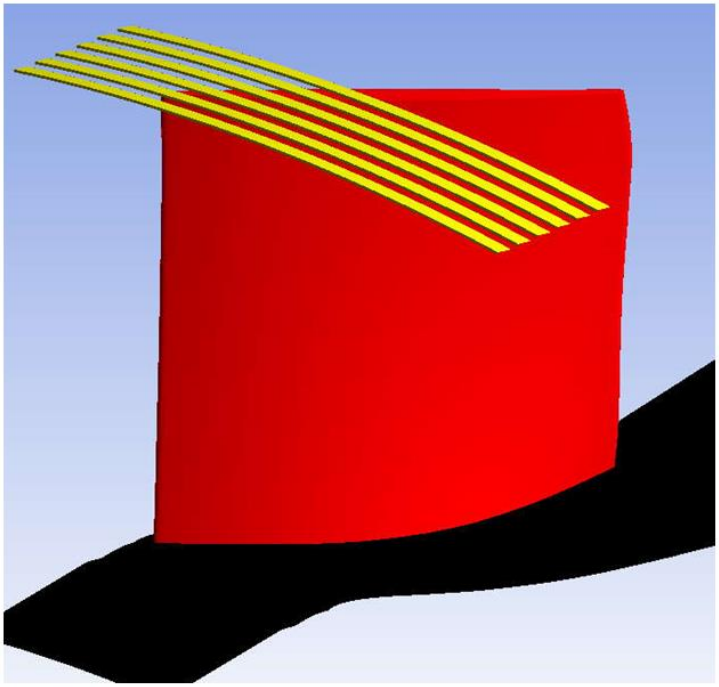

Figure 5.6: Final design of the casing treatment

5.2 General Assessment of Final Casing Treatment

Variations of total-to-total pressure ratio, total-to-total efficiency and stall margin with tip clearance are shown respectively in figures 5.7, 5.8 and 5.9 for the baseline rotor with and without the final casing treatment design.

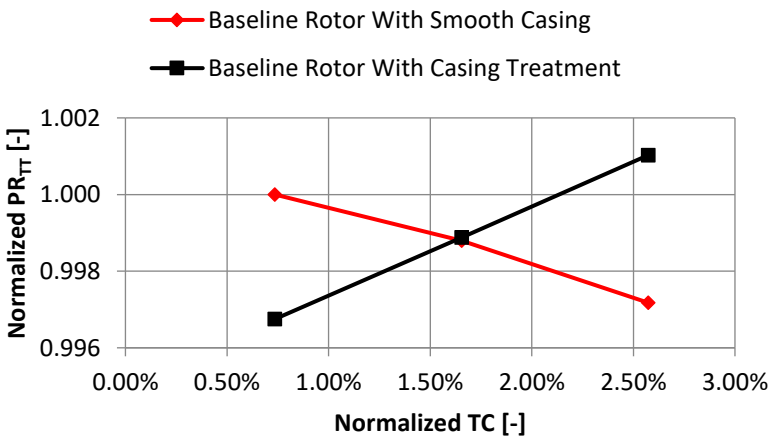

Figure 5.7: Design point total-to-total pressure ratio VS tip clearance

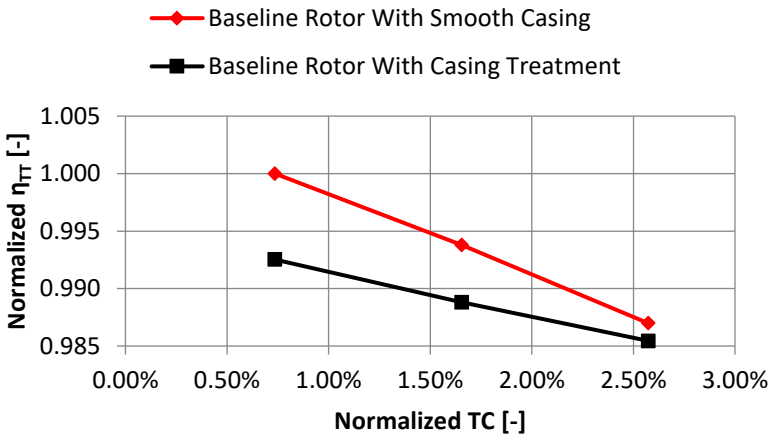

Figure 5.8: Design point total-to-total efficiency VS tip clearance

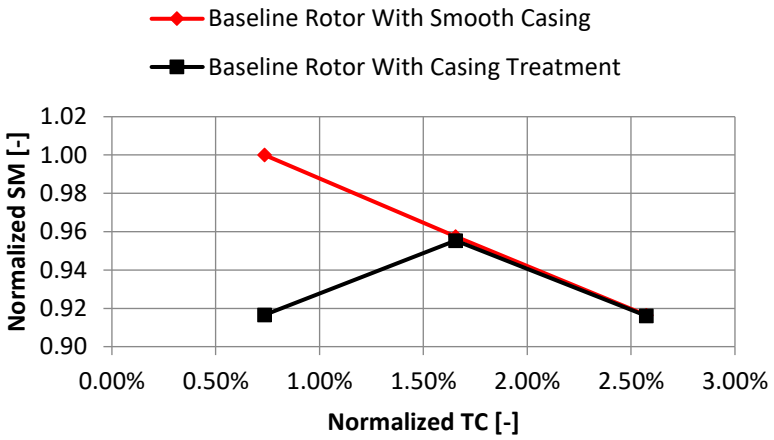

Figure 5.9: Stall margin VS tip clearance

These results from the CFD simulations indicate that the addition of the casing treatment to the baseline rotor causes a very small nominal total pressure ratio penalty of 0.33%, but reverses the total pressure ratio sensitivity with an increase of 0.43% from nominal to high tip clearance. In terms of efficiency, the final casing treatment incurs a 0.75% penalty but reduces the (negative) efficiency sensitivity. As such, the rotor loses 0.71% in efficiency from nominal to large tip clearance with this casing treatment instead of 1.30% without casing treatment. While the nominal pressure ratio and efficiency penalties associated with the final casing treatment fall short of the design constraints, they are the best that could be achieved for this casing treatment over this rotor. Finally, while the casing treatment decreases nominal stall margin by 8.3%, it improves its

sensitivity to tip clearance such that the stall margin increases between nominal and medium tip clearance and comes back to the nominal value at high tip clearance.

The next three sections investigate the source of the observed effect of the final casing treatment on the performance and sensitivity parameters.

5.3 Variation of pressure ratio with tip clearance

To investigate the source of pressure ratio penalty incurred by the presence of the final casing treatment, Figure 5.10 plots the spanwise distribution of change in pitch (mass)–averaged total pressure at the rotor outlet between the smooth shroud and the final casing treatment. While there is a small region (outer 3% span) of gain in exit total pressure, the rest of the tip region (80% to 97% span) experiences a significant reduction in exit total pressure. In the lower span region, a smaller drop in exit total pressure occurs. With the upstream inlet total pressure unchanged, the loss in exit total pressure experienced by the large majority of the span (and mass flow) translates into a total pressure penalty with the addition of the casing treatment.

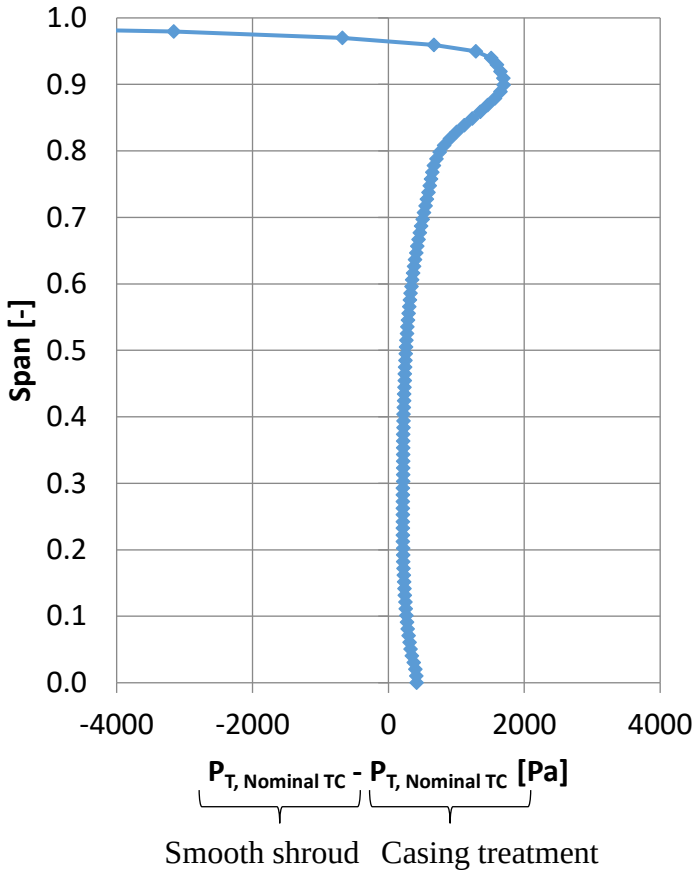

Figure 5.10: Difference in outlet total pressure pitch (mass)-averaged on the rotor trailing edge plane in the presence/absence of the final casing treatment

The source of local exit total pressure gain and loss on Figure 5.10 can be explained through Figure 5.11 which plots the contours of vorticity at the rotor trailing edge plane without and with casing treatment to highlight the change in the tip vortex. This figure indicates that the addition of the casing treatment causes the tip vortex to become more intense (larger vorticity) and to extend further toward the lower span but remaining much closer to the suction side than in the smooth casing case. This is consistent with the study by Cevik [8] which showed that the grooves re-inject the tip clearance leakage in the passage close to the suction side causing more mixing between that tip leakage and the incoming flow. This explains the radially larger and stronger tip clearance vortex observed in Figure 5.11. The enlarged region of tip clearance flow has higher mixing loss. Moreover, the lower streamwise velocity and higher trailing edge flow deviation in this region translates into lower flow turning (in the stationary frame) as shown in the left velocity triangles in Figure 5.12, resulting in less work done on the flow. These two factors combine to explain the exit

total pressure loss for the 80-97% span region observed in Figure 5.10. In parallel, the retreat of the tip vortex away from the pressure side and toward lower spans leaves more of the passage pitch in the upper span very close to the shroud free of tip clearance flow and its associated streamwise velocity deficiency. This explains the exit total pressure gain with casing treatment for the 97-100% span region.

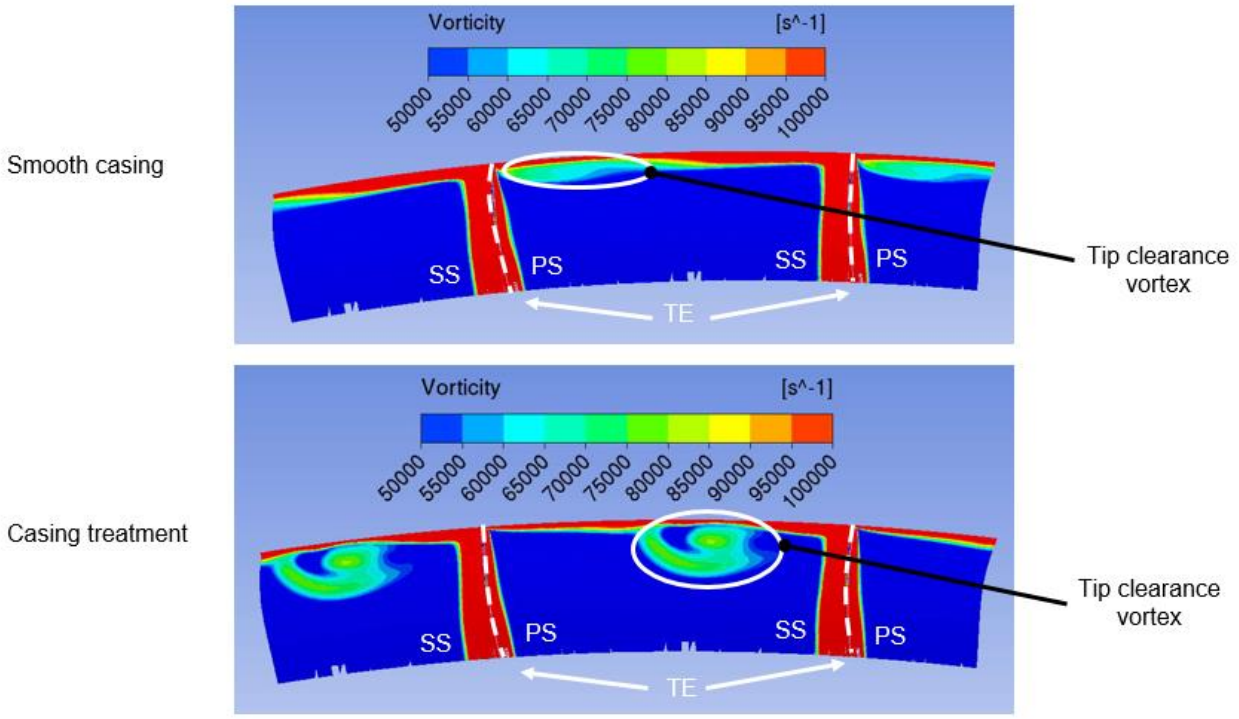

Figure 5.11: Vorticity at rotor trailing edge between 70% and 100% span in the presence/absence of the final casing treatment

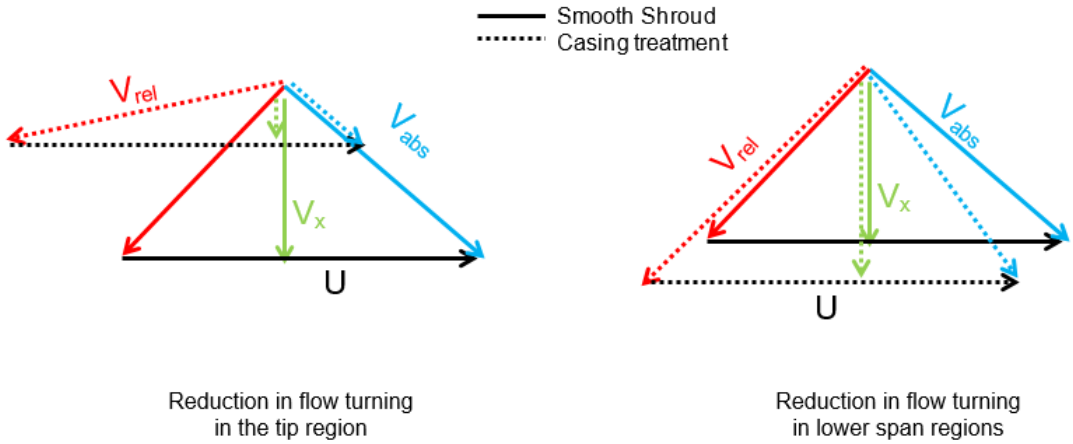

Figure 5.12: Reduction in flow turning in presence of the final casing treatment

Finally, in the lower span region, the enlarged tip vortex in the presence of the casing treatment diverts more flow toward the lower span leading to an increase in the relative streamwise velocity. As shown in the right velocity triangles in Figure 5.12, this effect leads to reduced flow turning (in the stationary frame) and thus to lower work on the flow and, by extension, lower exit total pressure for this region as observed in Figure 5.10.

Despite the total pressure ratio penalty, a very peculiar and counter-intuitive effect of the chosen casing treatment is its reversal of the total pressure ratio sensitivity, making the total pressure ratio increase with increasing tip clearance. Given the relatively insignificant changes in rotor inlet total pressure (see Appendix C), the rotor exit total pressure is used to investigate this effect. Figure 5.13 plots the contours of the change in rotor exit total pressure between the nominal and high tip clearance sizes in presence of the final casing treatment. Small ellipses on the figure highlight regions with total pressure gain (+) or loss (-). In the tip region, high-magnitude losses in total pressure occur near the shroud (mostly in the middle of the blade passage) while high-magnitude gains take place underneath. In the lower span region, the bulk of the core flow exhibits low-magnitude total pressure gains although a tiny area close to the blade suction side experiences total pressure losses. It is also noted that the pressure gain in the core flow increases as one gets closer to the tip vortex. From the magnitude of total pressure changes and respective areas (indicative of mass flow) of the loss and gain zones in the tip region, one can infer that there is a net loss in exit total pressure in this region. Therefore, the positive sensitivity of the pressure ratio must stem from the exit total pressure gain in the core flow, which contains the bulk of the mass flow.

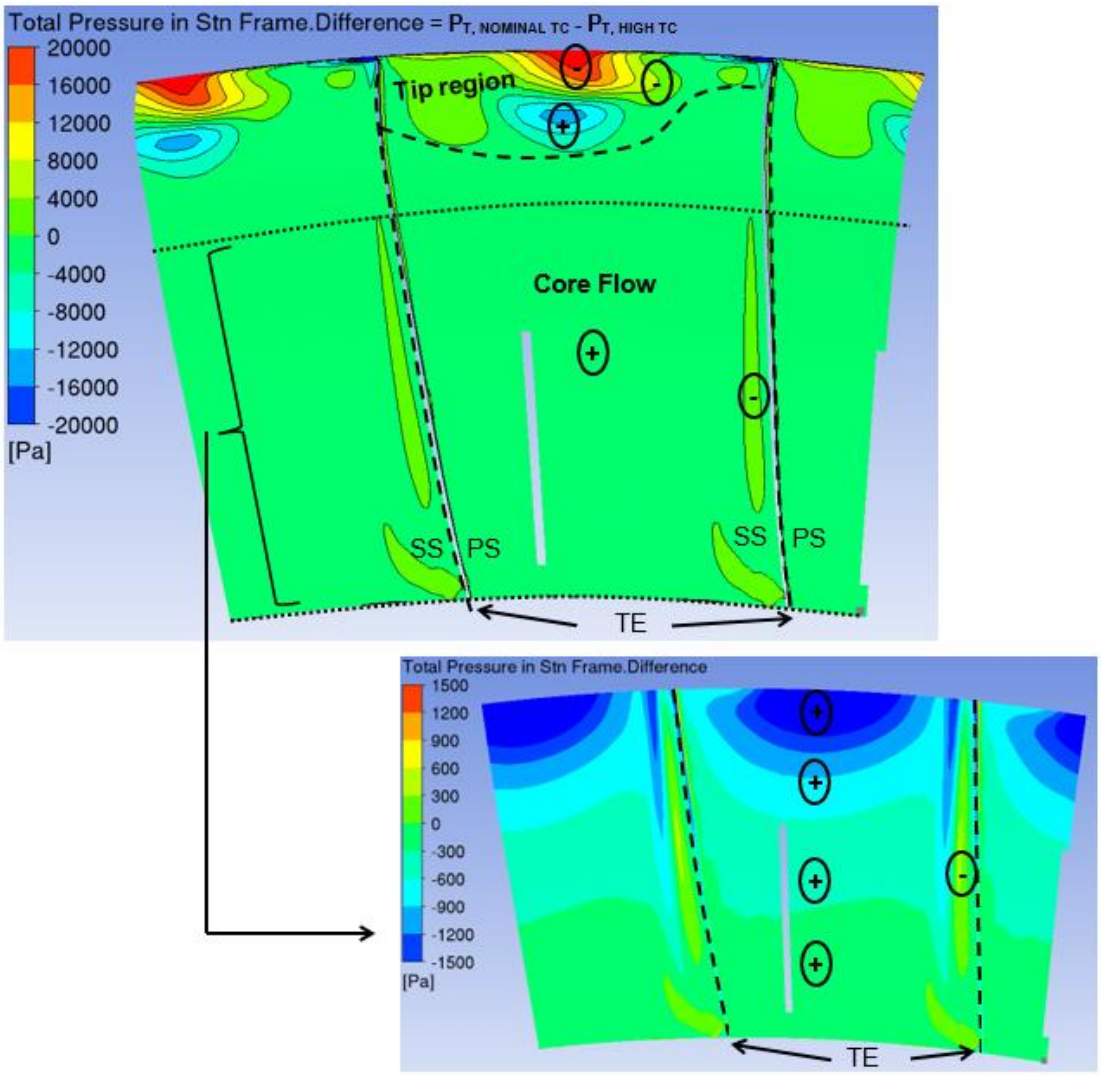

Figure 5.13: Difference in total pressure between nominal and high tip clearance at the rotor trailing edge plane with the final casing treatment

Thus, the source of the positive sensitivity of total pressure ratio from the casing treatment lies in the source of the total pressure increase in the core flow. Figure 5.14 plots the contours of spanwise velocity at the rotor exit plane with casing treatment at the nominal and maximum tip clearance. The tip vortex is indicated by adjacent regions of positive and negative spanwise velocity. These contours indicate that the strong tip vortex induced by the casing treatment grows in size (both circumferentially and radially) and strength as the tip clearance increases. This observation is consistent with more tip clearance fluid being aspirated and re-injected by the grooves in the adjacent blade passage at higher tip clearance. As shown by the arrows, the tip vortex induces rotation in the surrounding fluid in the core flow driving it toward the suction side. This effect is

accentuated as the tip vortex grows larger and stronger with increased tip clearance as indicated by the increase in spanwise velocity gradient in Figure 5.14. The deviation of the core flow toward the suction side leads to a reduction in exit relative flow angle and, as shown in the velocity triangles in Figure 5.15, an increase in flow turning (in the absolute frame). This leads to more work on the flow and, by extension, higher total exit pressure. The induced rotation in the core flow and resulting flow deviation increase as one gets closer to the tip vortex explaining the higher exit total pressure gain in the core flow closer to the vortex as observed in Figure 5.13.

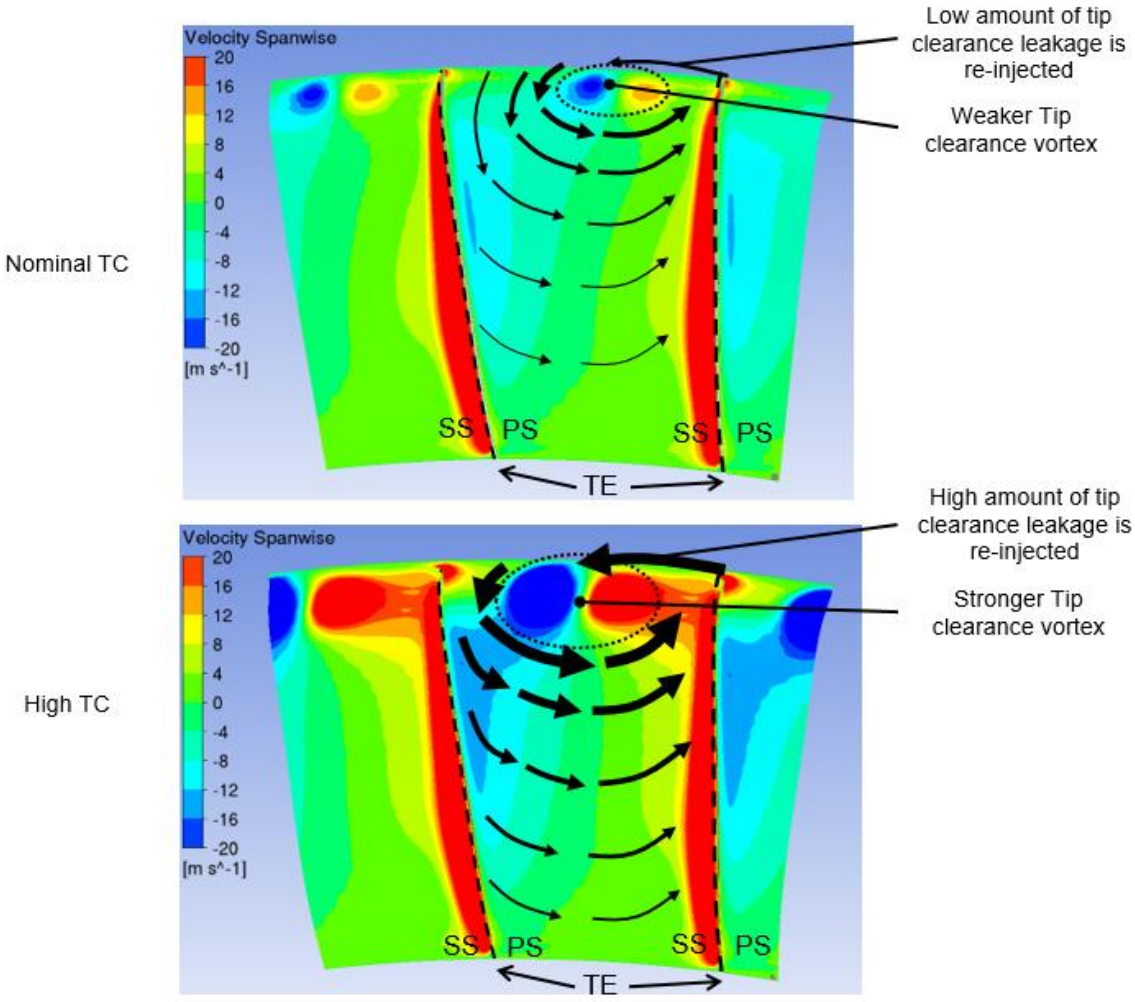

Figure 5.14: Spanwise velocity at the rotor trailing edge plane in the presence of the final casing treatment at nominal and large tip clearance

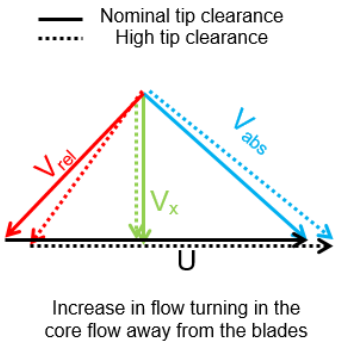

Figure 5.15: Change in velocity triangle as the tip clearance increases in the core flow away from the blades in the presence of the final casing treatment

5.4 Variation of efficiency with tip clearance

This section looks into the effect of the casing treatment on total-to-total efficiency. As mentioned in chapter 4, efficiency is directly related to losses in the blade passage and thus entropy changes across the rotor.

To investigate the source of nominal efficiency penalty brought about by the casing treatment, Figure 5.16 presents the spanwise distribution of difference in outlet static entropy between the baseline (smooth shroud) case and the case with the final casing treatment. The results show that virtually all the losses are generated in the tip region (85-100% span). In this region, the small portion near the shroud (97-100% span) shows an entropy drop (efficiency gain) with casing treatment while the larger portion underneath (85-97% span) shows high-magnitude entropy gain (efficiency drop). For the 97-100% span region, the retreat of the tip vortex toward the suction side and lower spans induced by the casing treatment (see Figure 5.11) leaves much of the passage pitch in the upper span very close to the shroud free of tip clearance flow. This explains the drop in entropy near the shroud. For the 85-97% span region, the radially larger and stronger tip clearance vortex induced by radial re-injection of tip clearance flow by the casing treatment grooves near the suction surface (observed in Figure 5.11) and its associated mixing loss explain the higher entropy. This mixing loss is thus responsible for the nominal efficiency penalty associated with this casing treatment.

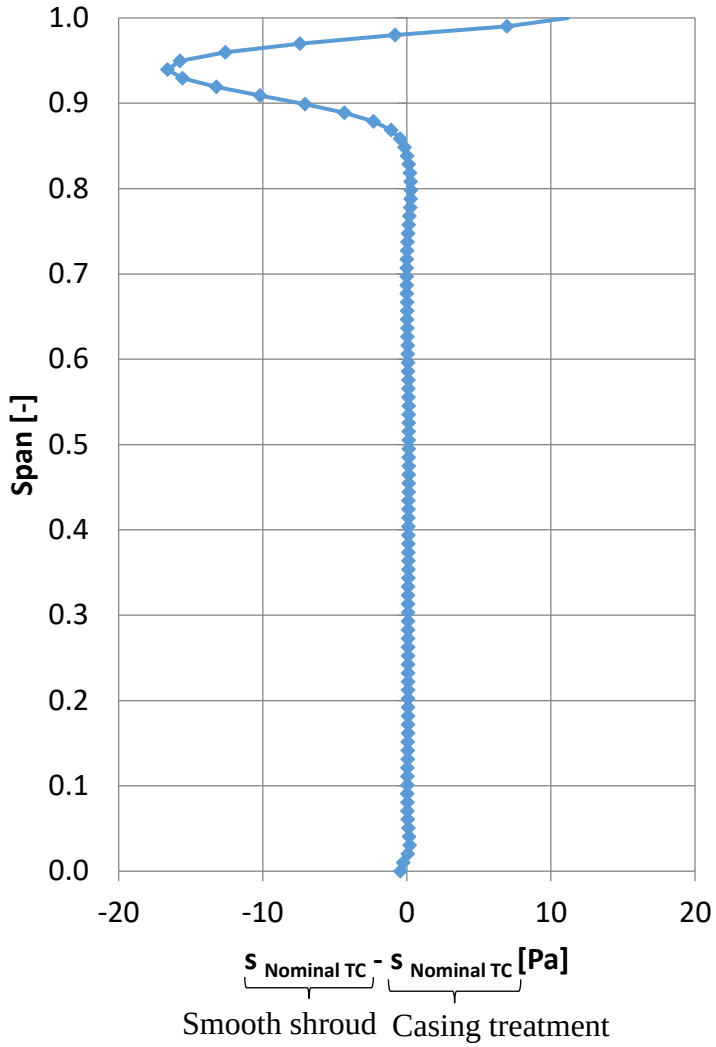

Figure 5.16: Difference in outlet static entropy pitch-averaged on the rotor trailing plane in the presence/absence of final casing treatment

Next, the source of the improvement in efficiency sensitivity is investigated. Since the inlet entropy change with tip clearance size is insignificant (see Appendix C), the entropy at the rotor exit plane can be used to investigate the change in efficiency. Figure 5.17 plots the contours of the change in rotor exit static entropy from nominal to high tip clearance in the presence of the final casing treatment. The data indicates that virtually all of the changes in entropy occur in the tip region as the tip clearance increases. Figure 5.18 compares the entropy contours between 70% and 100% span at different axial planes along the blade passage at nominal and high tip clearance for the smooth casing and casing treatment configurations. One can see that the growth of the tip clearance flow region/ tip vortex over the same tip clearance range is less significant in the presence of the

casing treatment. The reason is that the casing treatment completely removes double tip leakage as shown by the tip leakage flow streamlines taken in the tip region at nominal tip clearance in Figure 5.19. As explained by Erler [7], the reduction/absence of double leakage flow at nominal tip clearance leads to lower increase in double leakage and associated mixing losses, with tip clearance size, thus leading to lower efficiency sensitivity.

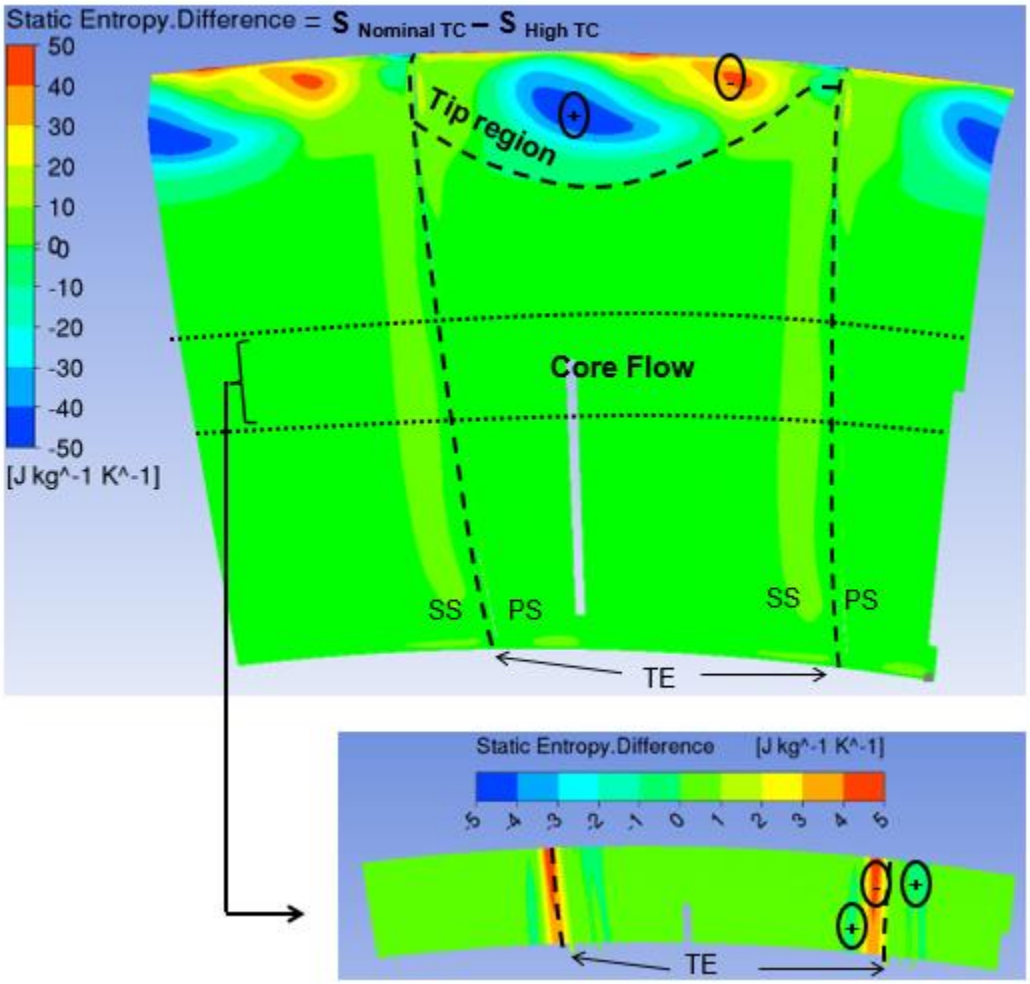

Figure 5.17: Difference in static entropy between nominal and high tip clearance at the rotor trailing edge plane in the presence of the final casing treatment

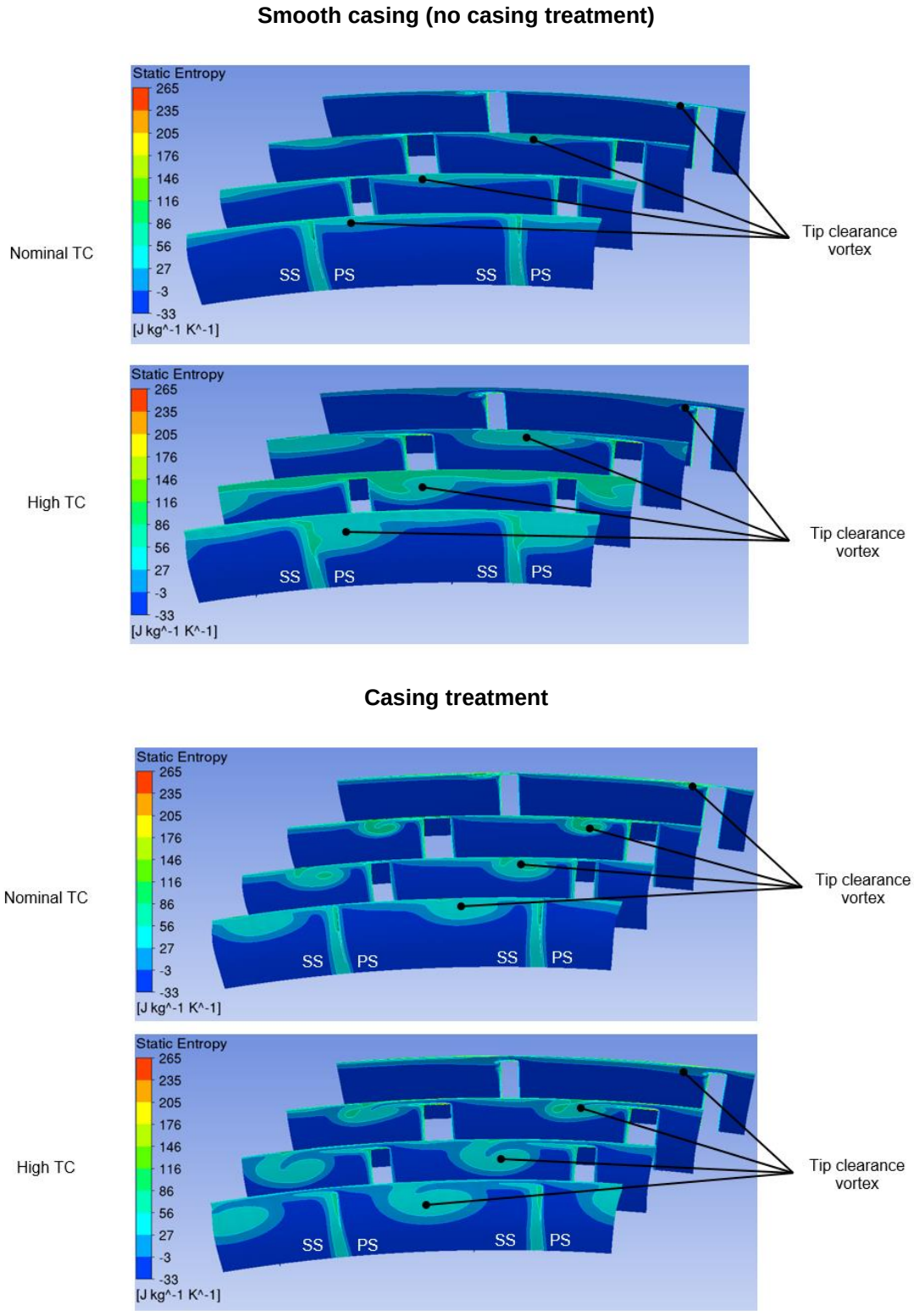

Figure 5.18: Entropy contours between 70% and 100% span at different axial planes for baseline rotor at nominal and large tip clearance with smooth casing and with final casing treatment

Figure 5.19: Double-leakage extent at the rotor tip plane at nominal tip clearance in the presence of the final casing treatment

5.5 Variation of stall margin with tip clearance

Figure 5.9 indicated that the addition of the final casing treatment to the baseline rotor causes a penalty in nominal stall margin, but has virtually no effect on the stall margin (thus stall mass flow) at medium and large tip clearance. To investigate the source of this phenomenon, the effect of the casing treatment on stall margin is thus analyzed through the monitoring of the incoming/tip clearance flow interface as was done in section 4.4 for the baseline rotor with smooth casing. Figure 5.20 shows the entropy contours at the blade tip plane of the baseline rotor with the final casing treatment at the stall point for each of the three simulated tip clearances.

The results show that at nominal tip clearance, a small leading edge spillage already occurred on the adjacent blade, which indicates spike stall inception. However, at the medium and large tip clearance (especially the large tip clearance where the stalling mass flow is the same as that at the small tip clearance, according to Figure 5.9), the incoming/tip clearance flow interface has moved into the blade passage, indicating modal stall inception.

Furthermore, a comparison of Figure 5.20 with Figure 4.11 (case with smooth shroud) at the medium and high tip clearance (same mass flow with or without casing treatment), indicates that the casing treatment moves the incoming/tip clearance flow interface downstream. This is consistent with the reduction/removal of double leakage by the casing treatment as indicated in Figure 5.19. The absence at nominal tip clearance of this effect by the casing treatment on the interface can be explained if the casing treatment, which in this case starts upstream of the leading

edge, allows for the tip clearance flow inside the blade passage to recirculate upstream of the leading edge plane and spill below the adjacent blade tip leading edge, causing a premature stall through spike stall inception. This effect is likely to occur when the blade tip is very close to the shroud (small tip clearance). As the tip clearance increases (as in the medium and large tip clearance cases here), the blade tip leading edge is far enough that this recirculated flow cannot spill below the leading edge blade tip. As a result, the interface at the blade tip plane is back inside the blade passage and stall occurs at a lower mass flow when the tip blockage causes the leveling-off of the total-to-static pressure rise speedline (modal stall inception). This hypothesis would explain the observed nominal stall margin penalty introduced by the casing treatment at nominal tip clearance.

Moreover, the upstream movement of the interface between the medium and large tip clearance in Figure 5.20 indicates that the strength of the tip clearance flow has grown with increasing tip clearance. This produces higher tip blockage and causes the leveling-off of the total-to-static pressure rise speedline to occur at a higher mass flow causing an earlier modal stall and thus reducing stall margin.

Finally, the casing treatment virtually did not change the stall point at the two higher tip clearances (especially at the medium tip clearance where the rotor exhibits modal stall with or without casing treatment) even though it moved the interface inside the blade passage (compared to Figure 4.11). This observation indicates that for the medium-to-large tip clearance range of this rotor, the additional mixing loss generated by the casing treatment neutralizes the reduction in loss from double leakage reduction with regard to the slope of the total-to-static speedline.

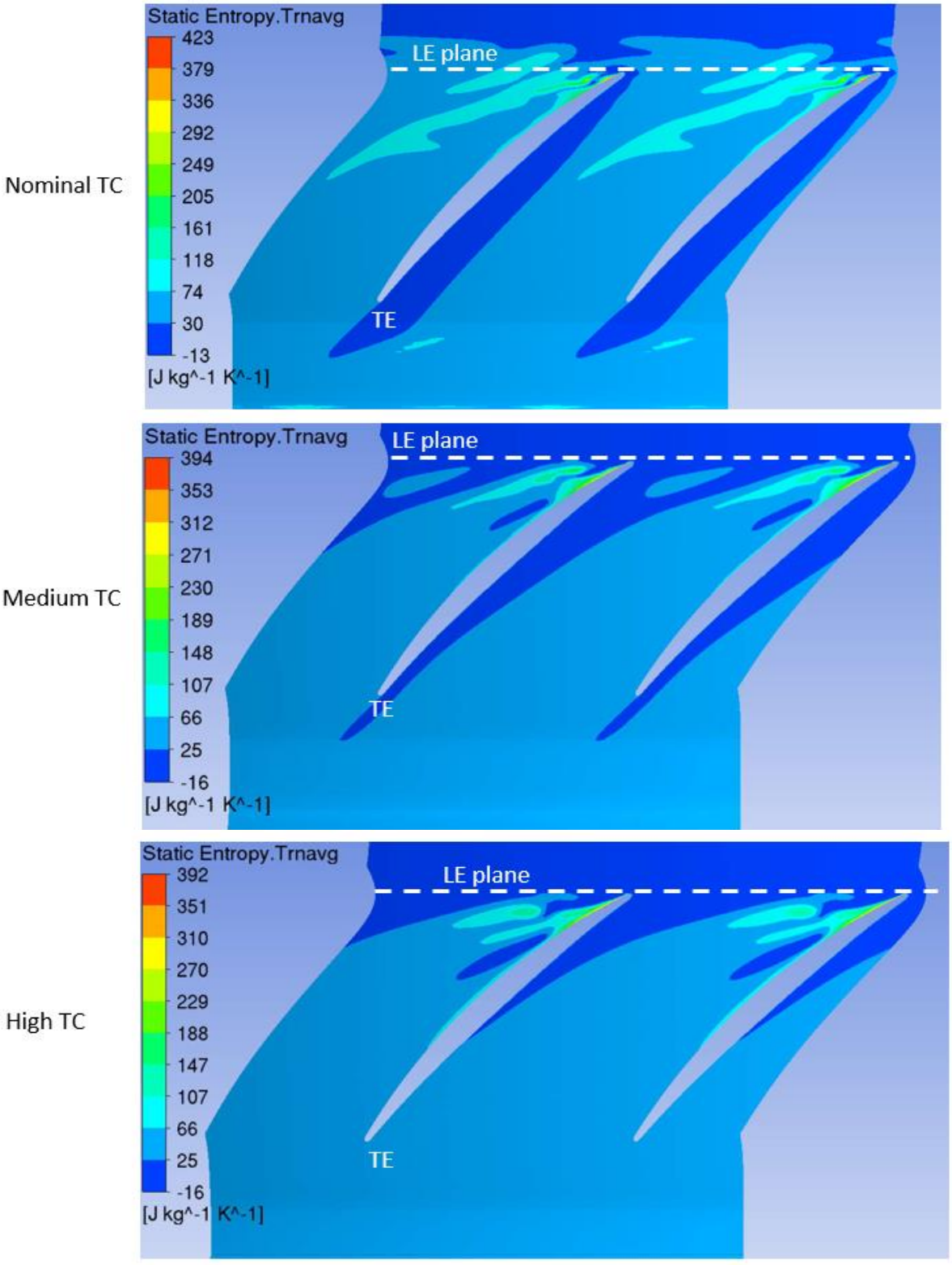

Figure 5.20: Entropy contours in blade tip plane of the baseline rotor with final casing treatment at the simulated stall points for the three tip clearances

CHAPTER 6 DESENSITIZED ROTOR DESIGN

6.1 Initial design

The initial methodology followed the design strategies recommended by Erler [7] from the first phase of this research program, namely full forward chordwise sweep and partial stagger angle reduction. These two strategies exploited the two desensitizing flow features identified by Erler [7] namely reduction of double-leakage and increase of the rotor tip meridional momentum. In this section, these two design strategies are applied to the baseline rotor of the current study. Once again, the design process would focus on the performance only. The stability would be verified only for successful final designs. The terminology used in this chapter to describe stacking-line changes is given in Appendix A.

Full Forward Chordwise Sweep

The full forward chordwise sweep rotor design by Erler [7] had a 20-degrees forward sweep in the stacking line while keeping the same spanwise distribution of the aerodynamic loading as the reference theoretical rotor used. In this study, a parametric study was carried out to determine the optimal chordwise sweep angle to be applied from hub to tip to the baseline rotor with a smooth shroud. Five different sweep angles were tested: 5, 10, 15, 20 and 23 degrees, the last being the limit beyond which the rotor leading edge would go beyond the tapered portion of the shroud. In each case, the spanwise distribution of aerodynamic loading was kept about the same as that of the baseline rotor. Figure 6.1 presents the variation of the nominal performance and sensitivity to tip clearance versus the chordwise sweep angle. The zero degree sweep angle represents the baseline rotor. Again, the sensitivity of total-to-total pressure ratio and efficiency is taken as the change in their respective values from nominal (minimum) tip clearance (0.74% span) to high tip clearance (2.57% span). The results indicate that while forward sweep improves nominal performance (with an optimum sweep angle of 20 degrees), the sensitivity is worse than the baseline rotor.

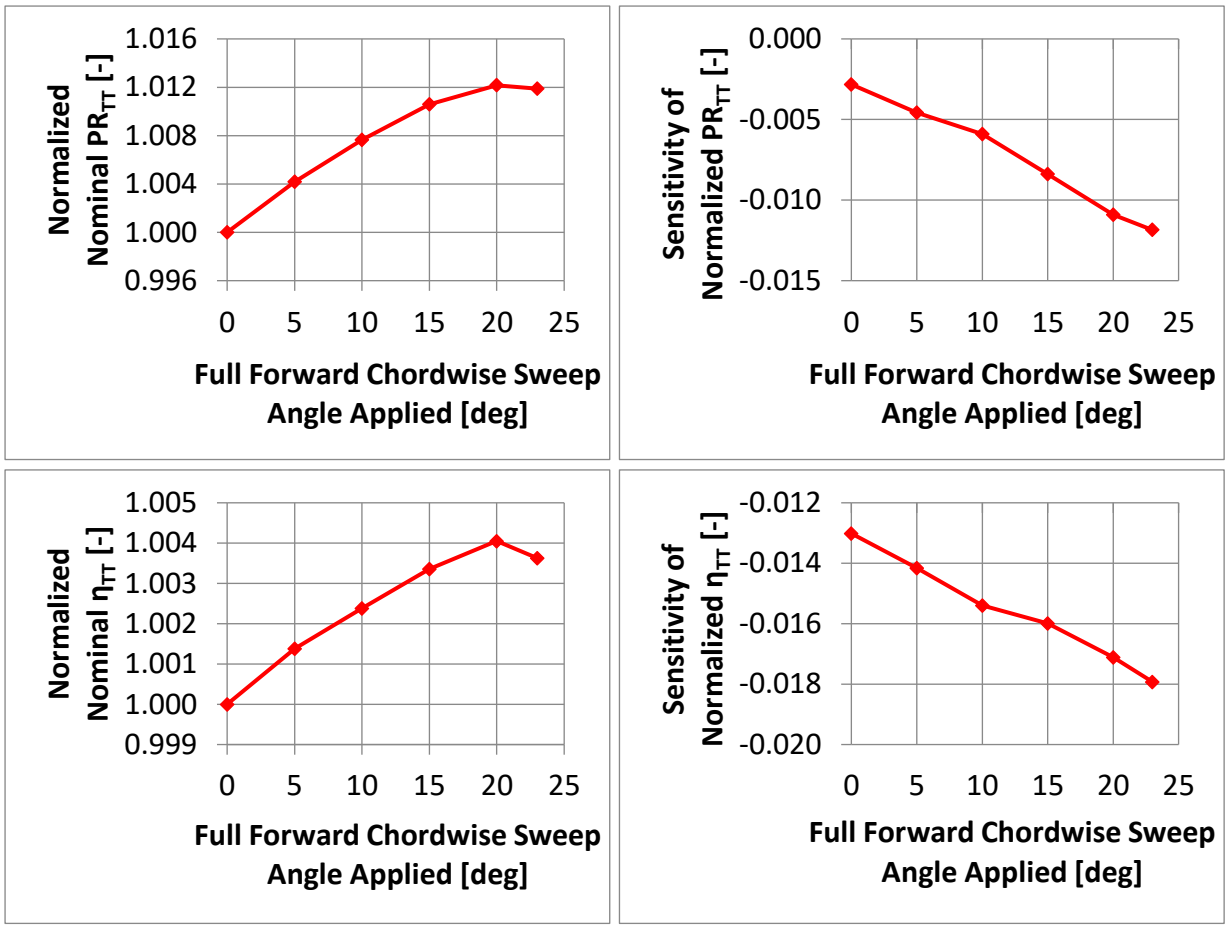

Figure 6.1: Parametric study on the full forward chordwise sweep angle

Partial stagger angle reduction

In her second proposed design, Erler [7] reduced the stagger angle linearly from 0 to 3 degrees from 50% to 100% span respectively while keeping the same spanwise distribution of the aerodynamic loading. The 3-degree-stagger angle reduction limit was set by rotor blade suction side boundary layer separation. This design strategy was applied to the present baseline rotor. In a parametric study with three configurations, the stagger angle of the baseline rotor in the outer 50% span was reduced linearly from 0 degree at 50% span to 1, 3 and 5 degrees at 100% span, while keeping a similar aerodynamic loading (by changing the trailing edge angle). The results are shown in Figure 6.2, with the zero-degree configuration representing the baseline rotor. The nominal performance improves for a tip stagger angle reduction of up to 3 degrees, beyond which tip blade suction side boundary layer separation is observed. However, the performance sensitivity only exhibits small changes or gets worse for tip stagger angle reductions lower or equal to 3 degrees.

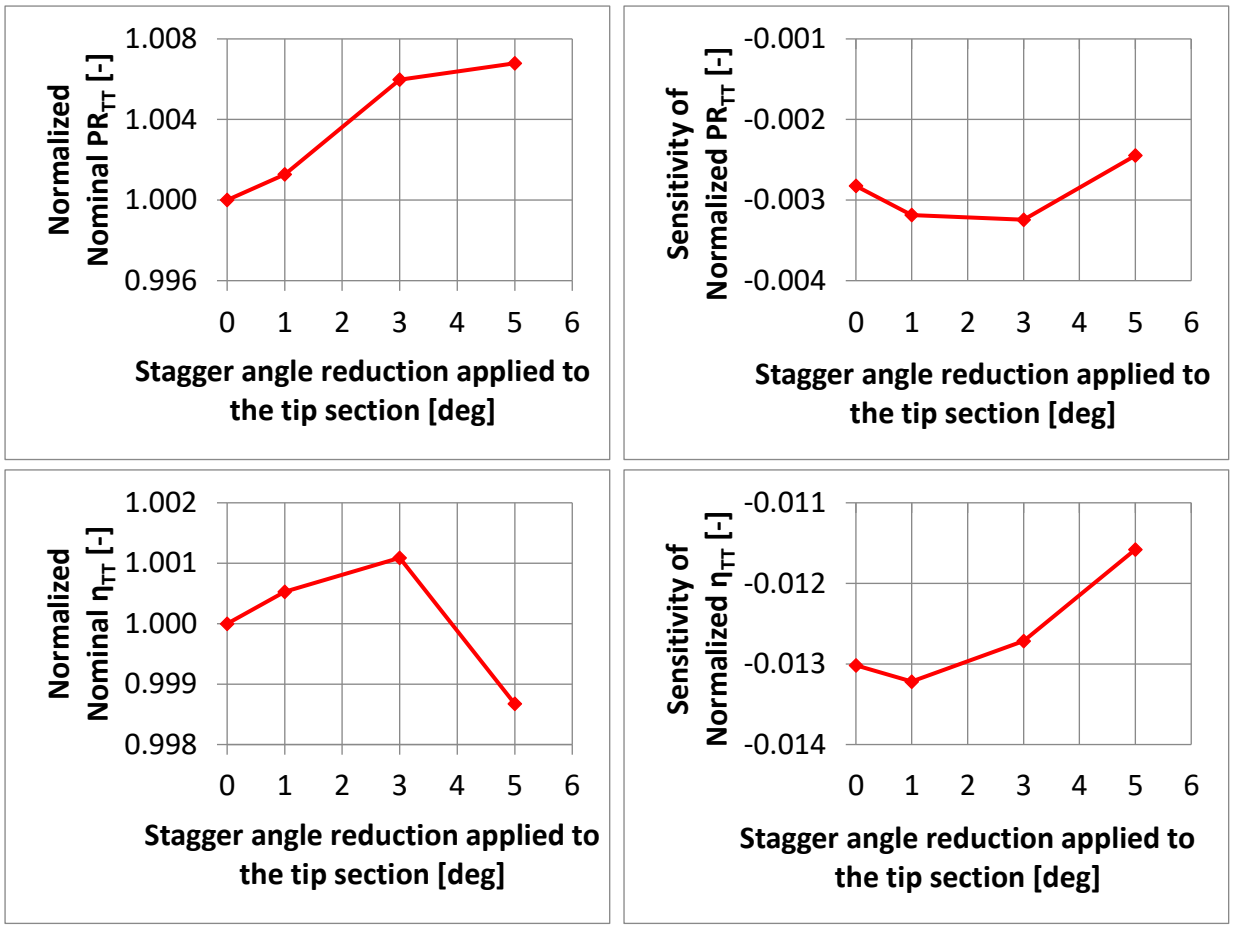

Figure 6.2: Parametric study on the linear stagger angle reduction applied from 50% to 100% span

Analysis of design strategies

This section verifies the spanwise loading distribution and the two desensitizing flow features for the best configuration from each of the two above strategies, namely the rotor with forward chordwise sweep of 20 degrees and the rotor which has a linear stagger angle reduction of 0 to 3 degrees from 50% to 100 % span. It is noted that sweep angle and stagger angle reduction are the same as those used by Erler [7] for her proposed designs.

Figure 6.3 compares the spanwise loading distributions for the two rotors with the baseline rotor. It verifies that the constraint of maintaining similar loading distributions is satisfied by both designs.

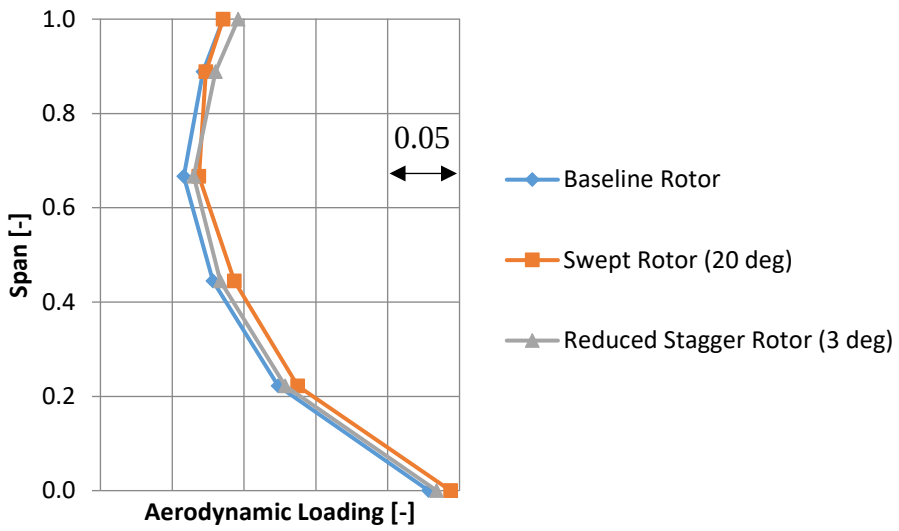

Figure 6.3: Aerodynamic loading of the swept rotor and reduced stagger rotor

Figure 6.4 compares the normalized incoming meridional momentum in the rotor tip region for the new rotors with the baseline rotor. It indicates that the swept rotor did not achieve the intended effect of improving incoming meridional momentum in the tip region, but rather experiences a loss in incoming meridional momentum. As expected, the reduced stagger design did not change incoming meridional momentum in the tip region.

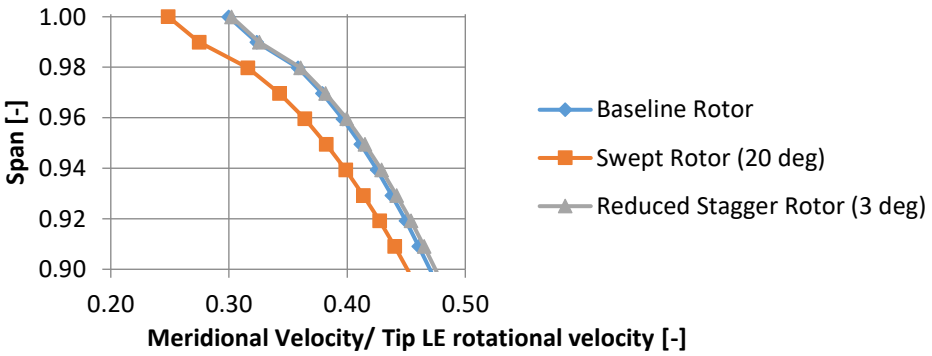

Figure 6.4: Tip meridional velocity of the swept rotor and reduced stagger rotor

Figure 6.5 qualitatively compares double leakage extent for the new rotors with the baseline rotor through tip clearance streamlines. None of the two new rotors show any noticeable reduction of double leakage extent from the baseline rotor, as was the intent behind these design strategies.

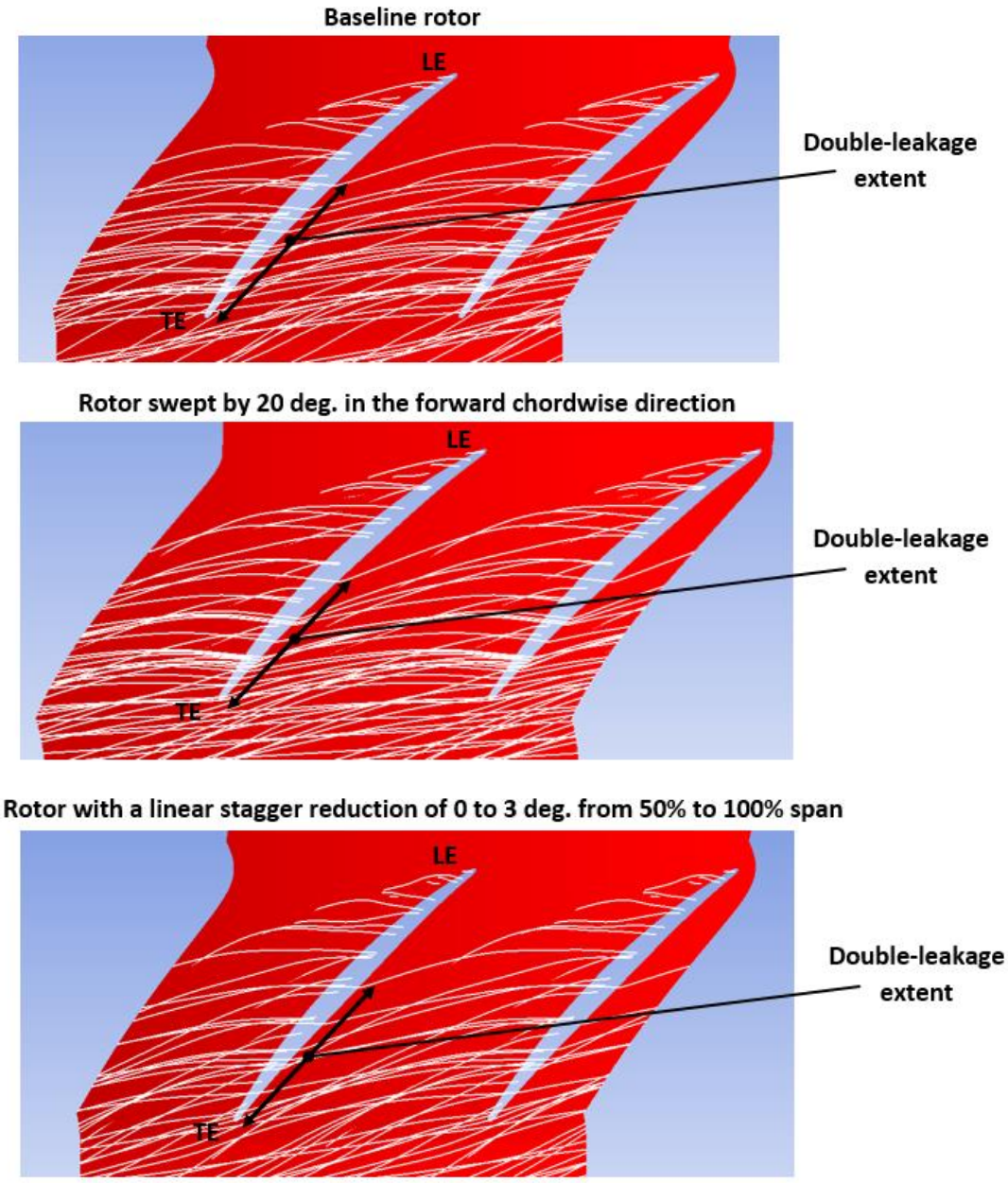

Figure 6.5: Double-leakage extent of the swept rotor and reduced stagger rotor at the blade tip plane

The above analysis of the two best designs from applying the design strategies proposed by Erler [7] to the current baseline rotor show that in this case they could not exploit the desensitizing flow features as intended. This explains their failure to improve performance sensitivity in any significant manner. While the theoretical rotor used by Erler [7] is close in performance and blade size to the baseline rotor in the current study, there are two important differences, namely the gas

path and inlet conditions, as illustrated in Figure 6.6. In terms of the gas path, the theoretical rotor of Erler [7] has a constant-radius shroud and a converging hub while the gas path of the real rotor has a tapered shroud and a diverging hub. As for the inlet conditions, the theoretical rotor of Erler [7] has an axial inlet flow while the current baseline rotor has a swirling inlet flow. One must conclude that these two physical differences are sufficient to render the desensitizing strategies ineffective for the current baseline rotor and a new approach must be taken.

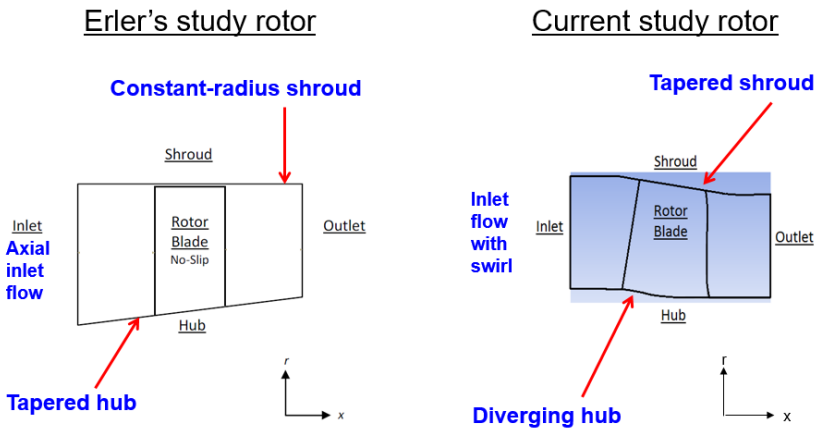

Figure 6.6: Differences between rotors used in Erler's study and in the current study – Adapted from [7]

6.2 Design methodology for the new rotor

This section presents a new design approach, based on the findings in chapter 5, to obtain a new version of the current baseline rotor with reduced performance sensitivity to tip clearance.

The analysis in chapter 5 to elucidate the mechanism by which the casing treatment reduces performance sensitivity for this rotor showed that:

1) The induction of rotation in the core flow by a large tip vortex strengthened by the casing treatment improves the total pressure ratio for the lower span region, which compensates for total pressure ratio losses in the tip region as tip clearance size increases, thus improving/reversing total pressure ratio sensitivity.

2) The reduction of double leakage by the casing treatment improves efficiency sensitivity.

Thus, to design a new desensitized version of the current rotor, one must apply blade design strategies that can generate rotation in the flow of the lower span region, and reduce double leakage.

Double leakage can be reduced if the chordwise location of maximum tip clearance flow (or maximum normal velocity of tip leakage flow) is shifted downstream. This is done by shifting the point of maximum loading (static pressure difference between the pressure and suction sides) at the blade tip toward the trailing edge.

Rotation in the core flow can be induced by creating an upward movement of the flow in the vicinity of the blade suction side through blade design strategies. As illustrated in Figure 6.7, the radially outward deflection of the flow near the suction side would combine with the radially inward flow movement near the pressure side due to tip clearance flow to induce flow rotation (vorticity) in the core flow at the lower span region.

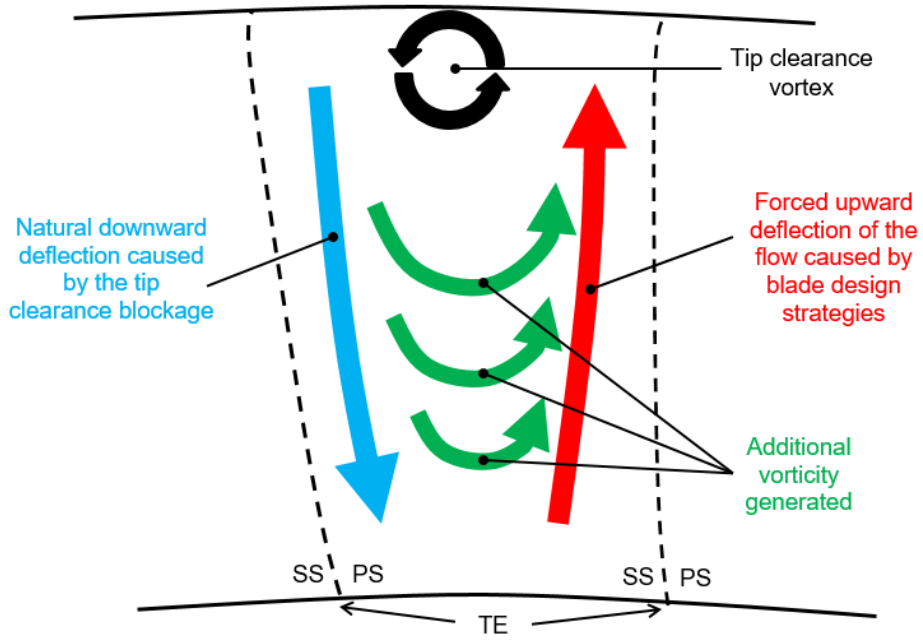

Figure 6.7: Strategy to induce rotation in the core flow

To induce a radially outward flow deflection near the blade suction side, the static pressure distribution on the blade suction side must be manipulated. In a compressor rotor, the flow crosses the blade passage while facing an adverse static pressure gradient in the streamwise direction. The flow will naturally move in the direction of least adverse static pressure gradient. Thus, the creation at each axial location of the highest adverse static pressure gradient in the hub region and the lowest adverse static pressure gradient in the tip region will deflect the flow toward the tip region, as illustrated in Figure 6.8. Put in different words, the rotor isobars should be tilted as much as possible from the hub leading edge to the tip trailing edge as depicted in Figure 6.9.

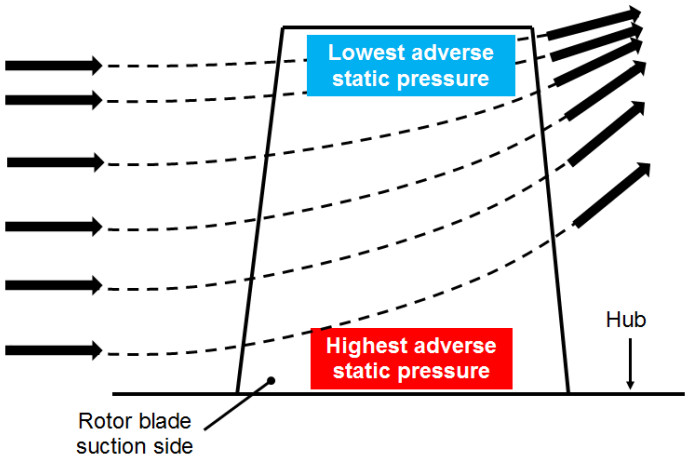

Figure 6.8: Spanwise deflection of the flow due to a strategic distribution of static pressure on the rotor suction side

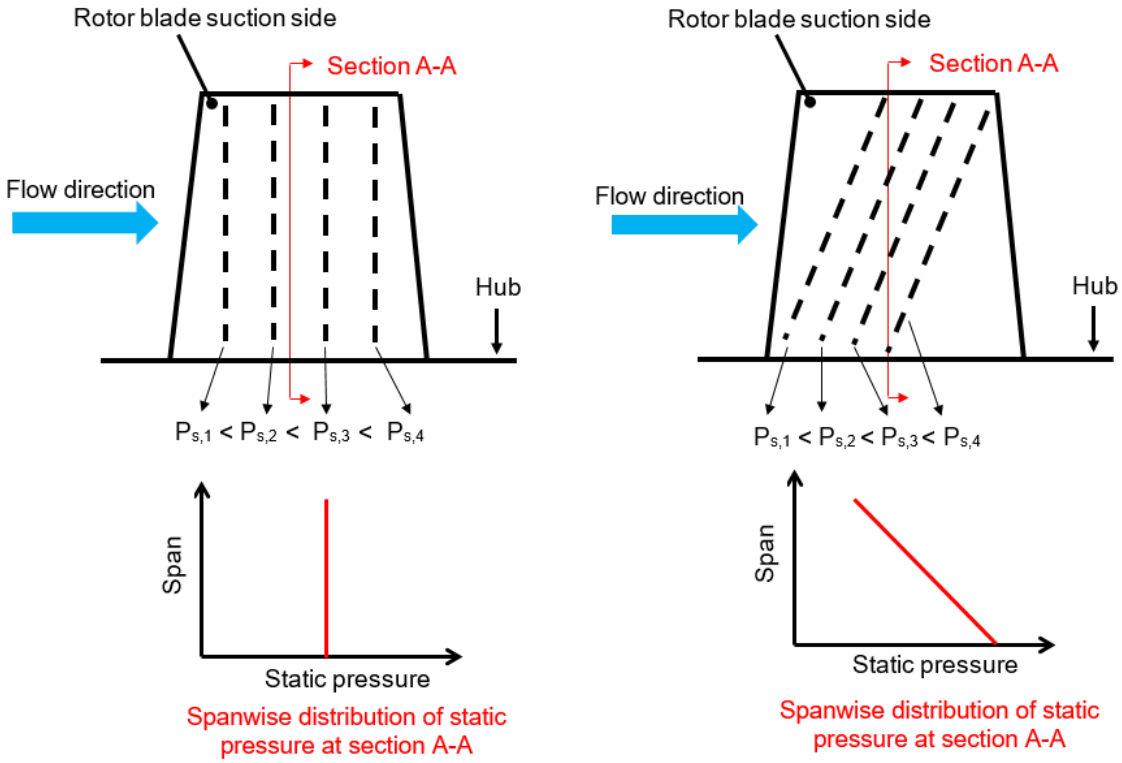

Figure 6.9: Orientation of isobars on rotor blade suction side for regular versus desensitized rotor

Four strategies involving camber line/blade section and stacking line changes have been devised through analytical reasoning and validated with CFD simulations (see Appendix D) to manipulate the shape and orientation of the rotor suction side isobars. These strategies are:

1) **Leading-edge metal angle (incidence)**: By closing the blade leading-edge (decreasing the incidence) at a certain span of the rotor, the local suction side isobars are displaced downstream. Opening the blade leading-edge has the reversed effect. Thus, to obtain the desired tilt of the isobar over the suction surface, the incidence should remain higher in the hub *relative* to the tip of the blade as shown in Figure 6.10.

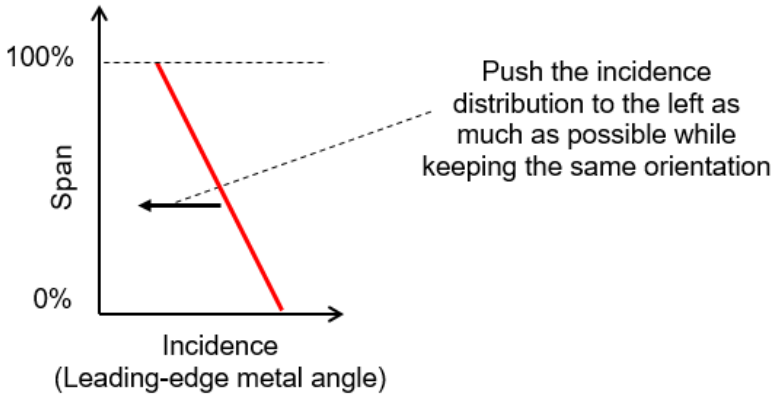

Figure 6.10: Variation of incidence from hub to tip

2) **Trailing-edge metal angle (aerodynamic loading)**: By opening the blade trailing edge (increasing the camber/aerodynamic loading) at a certain span of the rotor, the local suction side isobars are displaced upstream. Closing the blade trailing edge has the opposite effect. In this case, the aerodynamic loading should remain higher in the hub *relative* to the tip, as shown in Figure 6.11. The average value of the loading depends on the pressure ratio required from the rotor.

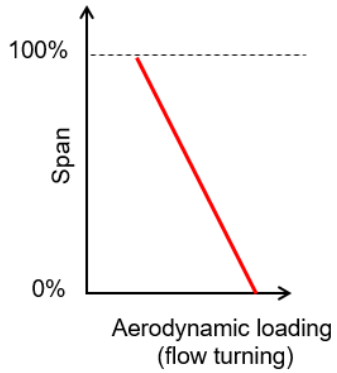

Figure 6.11: Variation of aerodynamic loading from hub to tip

3) **Chordwise position of the maximum camber (aft/front loading rotor sections):** By pushing the chordwise position of the maximum camber toward the trailing-edge (i.e. aft-loading the rotor section) at a certain span location of the rotor, the local suction side isobars are displaced downstream. In contrast, pushing the chordwise position of maximum camber toward the leading-edge (i.e. front loading the rotor section) has the opposite effect. In this case, the position of maximum camber should remain upstream in the hub *relative* to the tip, as shown in Figure 6.12. It is also noted that a rear position of the maximum camber at the blade tip also helps to reduce double leakage as previously discussed.

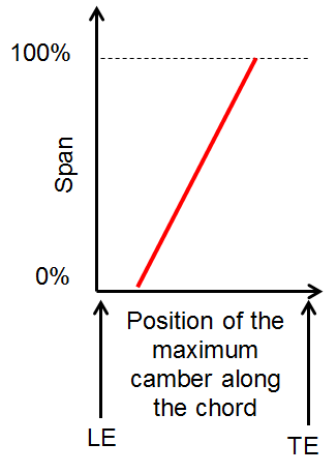

Figure 6.12: Variation of position of maximum camber from hub to tip

4) **Lean:** By applying a forward lean (stacking line tilted in the direction of the rotational velocity), the suction side isobars in the upper half of the rotor are displaced downstream while those in the lower half move upstream. Applying a backward lean has the opposite effect. In this case, the rotor should be gradually leaned forward from hub to tip. Due to structural considerations, a parabolic lean, as shown in Figure 6.13, is preferable to a linear lean to minimize structural problems.

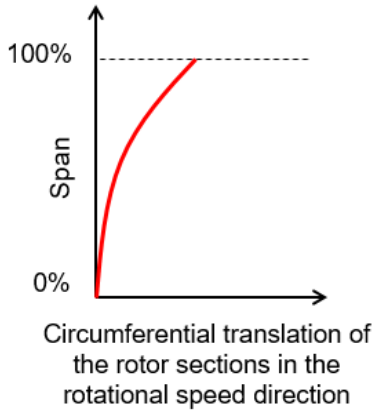

Figure 6.13: Amount of forward lean applied to the rotor

Beyond these four design strategies, there is an additional important factor to consider for maximizing the outward flow displacement over the blade surface. A reduction in streamwise velocity of the incoming flow will increase the outward flow deflection as illustrated in Figure 6.14.

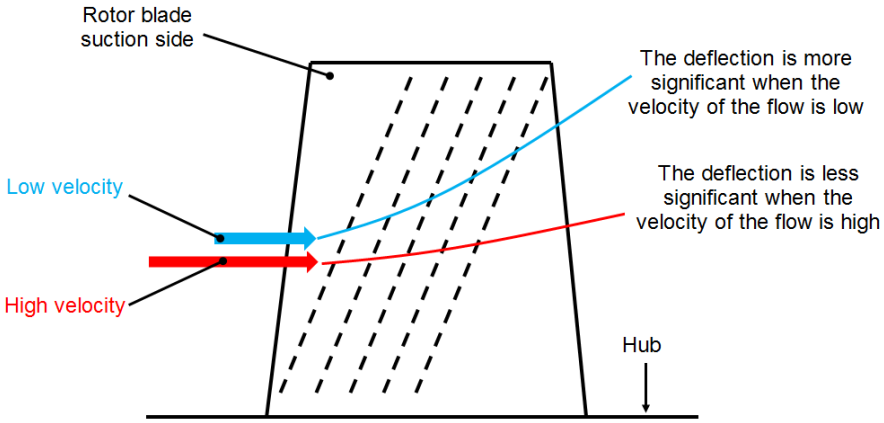

Figure 6.14: Variation of the spanwise flow deflection with the incoming flow speed

To control the velocity at which the flow enters the blade passage, the incidence of the rotor plays again an important role. A high incidence forces the incoming flow to accelerate at the rotor leading edge. In contrast, a low incidence decelerates the flow at the rotor leading edge. The importance of this factor to performance sensitivity is demonstrated in Appendix D for an intermediate aggressive blade design. Thus, the *average* value of the incidence distribution shown in Figure 6.10 should be kept as low as possible to achieve the lowest velocity for the incoming flow.

Based on multiple iterations where design strategies outlined above were applied to the baseline rotor, the final configuration for the new rotor is shown in Figure 6.15. Results from CFD simulations at the design mass flow shown in Figure 6.16 verify that the suction side isobars for the new rotor are more titled in the desired direction when compared with those of the baseline rotor. Figure 6.17 compares the spanwise distribution of the aerodynamic loading of the baseline versus new rotor. It shows that the new rotor maintains lower loading in the tip than the hub and it has higher tip loading than the baseline rotor. Thus, it does not sacrifice tip loading for reducing the sensitivity of the initial rotor, which is important given that the work per unit mass flow is the highest in the tip region.

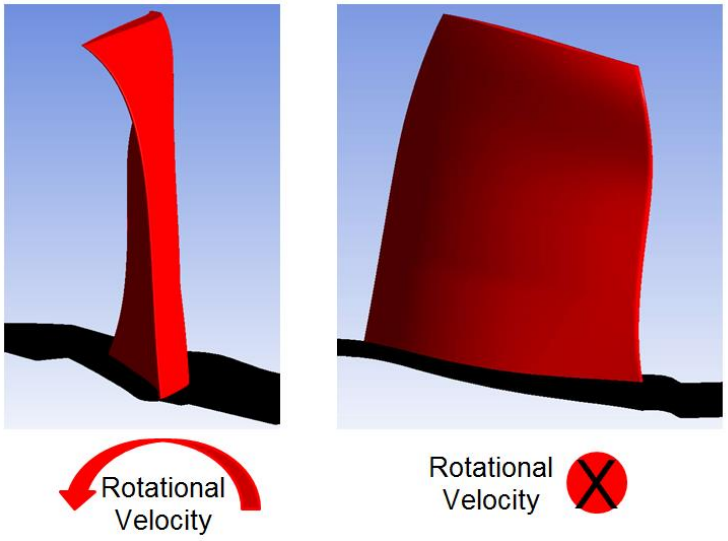

Figure 6.15: New rotor geometry

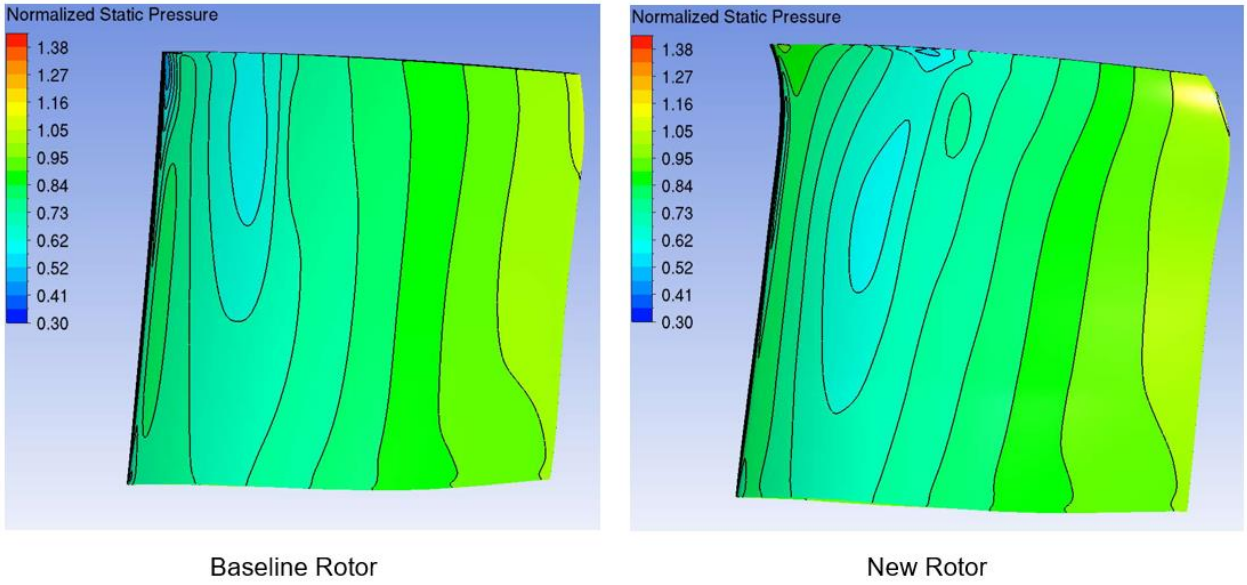

Figure 6.16: Orientation of the suction side isobars for the baseline rotor and new rotor

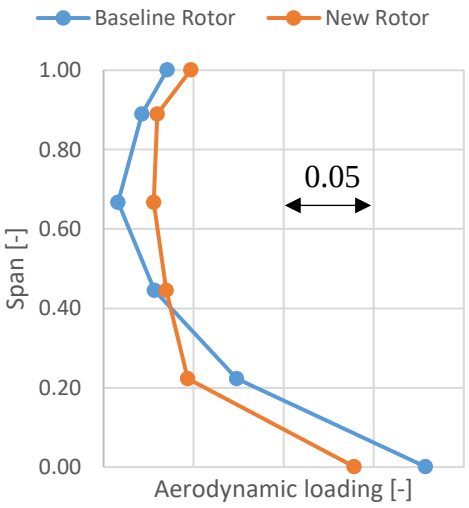

Figure 6.17: Aerodynamic loading for the baseline and new rotor

6.3 General Assessment of New Rotor Design

Figures 6.18, 6.19 and 6.20 plot the total-to-total pressure ratio, total-to-total efficiency and stall margin versus tip clearance, respectively, for the new rotor along with those for the baseline rotor with a smooth casing (chapter 4) and baseline rotor with casing treatment (from Chapter 5).

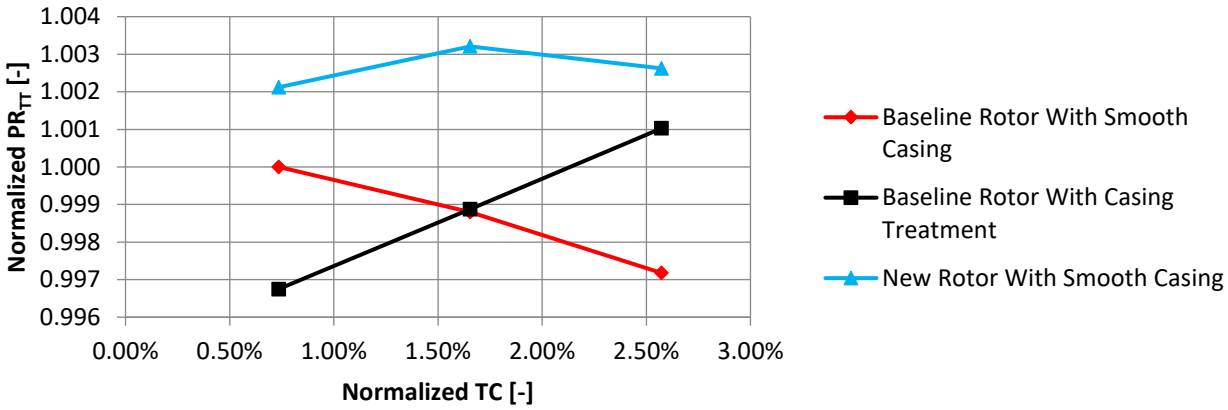

Figure 6.18: Design point total-to-total pressure ratio VS tip clearance

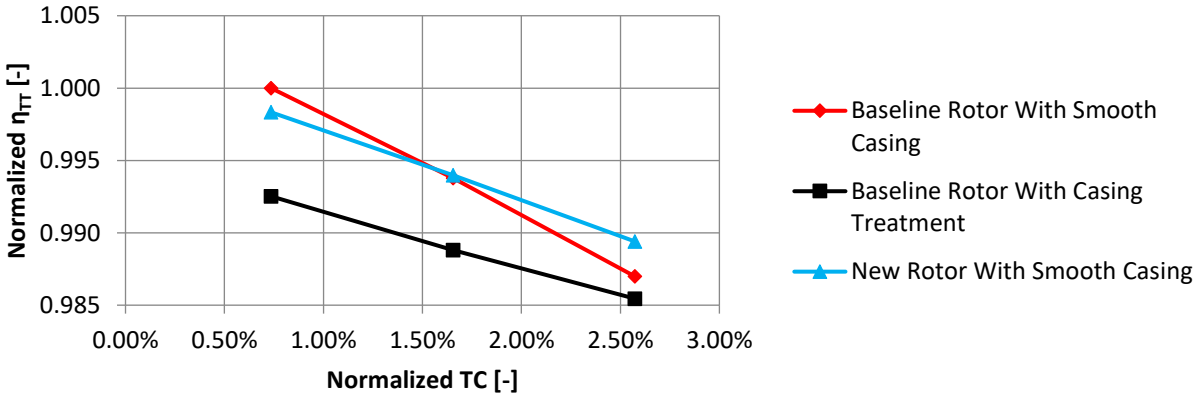

Figure 6.19: Design point total-to-total efficiency VS tip clearance

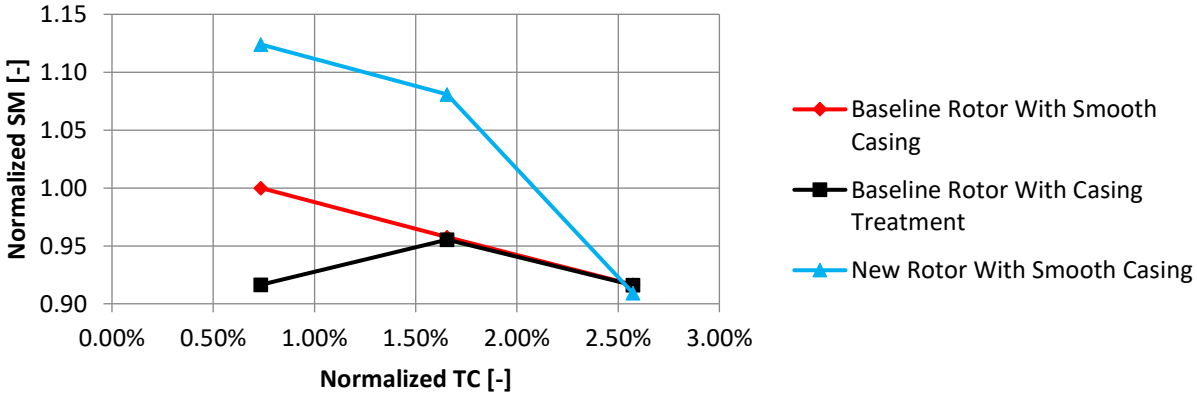

Figure 6.20: Stall margin VS tip clearance

The new rotor has a nominal pressure ratio that is higher by 0.17% than that of the baseline rotor. Moreover, while it does not have the positive sensitivity effect of the casing treatment, the new rotor basically desensitizes the total pressure ratio to tip clearance. In terms of efficiency, the new rotor incurs a nominal penalty of 0.23 point versus the baseline rotor, which is much lower than that of the casing treatment, while providing a sensitivity reduction that is not far from that obtained through the casing treatment. Finally, with regard to aerodynamic stability, there is a significant nominal stall margin improvement of 12.4% for the new rotor versus the baseline rotor. The sensitivity of stall margin between nominal and medium tip clearance is the same as the baseline rotor. However, this sensitivity deteriorates from medium to high tip clearance. Thus, the design of the new rotor meets all objectives, except for the stall margin sensitivity reduction.

6.4 Variation of pressure ratio with tip clearance

With the inlet total pressure for the new rotor remaining virtually unchanged with increasing tip clearance (see Appendix C), the variation with tip clearance of the rotor exit total pressure is again used to investigate the source of total pressure ratio sensitivity. Figure 6.21 presents the contour plot of the difference in total pressure between nominal and high tip clearance taken at the new rotor trailing edge plane. Small ellipses on the figure highlight regions with total pressure gain (+) or loss (-) as the tip clearance increases. The net total pressure changes in the tip region correspond clearly to total pressure loss (in magnitude and in extent). Therefore, the slight increase in total pressure ratio for the new rotor as the tip clearance increases (Figure 6.18) must originate from lower span regions. In fact, the high mass flow going through these regions combined to the low-magnitude total pressure gains experienced by them are sufficient to compensate for net total pressure losses in the tip region.

In fact, a comparison of the Figure 6.21 with the equivalent figure for the baseline rotor in chapter 4 (Figure 4.5) shows that the region of exit total pressure gain in the lower span region is much larger for the new rotor, which can be explained by the higher rotation of the core flow for the new rotor. At the same time, this region of total pressure gain is not as extensive as that shown in Chapter 5 (Figure 5.13) for the baseline rotor with casing treatment. Assuming that the level of flow rotation in the core can be inferred by the vorticity of the tip region, the comparison of tip vorticity in Figure 6.22 for the three configurations shows that the reduction in pressure ratio sensitivity correlates, at least in trend, with the strength (size times vorticity, i.e. circulation) of the

tip vortex. It is interesting to note that although the proposed design strategy for the new rotor does not aim to influence directly the tip clearance vortex, this latter vortex is impacted.

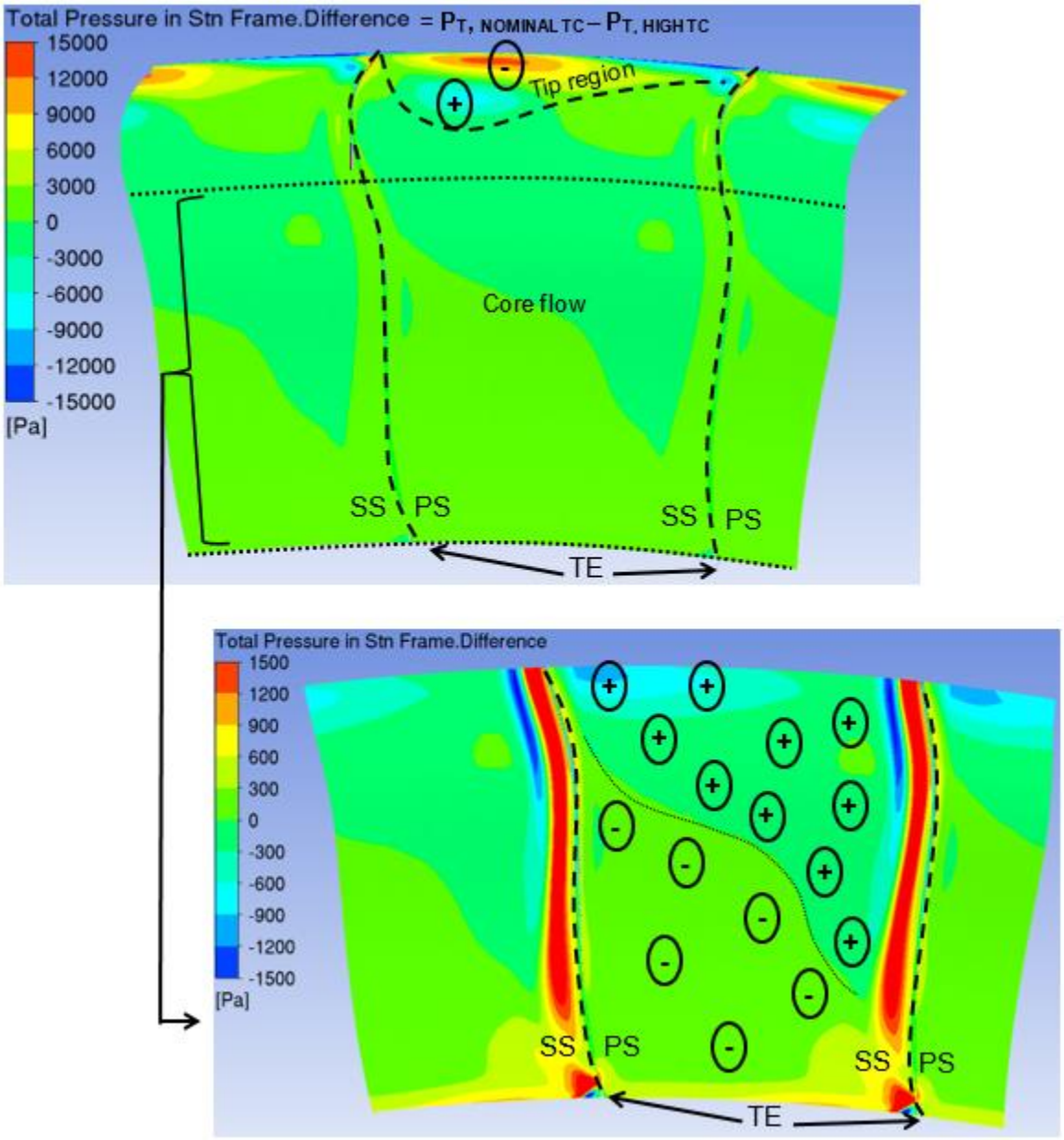

Figure 6.21: Difference in total pressure between nominal and high tip clearance at the new rotor trailing edge plane

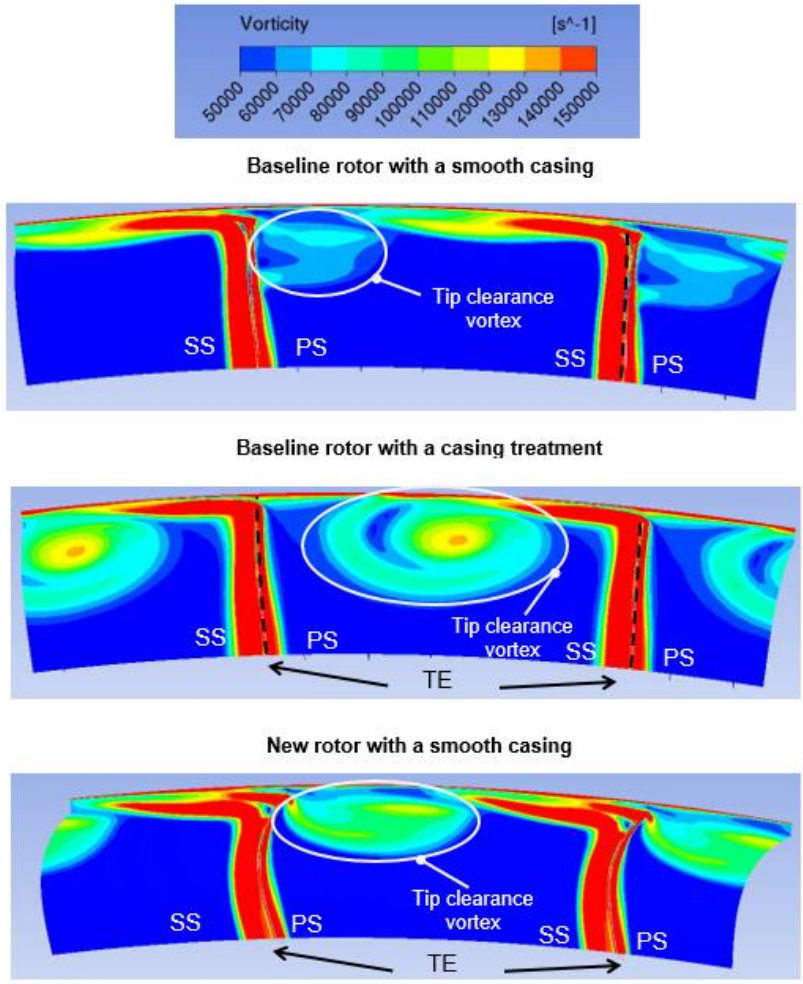

Figure 6.22: Vorticity at the rotor trailing edge plane between 70% and 100% span for all cases investigated in this study

6.5 Variation of efficiency with tip clearance

With the entropy of the inlet flow unaffected by the increase in tip clearance (see Appendix C), the change in entropy distribution at the rotor exit with tip clearance increase is used to look into the source of the reduction in sensitivity of efficiency for the new rotor. Figure 6.23 is a contour plot of the difference in static entropy between nominal and high tip clearance at the rotor trailing edge plane. As before, small ellipses on the figure highlight regions with entropy increase (+) or decrease (-) as the tip clearance increases.

When compared to the equivalent plot in Chapter 4 for the baseline rotor (see figure 4.7), one can observe a zone of entropy decrease (efficiency gain) in the tip region for the new rotor that is not

present for the baseline rotor. This zone is the result of the displacement of the tip vortex from near mid-pitch at nominal tip clearance to near pressure side at high tip clearance. The presence and position of this zone next to the shroud is consistent with a reduction in double leakage. This is qualitatively confirmed by comparing the tip clearance flow streamlines for the new rotor (Figure 6.24) with those of the baseline rotor (Figure 4.8) which show that the chordwise extent of double leakage is lower for the new rotor. Based on the findings of Erler [7], a lower double leakage at nominal tip clearance leads to its lower growth (along with its associated losses in the tip region, thus lower drop in efficiency) with tip clearance increase. This is consistent with the observed growth in the tip blockage region between the two rotors when comparing the contours of rotor exit static entropy at nominal and maximum tip clearance for the new rotor (Figure 6.25) versus the baseline rotor (Figure 4.9). One can observe that the tip blockage region (represented by the zone of high entropy in the tip region) grows less between the two tip clearances for the new rotor than for the baseline rotor.

Based on the above observations, the reduction in efficiency sensitivity for the new rotor design can be explained by the reduction in double leakage.

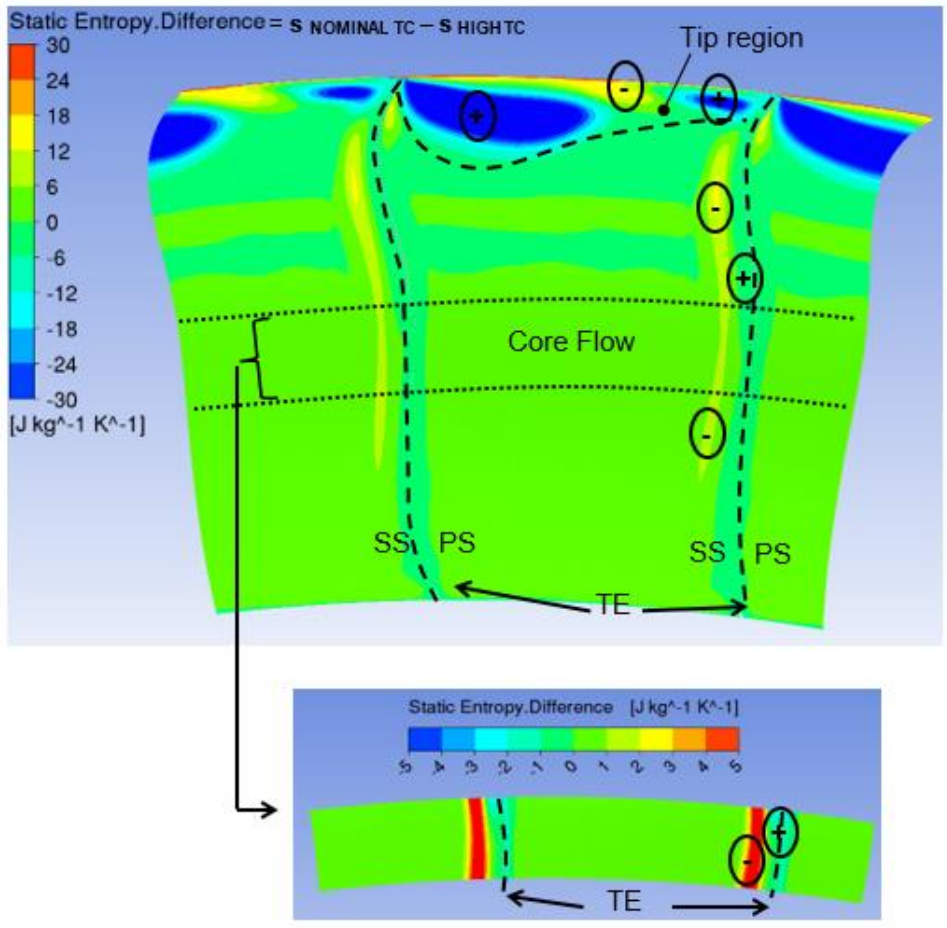

Figure 6.23: Difference in static entropy between nominal and high tip clearance at the new rotor trailing edge plane

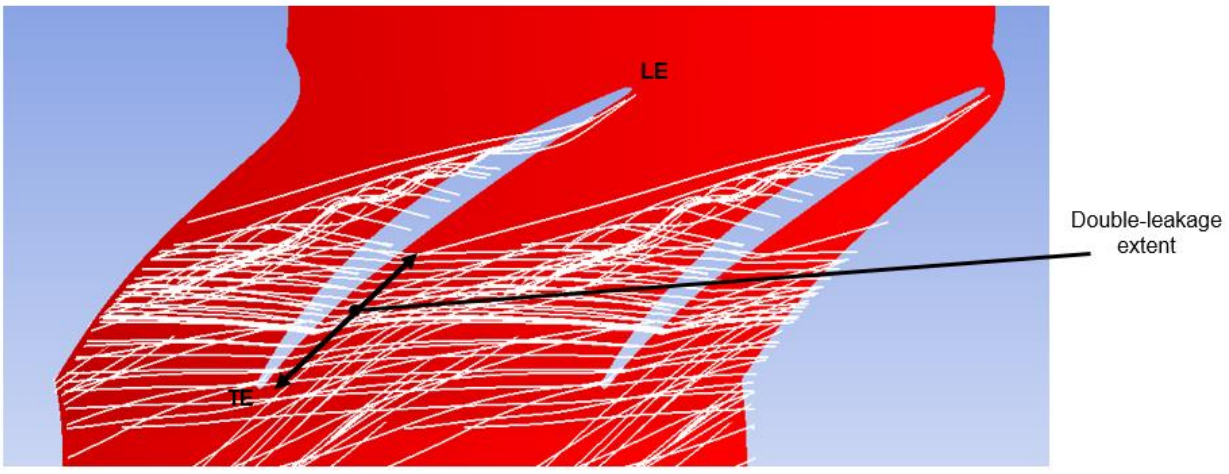

Figure 6.24: Double-leakage extent at the rotor tip plane at nominal tip clearance for the new rotor

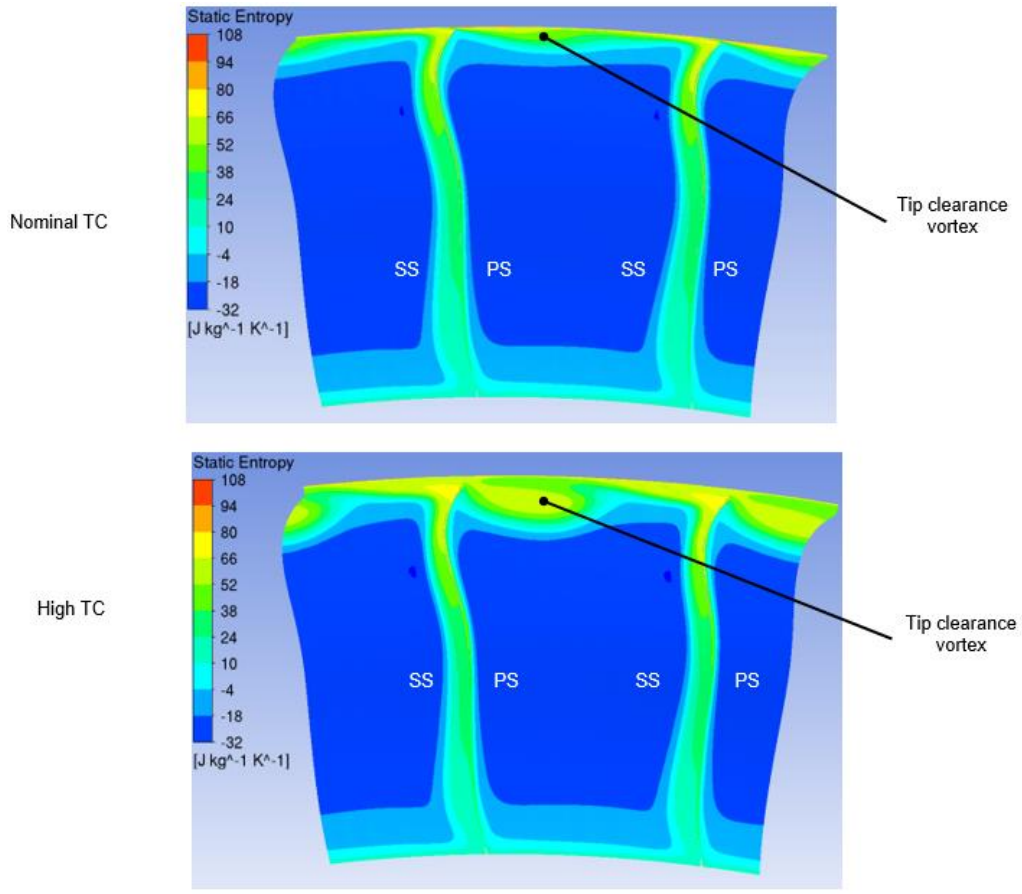

Figure 6.25: Entropy contours at the new rotor trailing edge plane

6.6 Stability Results

Figure 6.20 showed that the new rotor produced a significant stall margin improvement over the baseline rotor at nominal and medium tip clearance with about the same sensitivity in this range. However, there is a worsening of stall margin sensitivity at higher tip clearance that neutralizes the stall margin advantage of the new rotor at large tip clearance. The investigation into this behaviour starts with an analysis based on the monitoring of the incoming/tip clearance flow interface as was done in section 4.4 for the baseline rotor.

Figure 6.26 shows the entropy contours at the blade tip plane of the new rotor at the stall point for each of the three simulated tip clearances. At nominal and medium tip clearances, the interface between the incoming flow and tip clearance flow is still inside the blade passage, inferring modal stall inception. One can also observe that the interface is slightly closer to the leading edge plane at medium tip clearance even though the mass flow is higher (lower stall margin, as indicated in

Figure 6.20) than that at nominal tip clearance. This means that the strength of the tip clearance flow and resulting tip blockage have grown from nominal to medium clearance to cause the leveling-off (reaching zero slope) of the total-to-static pressure rise speedline to occur at a higher mass flow, resulting in an earlier modal stall and thus reduced stall margin.

The stall margin improvement seen at the nominal and medium tip clearances can be explained through Figure 6.27 which shows the entropy contours at the rotor exit plane for the new rotor and the baseline rotor at nominal tip clearance and at the common mass flow corresponding to that of the stall point of the baseline rotor. One can see that the tip blockage region is smaller for the new rotor such that it would enable the total-to-static pressure rise speedline of this rotor to level-off at a lower mass flow, thus improving its stall margin.

For the new rotor at large tip clearance, the stall point occurs at an even higher mass flow (lowest stall margin according to Figure 6.20) and yet the interface at this point has already reached the leading edge plane, signaling a spike stall inception. This indicates that the strength of the tip vortex has grown further between the medium and large tip clearance, causing a premature stall by spike stall inception (i.e. before the tip blockage can cause the leveling-off of the total-to-static pressure rise speedline and modal stall inception). This explains the discontinuity in stall margin variation with tip clearance observed between the medium and large tip clearance values.

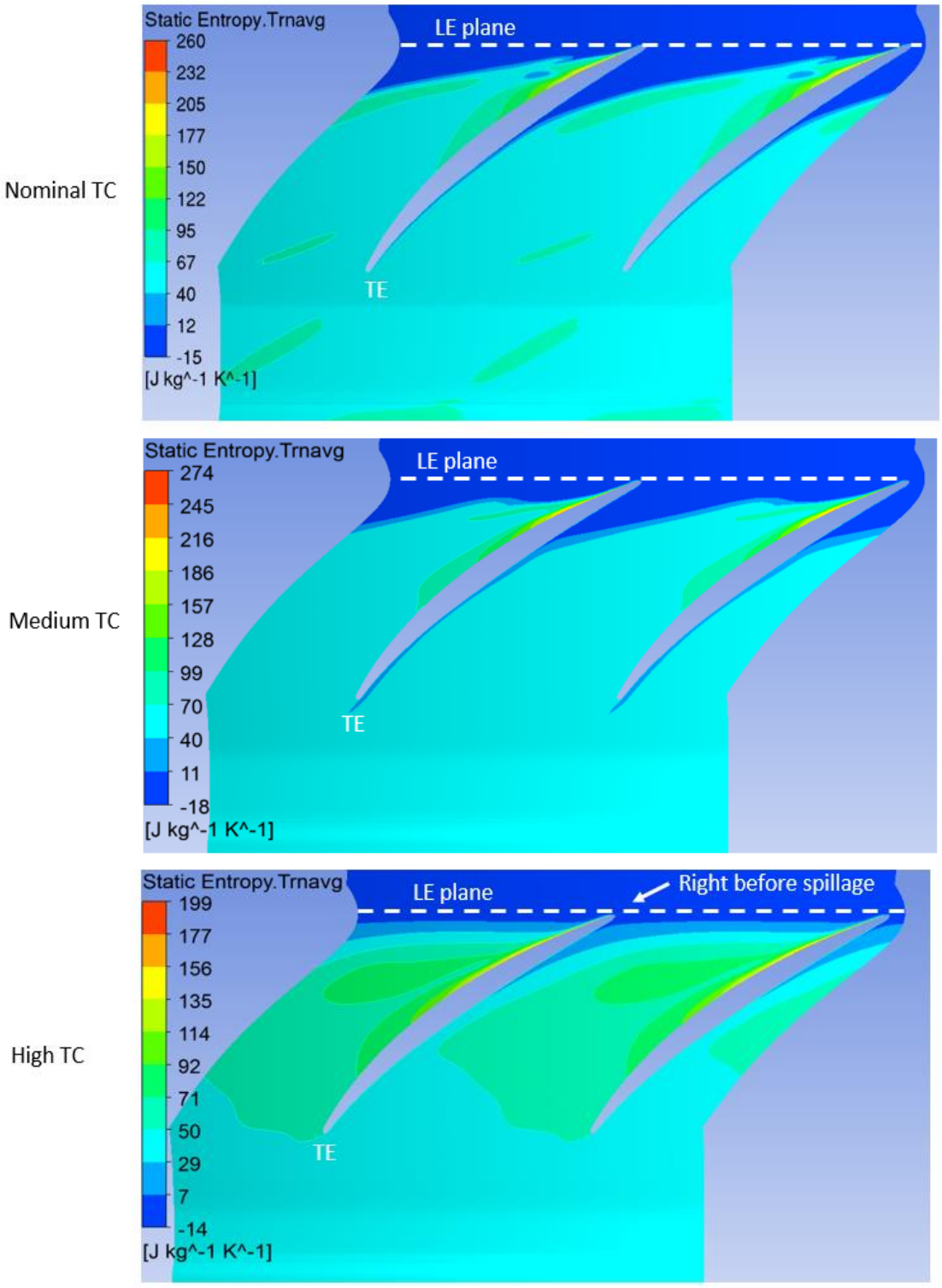

Figure 6.26: Entropy contours in blade tip plane of the new rotor at the simulated stall points for the three tip clearances

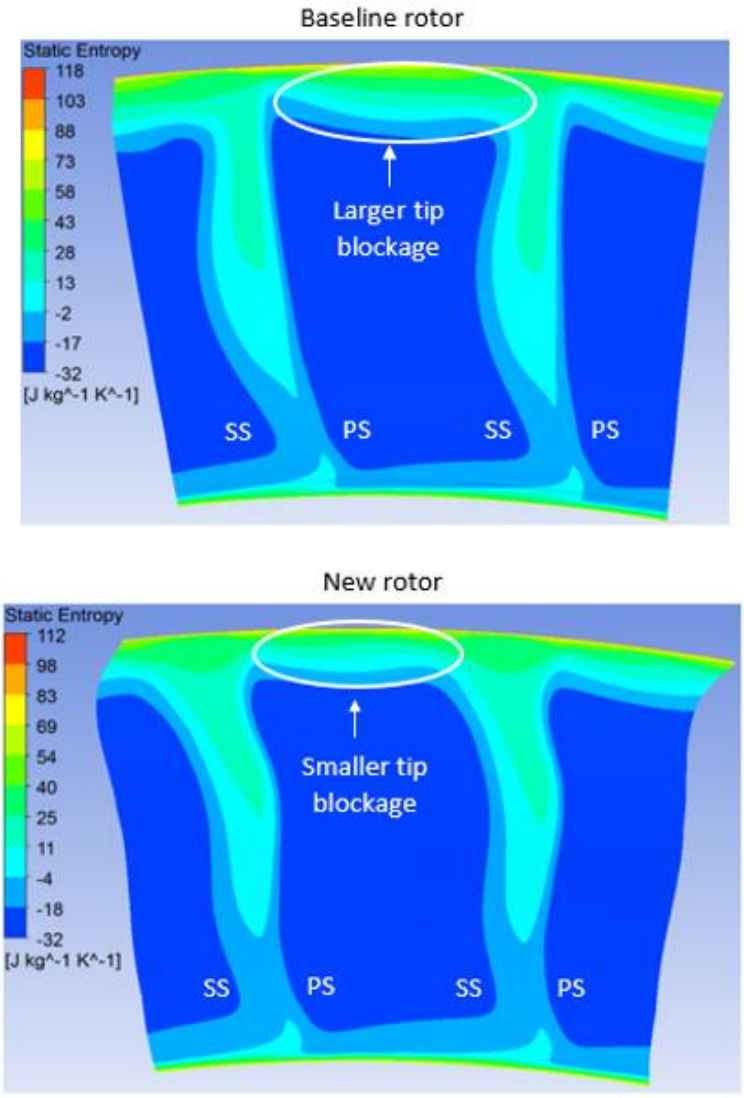

Figure 6.27: Entropy contours at the rotor trailing edge plane for the new rotor and the baseline rotor at nominal tip clearance and at the common mass flow corresponding to that of the stall point of the baseline rotor

CHAPTER 7 CONCLUSION AND FUTURE WORK

Two different strategies were applied to an aero-engine axial compressor rotor to reduce its performance and stall margin sensitivity to tip clearance increase. On one hand, a previously discovered casing treatment made up of shallow negative saw-tooth shaped circumferential grooves was refined for the current study. On the other hand, the rotor blade was redesigned by modifying the static pressure field on its suction side. The main findings are:

1. Two zones of the blade passage are affected differently by the increase in tip clearance. The first zone is the tip region which consists of the tip clearance vortex and the surrounding low-momentum flow. The second zone is the lower span region which refers to the rest of the blade passage, made up of the core flow and blade /hub boundary layers.
2. For the baseline rotor, the tip region and the lower span region contribute about equally to the total pressure ratio sensitivity. In contrast, the efficiency sensitivity is mainly driven by the mixing losses in the tip region.
3. The casing treatment reverses the total pressure ratio sensitivity by amplifying the tip vortex through radial flow injection from the grooves, which in turn induces rotation in the core flow leading to additional flow turning in the lower span region with tip clearance increase. The reduction in efficiency sensitivity stems from the elimination of double-leakage by the casing treatment.
4. Blade design strategies that manipulate the suction side static pressure distribution to create flow rotation in the core flow can be successful in decreasing the performance sensitivity.

The main novel contributions of this project are:

1. Explanation of the positive (reversed) sensitivity to tip clearance of the pressure ratio brought about by a circumferential grooves casing treatment.
2. A new blade design strategy based on core flow rotation that can completely desensitize the total pressure ratio and significantly reduce the efficiency sensitivity.

From the current research, the recommendations for future work include:

1. Experimental validation of the performance and stability of the casing treatment and new rotor.
2. Verify the generic nature of the new blade design strategy to other axial compressor rotors.

BIBLIOGRAPHY

[1] S. Yoon, E. Curtis, J. Denton, and J. Longley, "The Effect of Clearance on Shrouded and Unshrouded Turbines at Two Levels of Reaction," *Journal of Turbomachinery,* vol. 136, pp. 021013-021013-9, 2013.

[2] J. A. Storer and N. A. Cumpsty, "An Approximate Analysis and Prediction Method for Tip Clearance Loss in Axial Compressors," *Journal of Turbomachinery,* vol. 116, pp. 648-656, 1994.

[3] H. D. Vo, "Role of Tip Clearance Flow on Axial Compressor Stability," Ph.D. Thesis, Massachusetts Institute of Technology, Boston, Massachusetts, USA, 2001.

[4] P. Seshadri, S. Shahpar, and G. T. Parks, "Robust compressor blades for desensitizing operational tip clearance variations," in *ASME Turbo Expo 2014: Turbine Technical Conference and Exposition, GT 2014, June 16, 2014 - June 20, 2014*, Dusseldorf, Germany, 2014, p. International Gas Turbine Institute.

[5] R. A. Berdanier and N. L. Key, "The effects of tip leakage flow on the performance of multistage compressors used in small core engine applications," *Journal of Engineering for Gas Turbines and Power,* vol. 138, 2016.

[6] X. Zheng and H. Yang, "Influence of Tip Clearance on the Performance and Matching of Multistage Axial Compressors," p. V02AT37A008, 2016.

[7] E. Erler, "Axial Compressor Blade Design for Desensitization of Aerodynamic Performance and Stability to Tip Clearance " Ph.D. Thesis, École Polytechnique de Montréal, Montréal, Canada, 2012.

[8] M. Cevik, "Axial Compressor Gas Path Design for Desensitization of Aerodynamic Performance and Stability to Tip Clearance.," Ph.D. Thesis, École Polytechnique de Montréal, Montréal, Canada, 2013.

[9] H. D. Vo, M. Cevik, and E. Erler, "Compressor casing," ed: Google Patents, 2016.

[10] M. Inoue, M. Kuroumaru, and M. Fukuhara, "Behavior of tip leakage flow behind an axial compressor rotor," *Journal of Engineering for Gas Turbines and Power,* vol. 108, pp. 7-14, 1986.

[11] J. A. Storer and N. A. Cumpsty, "Tip Leakage Flow in Axial Compressors," *Journal of Turbomachinery,* vol. 113, pp. 252-259, 1991.

[12] C. Hah, "Effects of double-leakage tip clearance flow on the performance of a compressor stage with a large rotor tip gap," *Journal of Turbomachinery,* vol. 139, 2017.

[13] Khalid S. Arif, A. S. Khaisa, I. A. Waltz, C. S. Tan, E. M. Greitzer, N. A. Cumpsty, *et al.*, "Endwall blockage in axial compressors," in *ASME 1998 International Gas Turbine and Aeroengine Congress and Exhibition, GT 1998, June 2, 1998 - June 5, 1998*, Stockholm, Sweden, 1998, p. International Gas Turbine Institute.

[14] T. R. Camp and J. Day, "A study of spike and modal stall phenomena in a low-speed axial compressor," in *ASME 1997 International Gas Turbine and Aeroengine Congress and Exhibition, GT 1997, June 2, 1997 - June 5, 1997*, Orlando, FL, United states, 1997, p. International Gas Turbine Institute.

[15] F. K. Moore and E. M. Greitzer, "Theory of post-stall transients in axial compression systems: Part I - Development of equations," *Journal of Engineering for Gas Turbines and Power,* vol. 108, pp. 68-76, 1986.

[16] H. D. Vo, C. S. Tan, and E. M. Greitzer, "Criteria for spike initiated rotating stall," *Journal of Turbomachinery,* vol. 130, 2008.

[17] C. Freeman, "Effect of tip clearance flow on compressor stability and engine performance," *Von Karman Institute for Fluid Dynamics Lecture Series,* vol. 5, 1985.

[18] G. S. McNulty, J. J. Decker, B. F. Beacher, and S. A. Khalid, "The impact of forward swept rotors on tip clearance flows in subsonic axial compressors," *Journal of Turbomachinery,* vol. 126, pp. 445-454, 2004.

[19] A. R. Wadia, H. C.;, and R. D., "The Impact of Forward Sweep on Tip Clearance Flows in Transonic Compressors," in *24th International Congress of the Aeronautical Sciences*, Yokohoma, Japan, 2004.

[20] C. V. Halbe, Y. S. Chati, J. T. George, A. M. Pradeep, B. Roy, H. Yu, *et al.*, "Study of effects of rotor tip tailoring in axial flow compressors," in *ASME Turbo Expo 2015: Turbine Technical Conference and Exposition, GT 2015, June 15, 2015 - June 19, 2015*, Montreal, QC, Canada, 2015, p. International Gas Turbine Institute.

[21] G. D. J. Smith and N. A. Cumpsty, "Flow phenomena in compressor casing treatment," *Journal of Engineering for Gas Turbines and Power,* vol. 106, pp. 532-541, 1984.

[22] B. H. Beheshti, J. A. Teixeira, P. C. Ivey, K. Ghorbanian, and B. Farhanieh, "Parametric Study of Tip Clearance—Casing Treatment on Performance and Stability of a Transonic Axial Compressor," *Journal of Turbomachinery,* vol. 126, pp. 527-535, 2004.

[23] M. Cevik, H. Duc Vo, and H. Yu, "Casing Treatment for Desensitization of Compressor Performance and Stability to Tip Clearance," *Journal of Turbomachinery,* vol. 138, pp. 121008-121008-16, 2016.

[24] C. Guinet, J. A. Streit, H.-P. Kau, and V. Gummer, "Tip gap variation on a transonic rotor in the presence of tip blowing," in *ASME Turbo Expo 2014: Turbine Technical Conference and Exposition, GT 2014, June 16, 2014 - June 20, 2014*, Dusseldorf, Germany, 2014, p. International Gas Turbine Institute.

[25] A. P. Singh, A. R. Paul, and P. Ranjan, "Investigation of reattachment length for a turbulent flow over a backward facing step for different step angle," *Int J Eng Sci Technol,* vol. 3, pp. 84-88, 2011.

[26] ANSYS. (2013). *ANSYS CFX-Solver Modeling Guide*. Available: http://148.204.81.206/Ansys/150/ANSYS%20CFX-Solver%20Modeling%20Guide.pdf

[27] D. E. Van Zante, A. J. Strazisar, J. R. Wood, M. D. Hathaway, and T. H. Okiishi, "Recommendations for Achieving Accurate Numerical Simulation of Tip Clearance Flows in Transonic Compressor Rotors," p. V001T03A057, 1999.

[28] S. Yin, D. Jin, X. Gui, and F. Zhu, "Application and comparison of SST model in numerical simulation of the axial compressors," *Journal of Thermal Science,* vol. 19, pp. 300-309, August 01 2010.

[29] Y. Liu, X. Yu, and B. Liu, "Turbulence models assessment for large-scale tip vortices in an axial compressor rotor," *Journal of Propulsion and Power,* vol. 24, pp. 15-25, 2008.

APPENDIX A BLADE TERMINOLOGY

The terminology used in the text to describe stacking-line changes is shown in the figure below:

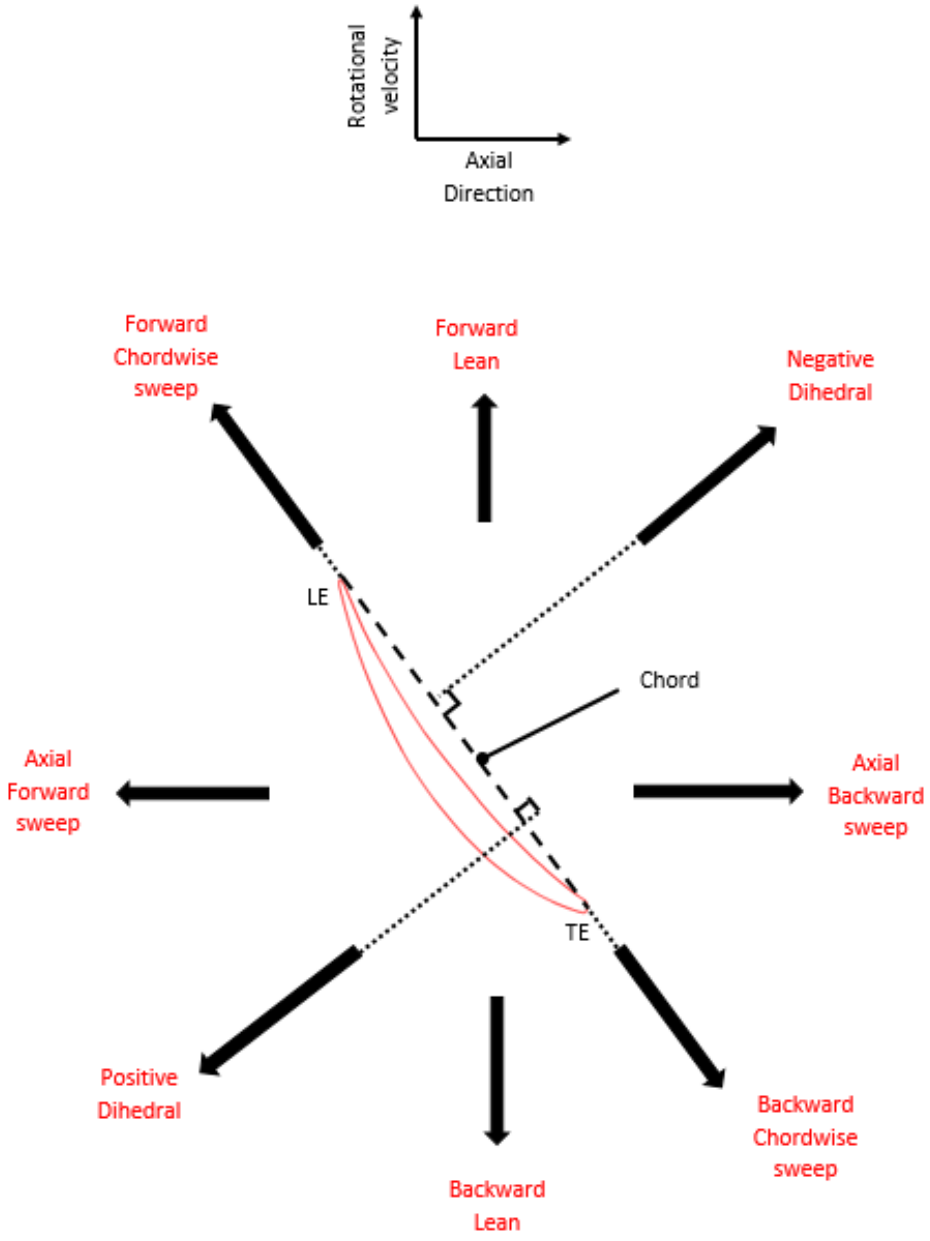

Figure A.1: Terminology used for stacking-line changes

APPENDIX B MESH CONVERGENCE STUDIES

Mesh study on the IGV, Rotor and Stator

A mesh convergence study was carried out by refining simultaneously the meshes of the IGV, the rotor and the stator. The baseline rotor with nominal tip clearance at design conditions served as the basis for this mesh study. The convergence of the results was checked using the total-to-total pressure ratio and efficiency of the entire system (IGV, Rotor and Stator). These two parameters were measured 10% axial chord upstream of the IGV leading-edge and 10% axial chord downstream of the stator trailing-edge. The results obtained are shown in figures B.1 and B.2. From these figures, the mesh selected is that having a total number of nodes of 8.4 million. This mesh density is kept the same throughout the design process.

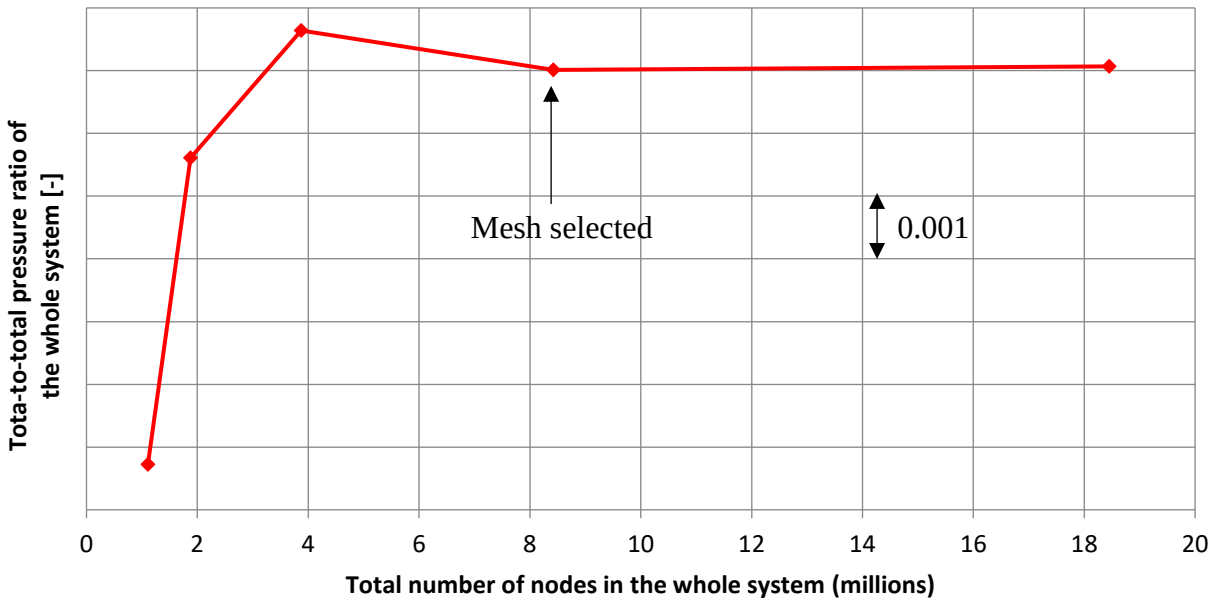

Figure B.1: Convergence of the IGV, rotor and stator meshes using total-to-total pressure ratio

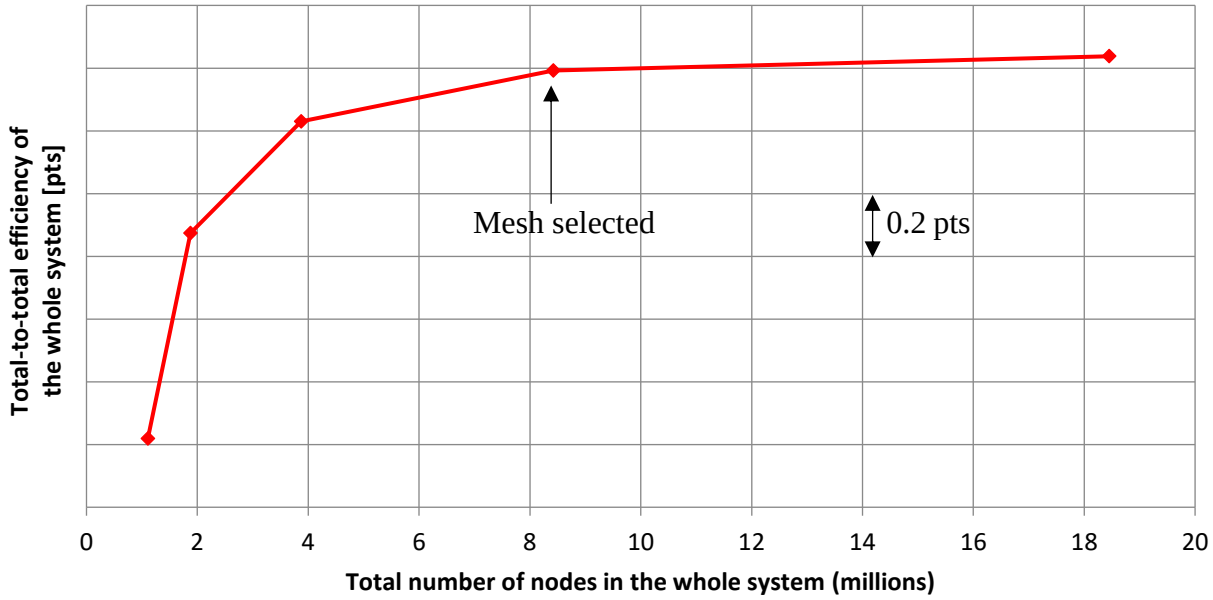

Figure B.2: Convergence of the IGV, rotor and stator meshes using total-to-total efficiency

Mesh study on the casing treatment

A mesh convergence study was carried out on a casing treatment corresponding to four grooves with the following dimensions expressed as a percentage of the rotor mean span: a depth of 0.6%, an indentation width of 30.3% and a location equal to 9.4% chord upstream of the rotor tip leading-edge. Once again, the baseline rotor at design conditions with nominal tip clearance was used. The meshes of the IGV, Rotor and Stator used in this new mesh study were the final meshes selected in the above section (8.4 million nodes in total). Since the casing treatment lies above the rotor alone, it was deemed more convenient to use the total-to-total pressure ratio and efficiency of the rotor alone to check the convergence of the casing treatment mesh. These two parameters were measured 10% axial chord upstream/downstream of the rotor leading-edge/trailing-edge respectively. The results obtained are shown in figures B.3 and B.4. The total number of nodes per groove chosen in this study is 128 000. This mesh density is kept the same throughout the design process.

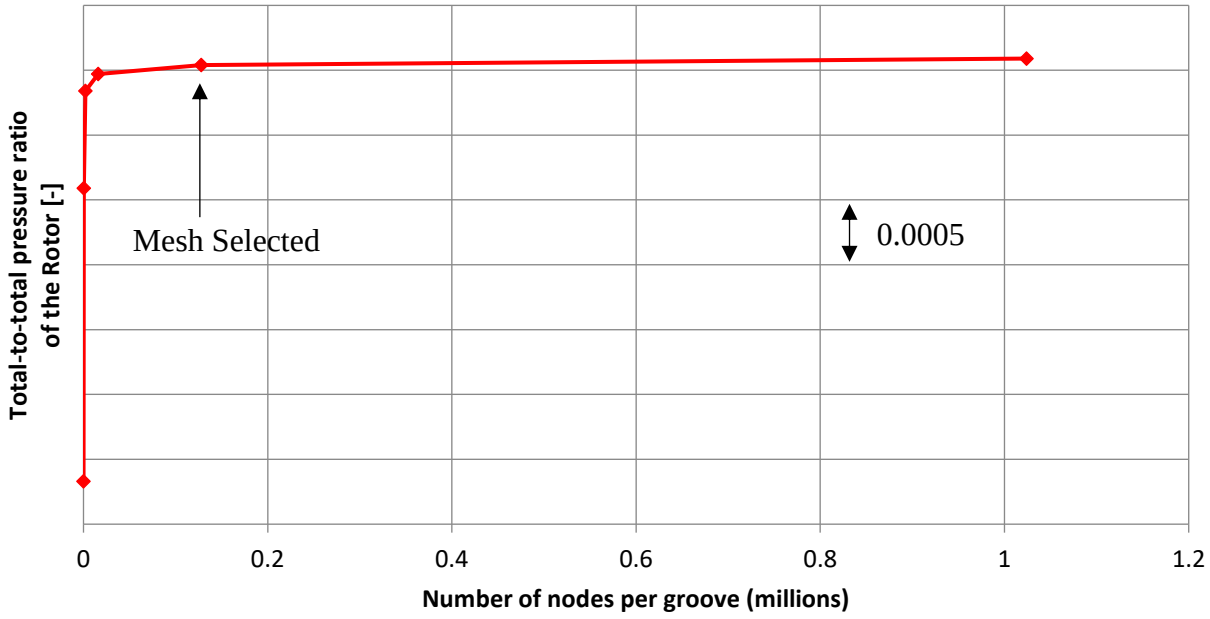

Figure B.3: Convergence of the casing treatment mesh using total-to-total pressure ratio

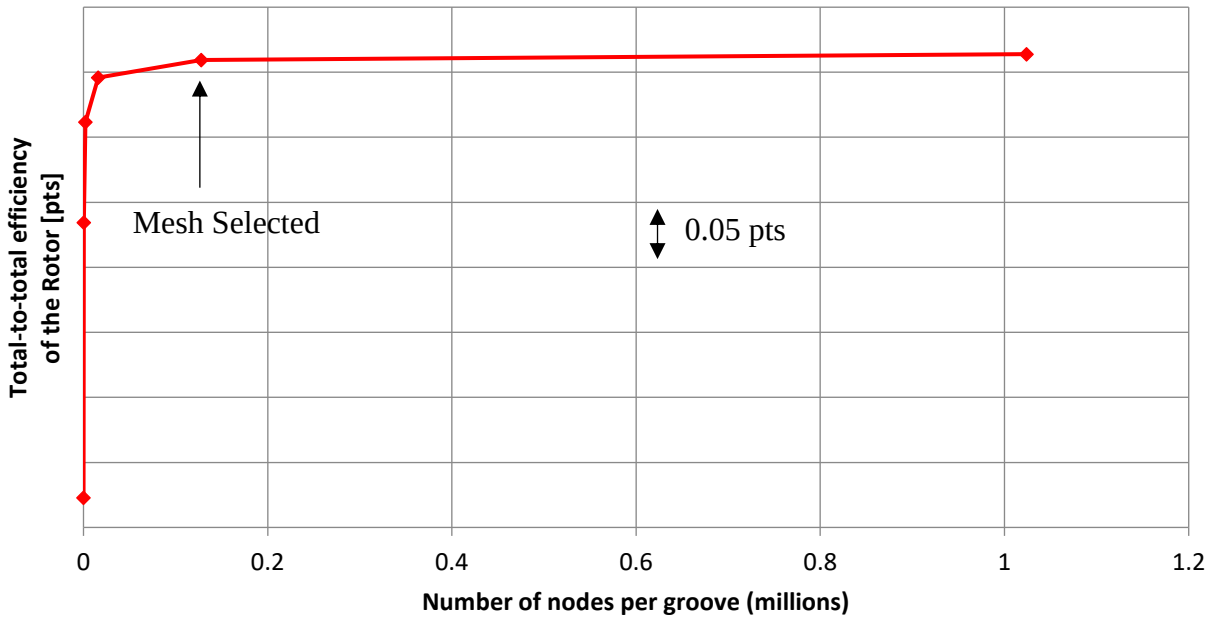

Figure B.4: Convergence of the casing treatment mesh using total-to-total efficiency

APPENDIX C VARIATION OF TOTAL PRESSURE AND STATIC ENTROPY IN THE ROTOR INLET/OUTLET

The changes in total pressure and static entropy from nominal to high tip clearance for the three cases investigated in chapters 4, 5 and 6 appear in the table below.

Table C.1: Changes in total pressure and static entropy as the tip clearance increases at the rotor inlet/outlet

	Inlet ΔP_T	Outlet ΔP_T	Inlet Δs	Outlet Δs
Baseline rotor with a smooth shroud	0.01%	0.29%	0.58%	16.57%
Baseline rotor with a casing treatment	0.01%	0.42%	0.84%	6.69%
New rotor with a smooth shroud	0.02%	0.11%	0.43%	18.27%

APPENDIX D DETAILTS ABOUT THE DESIGN STRATEGY OF THE DESENSITIZED ROTOR

In this appendix, the modifications to the shapes of the rotor suction side isobars resulting from the application of the three camber line changes and the stacking line change proposed in the design methodology of chapter 6 are explained.

Inlet metal angle/incidence

By decreasing the incidence (i.e. closing the leading-edge), the diffusion at a certain blade section starts at a more downstream axial location and vice versa. This is illustrated in figure D.1 by two sections having different incidences while having the same outlet metal angle.

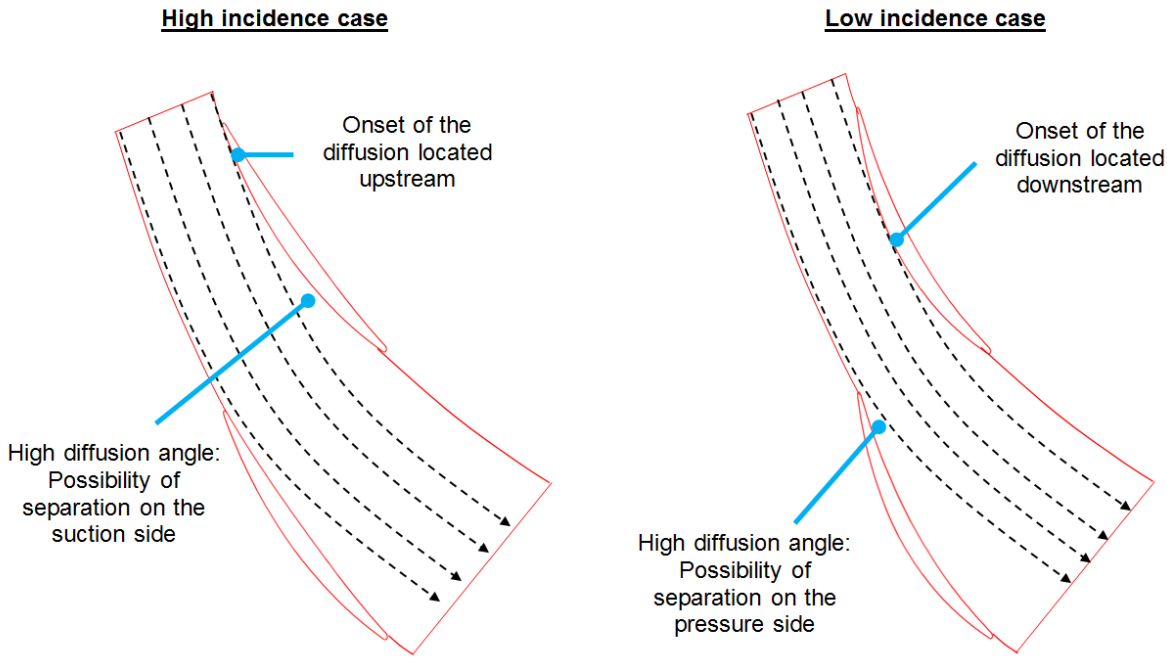

Figure D.1: Effect of the incidence on the location where the diffusion starts at a certain rotor span location

Therefore, by decreasing the incidence, the same static pressure is found at a more downstream location. This is illustrated in figure D.2 by CFD results obtained on the baseline rotor where the incidence was aggressively modified at 64% span without changing the trailing edge metal angle. In this figure, isobars selected in the three rotors are the same (i.e. same static pressure).

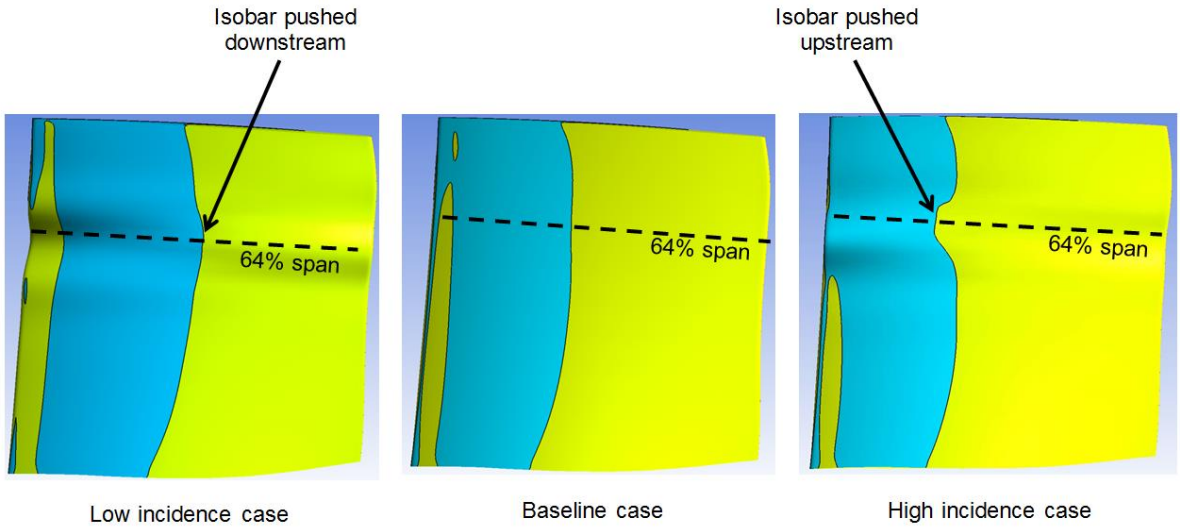

Figure D.2: Change in the rotor suction side isobar shape when incidence is modified

When applying this camber line change, attention should be taken not to induce a blade boundary layer separation either on the suction or the pressure side when respectively increasing or decreasing the blade incidence. That is to avoid penalizing the nominal efficiency. Also, an excessively high incidence might cause an early modal stall preceded by a suction side boundary layer separation which is not desirable.

Outlet metal angle/aerodynamic loading

By decreasing the amount of aerodynamic loading (i.e. by closing the trailing edge), the same static pressure is found at a more downstream location because a longer diffusion distance is required to achieve the same static pressure compared to a more loaded rotor. This is illustrated in figure D.3 by two sections having the same incidence while having different trailing edge metal angles.

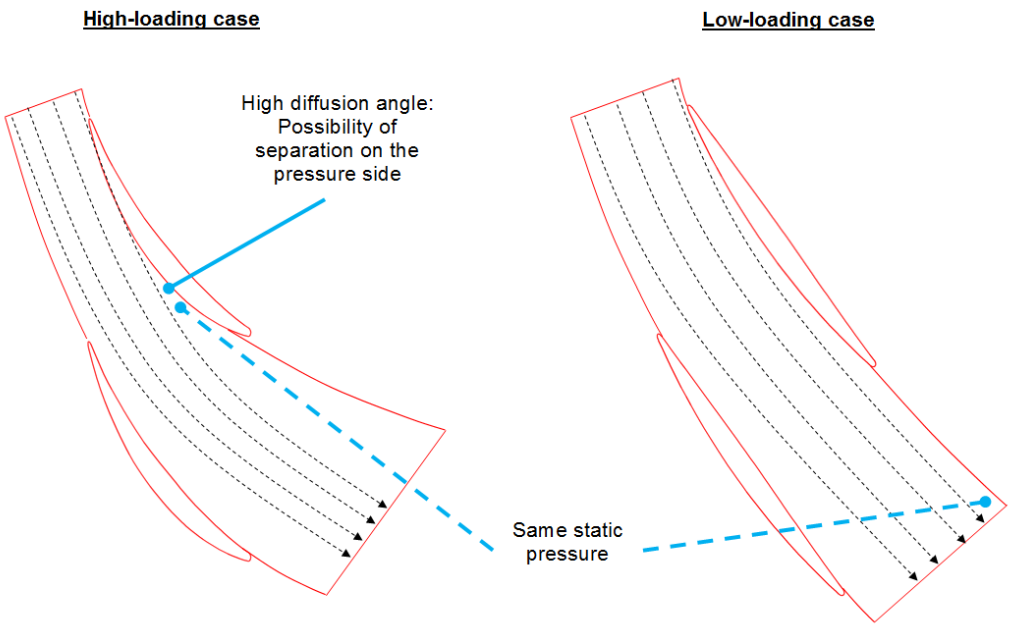

Figure D.3: Effect of the aerodynamic loading on the static pressure distribution at a certain rotor span location

An aggressive change was applied to the trailing edge metal angle of the baseline rotor at 64% span without changing the leading edge metal angle. The resulting effect on a suction side isobar obtained by CFD is shown in figure D.4.

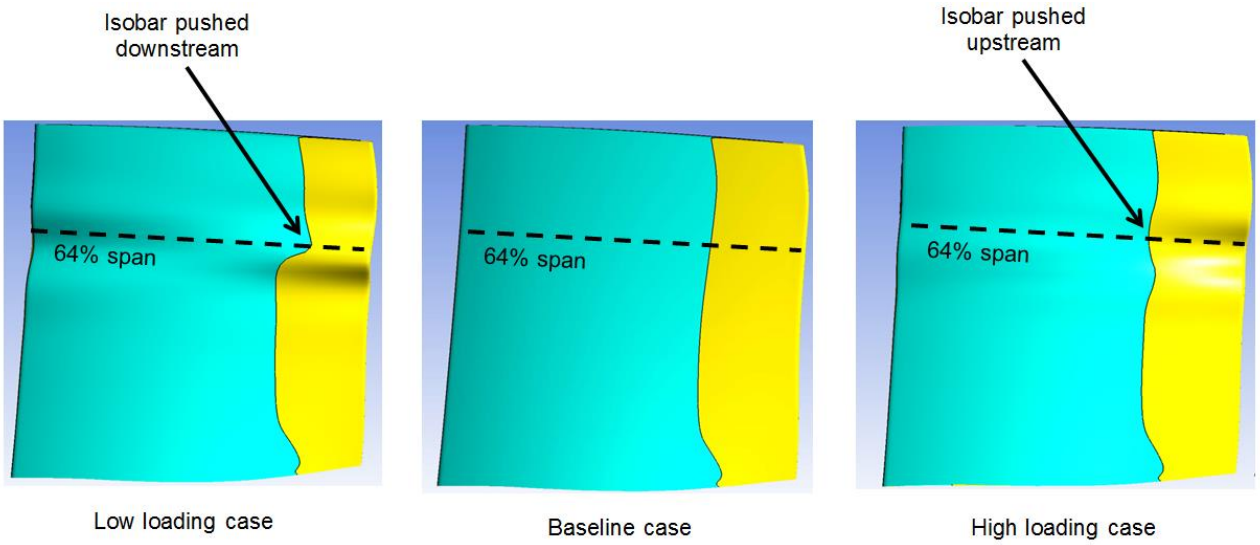

Figure D.4: Change in the rotor suction side isobar shape when the aerodynamic loading is modified

By applying that change, the rotor total pressure ratio is obviously modified. Attention should be taken again in the high-loading case not to cause a suction side boundary layer separation which would affect the nominal performance and stability.

Chordwise position of the maximum camber

The chordwise position of the maximum camber plays also a role on the location where the diffusion starts. In fact, an aft-loaded airfoil would start diffusing at a more downstream location compared to a front-loaded airfoil. This is illustrated in figure D.5 by two sections having different chordwise positions of the maximum camber while having the same leading edge/trailing edge metal angles.

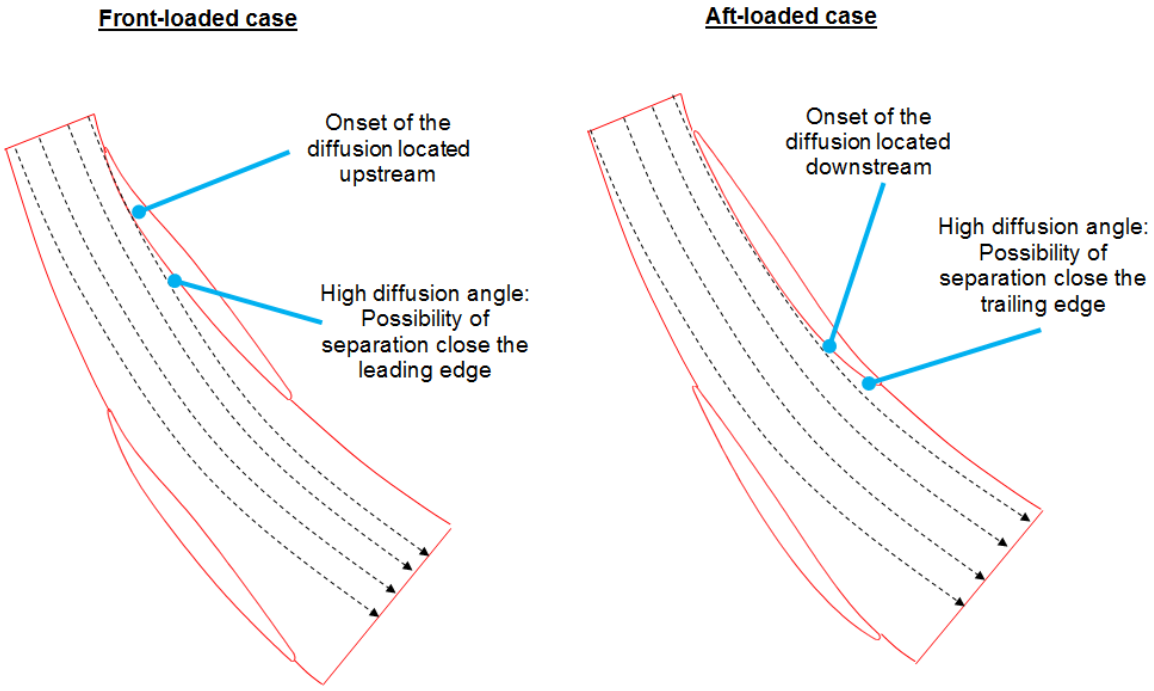

Figure D.5: Effect of the position of the maximum camber on the location where the diffusion starts at a certain rotor span location

An aggressive change in the chordwise position of the maximum camber was applied to the baseline rotor at 64% span. The change experienced by a suction side isobar obtained by CFD is shown in figure D.6.

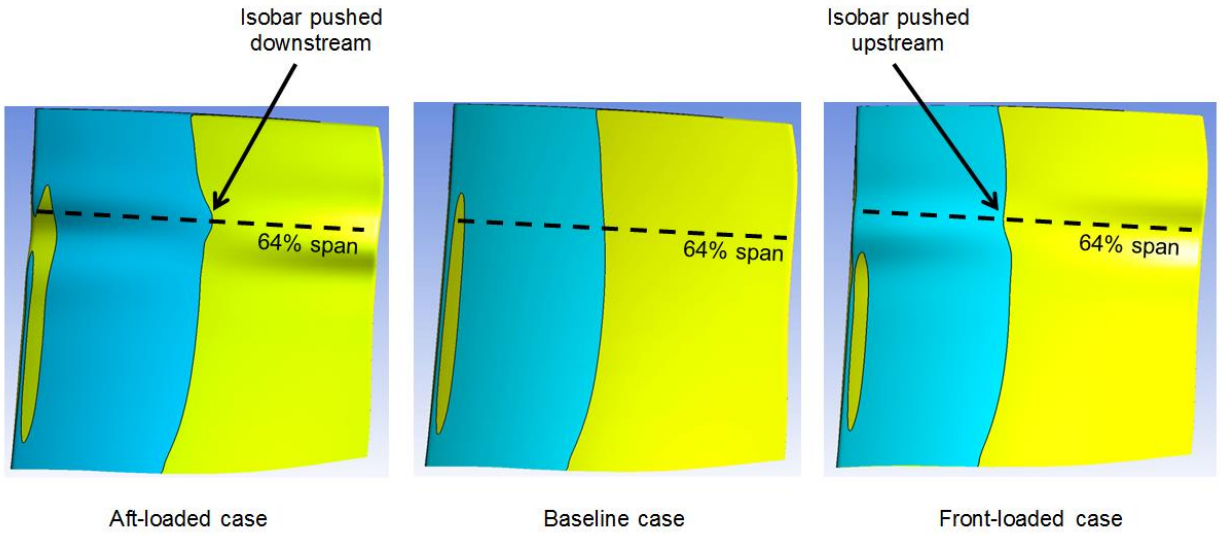

Figure D.6: Change in the rotor suction side isobar shape when the chordwise position of the maximum camber is modified

When applying this change, a high concentration of loading at a certain chordwise position might cause a suction side boundary layer separation close to the leading edge or close to the trailing edge respectively for a front-loaded or an aft-loaded section. This might cause penalties in efficiency and stall margin. Also, even by keeping the same leading edge/trailing edge metal angles and by having an attached flow (with no separation), an aft-loaded airfoil is known to have a lower pressure ratio than a front-loaded airfoil. Therefore, an aft-loaded airfoil might also cause a penalty in pressure ratio.

Moreover, aft-loading the tip airfoil is the strategy mentioned in the outset of chapter 6 to decrease the amount of double-leakage and reduce the sensitivity to tip clearance of the efficiency.

Blade lean

The blade lean is the stacking line change found to have an important effect on the shape of suction side isobars. A forward blade lean is referred to as a circumferential translation of a rotor section in the rotational speed direction while a backward blade lean is a circumferential translation in the opposite direction. This is illustrated in Appendix A.

A linear lean of the entire rotor blade which refers to a linearly increasing circumferential translation of the rotor sections from hub to tip was found to literally bend suction side isobars. In fact, a linear *forward* lean bends isobars toward the downstream direction in the tip of the rotor and

toward the upstream direction in the hub of the rotor while a linear *backward* lean has the opposite effect. This is illustrated in figure D.7[3] after applying an aggressive linear lean to the baseline rotor.

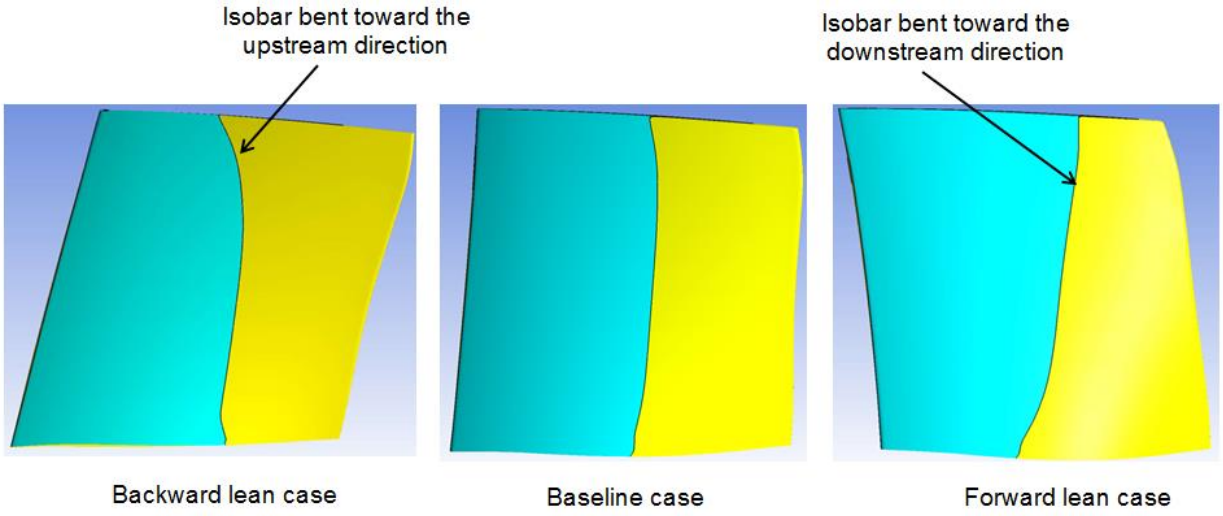

Figure D.7: Change in the rotor suction side isobar shape when lean is applied to the blade

To understand why the lean has such effect, the normalized static pressure field is taken at mid-chord for the three cases above and put in figure D.8. When the rotor is leaned backward, the lowest adverse pressure is found along the hub suction side which means that the entire incoming flow is directed toward that spot. In contrast, the lowest adverse pressure is found along the tip suction side when the rotor is leaned forward. The entire incoming flow is therefore attracted toward the tip. For the baseline rotor case, the lowest adverse pressure is uniformly distributed along the suction side. The incoming flow, having no preference between the hub and the tip, convects downstream without being deflected in the spanwise direction.

[3] In this figure, it is important to understand that **no** axial sweep (which refers to rotor sections translated *axially*) was applied to the three rotors shown. Leaned rotors appear to be titled axially only because the gas path is not horizontal.

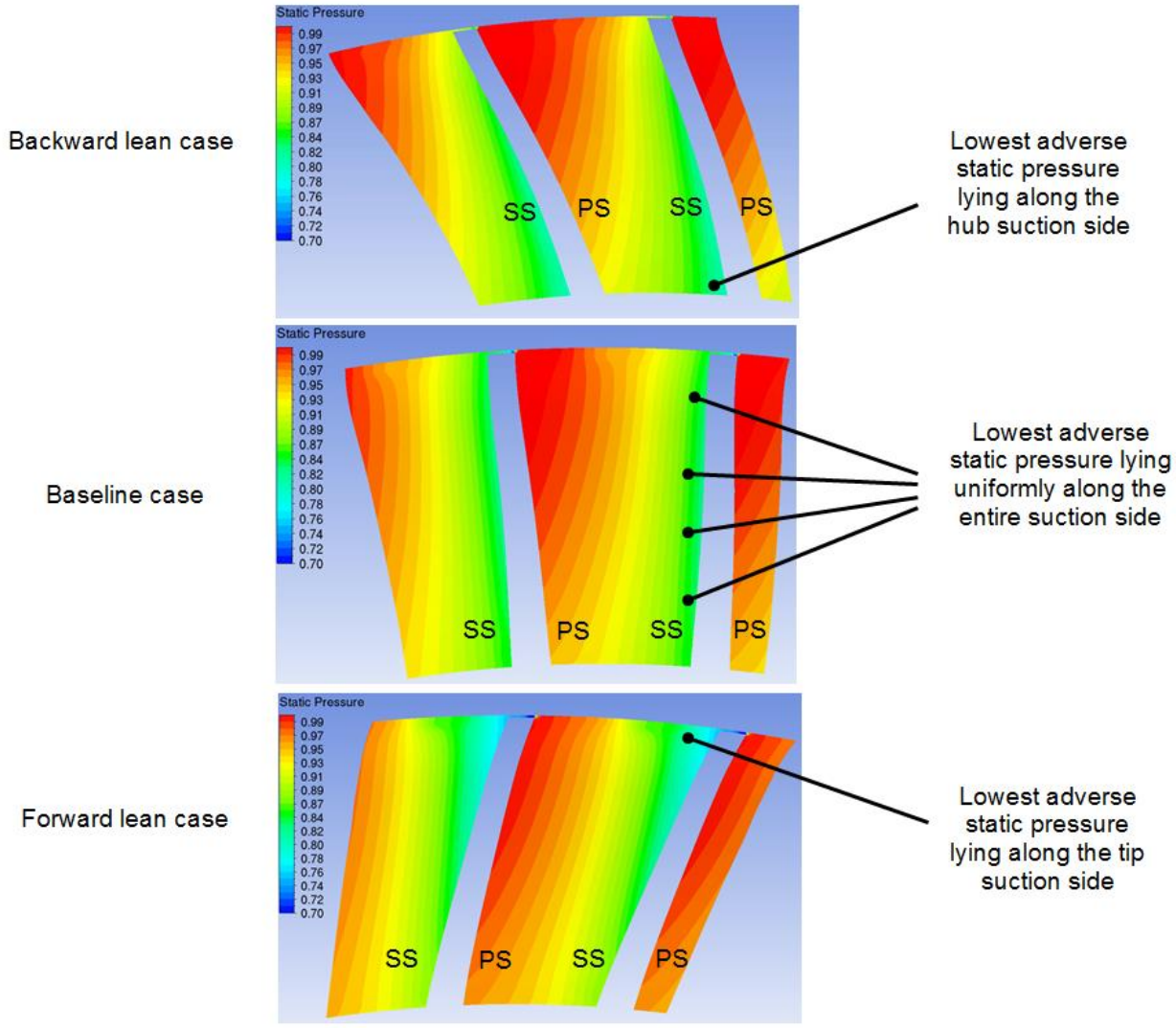

Figure D.8: Modification of the static pressure field in the passage following a blade lean

In a real design context, the only drawback of a lean is the high bending moment created by the centrifugal force at the rotor hub which might cause structural issues. To overcome this problem, a *parabolic* lean could be applied to the rotor (rather than a *linear* lean) in order to keep more matter in lower span regions close to the theoretical radial stacking line which would avoid creating a high bending moment in the hub.

Importance of the incidence on the sensitivity to tip clearance

After combining the four design strategies mentioned above to the baseline rotor in order to tilt its suction side isobars in the desired orientation shown in figure 6.9, a new rotor is obtained and called

"High-incidence rotor". This rotor is shown in figure D.9 and its suction side isobars are compared to the baseline rotor in figure D.10.

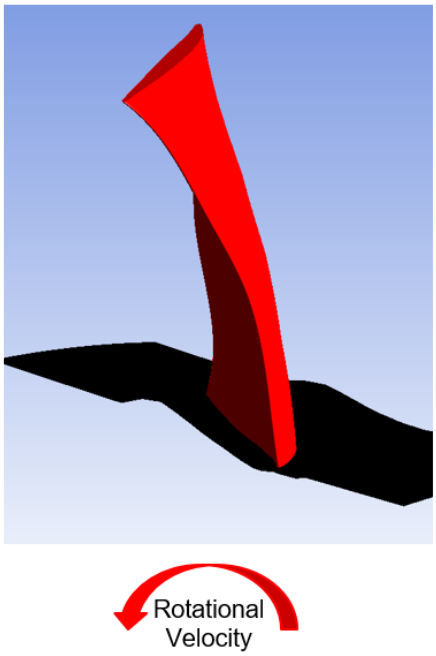

Figure D.9: "High-incidence" rotor geometry

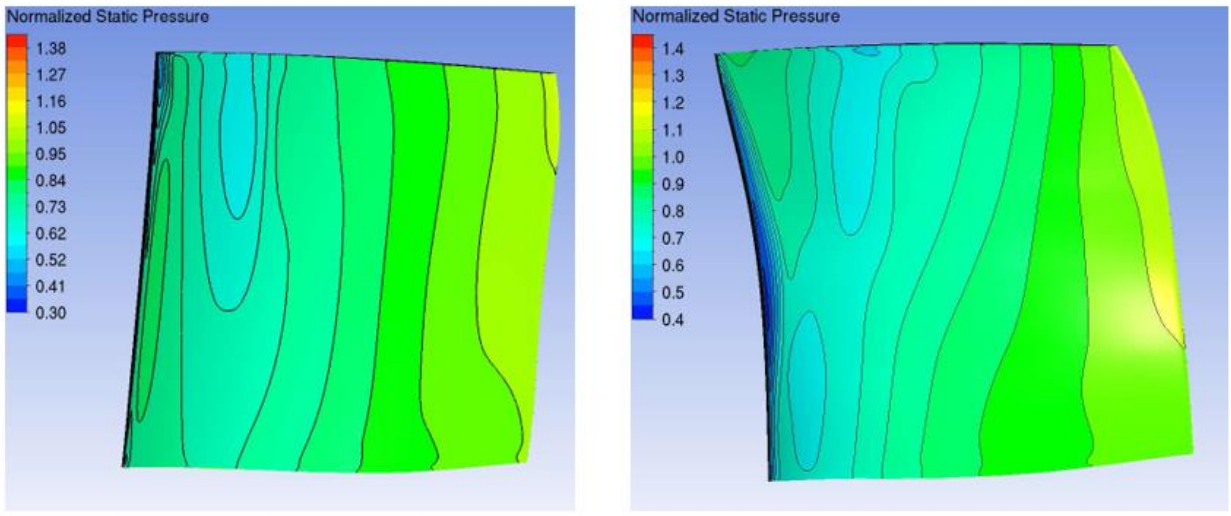

Figure D.10: Suction side isobars of the baseline and "high-incidence" rotors

Afterwards, the incidence of that rotor was uniformly decreased by 5 degrees from 0% to 82% span and then linearly decreased from 5 to 0 degrees from 82% to 100% span respectively. Therefore,

the rotor tip section and tip clearance flow are not affected by this change at all. Also, the reduction in incidence for the modified sections affected only 20% of the chord starting from the leading-edge. The resulting new rotor is called “Low-incidence rotor”. The spanwise distributions of aerodynamic loading for low/high incidence rotors are shown in figure D.11. The tip loading is the same for both rotors.

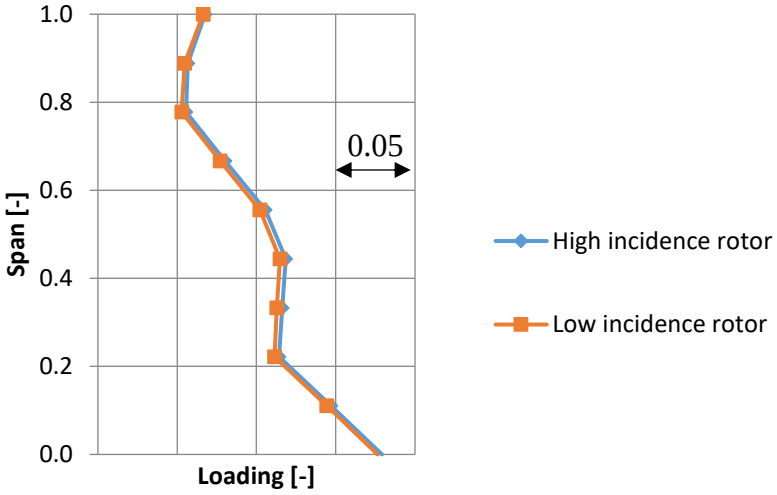

Figure D.11: Aerodynamic loading for the two rotors designed with different incidences

The resulting effect of the incidence on the rotor could be identified in figure D.12 by the difference in vorticity of the tip clearance vortex at high tip clearance size at the rotor trailing-edge plane. The low-incidence rotor vortex is stronger than that of the high-incidence rotor. The impact on the sensitivity to tip clearance of the pressure ratio and efficiency is important as shown in figures D.13 and D.14. It is worth mentioning that sensitivities to tip clearance of the pressure ratio (which is positive) and efficiency for the low-incidence rotor (having a smooth shroud) are very close to those obtained when the casing treatment was applied to the baseline rotor in chapter 5 (see figures 5.7 and 5.8). In addition, the low/high incidence rotors show almost no nominal performance penalty as depicted on table D.1. However, since the low-incidence rotor has an aggressive forward lean, its structural integrity could not be assured. Therefore, it is not retained as the final rotor design.

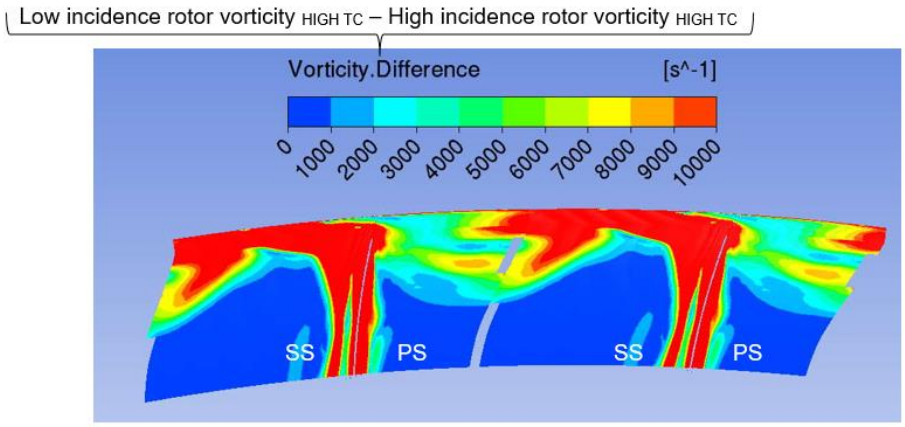

Figure D.12: Effect of the incidence on the vorticity of the tip clearance vortex at the rotor trailing edge plane between 70% and 100% span

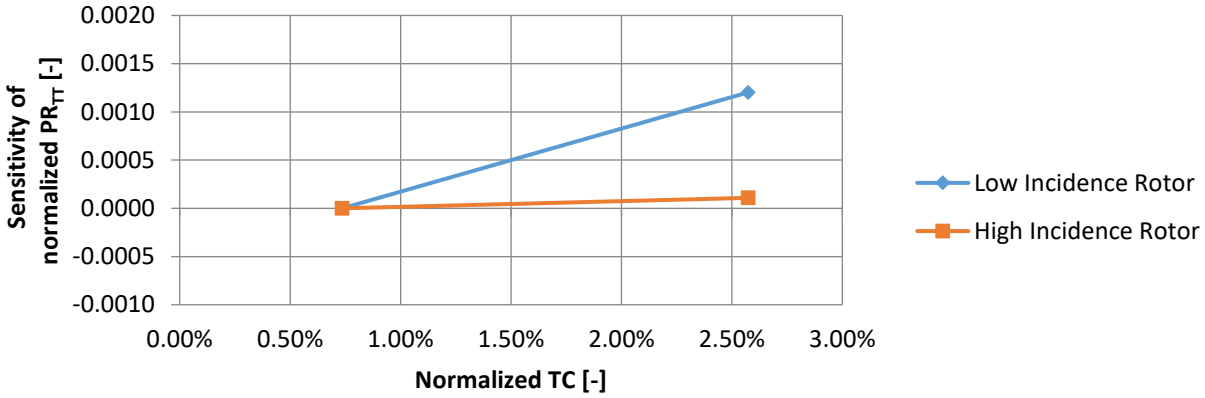

Figure D.13: Change of the sensitivity to tip clearance of the pressure ratio with incidence

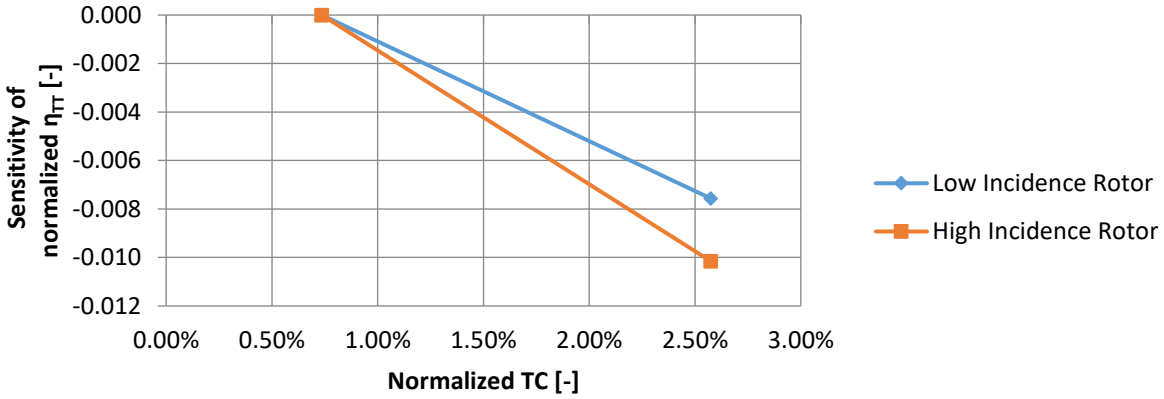

Figure D.14: Change of the sensitivity to tip clearance of the efficiency with incidence

Table D.1: Nominal performance of the two rotors having different incidences

	Normalized Nominal PR_{TT}	Normalized Nominal η_{TT}
Low-incidence rotor	1.003	0.999
High-incidence rotor	1.006	1.002

When the low-incidence rotor was obtained from the high-incidence rotor by a change in the incidence only, the sensitivity to tip clearance of efficiency decreased as shown in figure D.14 without aft-loading the rotor tip section. Actually, the sensitivity to tip clearance of the efficiency was reduced without even modifying the tip section. It is hypothesized that the high vorticity of the tip clearance vortex reduced also double-leakage (and sensitivity to tip clearance of the efficiency) by deflecting the tip clearance leakage toward lower span regions preventing it from reaching the adjacent blade. This hypothesis is illustrated in figure D.15.

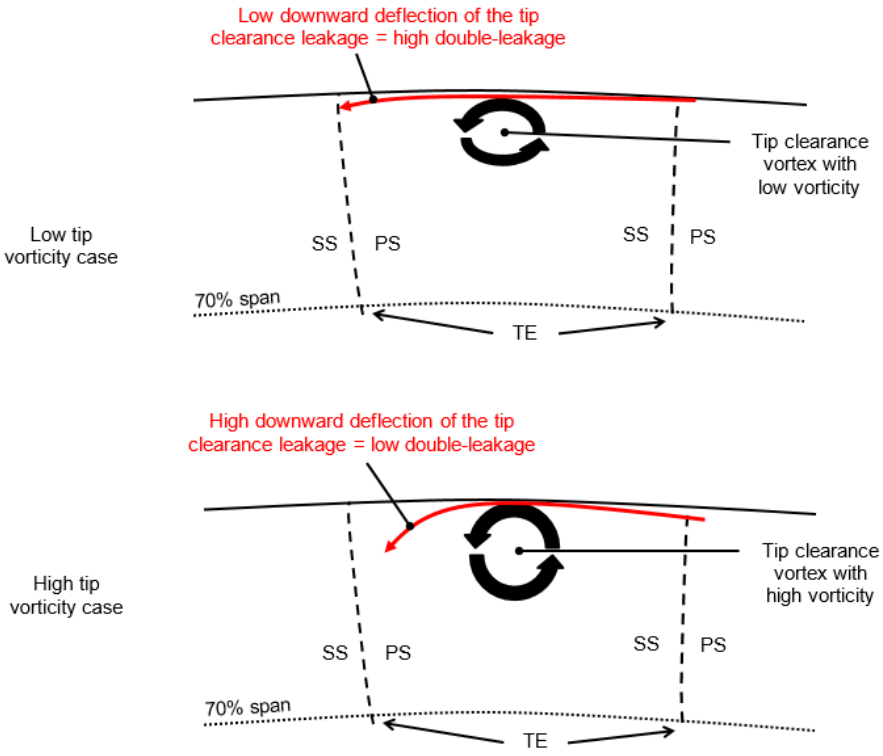

Figure D.15: Hypothesised effect of the vorticity of the tip clearance vortex on the tip clearance trajectory and double-leakage